POLITECNICO DI MILANO

Scuola di Ingegneria Industriale e dell'Informazione

Corso di Laurea Magistrale in Ingegneria Biomedica

Finite element fracture risk assessment of metastatic femur using deep-learning lesion segmentation

Relatore: Prof. Pasquale Vena

Correlatori: Prof. Nico Verdonschot

Prof. Esther Tanck

Dr. Florieke Eggermont

Ing. Ali Ataei

Tesi di laurea magistrale di:

Andrea D'Aurizio, 927215

Anno accademico 2021/2022

Contents

Sommario

Abstract

L'obbiettivo di questo studio è sia quello di determinare se l'utilizzo della tecnica degli elementi finiti combinata con segmentazioni delle lesioni (derivate sia da un algoritmo di deep learning sia manualmente) sia migliore nel determinare l'indice di rischio per metastasi ossee litiche nel femore rispetto all'utilizzo della sola tecnica agli elementi finiti, sia di trovare un modo per implementare le proprietà meccaniche delle metastasi blastiche nel modello ad elementi finiti.

8 pazienti litici e 6 blastici sono stati analizzati con 5 segmentazioni ed una segmentazione rispettivamente. Il modello ad elementi finiti specifico per ogni paziente è stato costruito partendo dalle immagini CT. Nei pazienti litici si è analizzato il coefficiente di Dice, il BOS score (il carico di fallimento normalizzato per il peso corporeo) e la classifica dei carichi di fallimento. Dato che i BOS score ottenuti dalla segmentazioni manuale erano positivi, si è deciso di allargare lo studio a 33 pazienti. Su di essi, si sono calcolati i valori di sensitività, specificità e di valore predittivo positivo e negativo. Per le metastasi blastiche, si è cercata una relazione tra la riduzione del modulo di Young delle metastasi e la differenza tra i carichi di fallimenti tra il modello standard e quello modificato con la segmentazione.

Per i pazienti litici, la segmentazione automatica più simile alla segmentazione manuale ha ottenuto un coefficiente di Dice pari a 64,43%. La segmentazione manuale ha una classifica dei carichi di fallimento molto diversa dalle segmentazioni automatiche e dal modello standard. Le segmentazioni automatiche hanno una classifica molto simile tra loro e al modello standard. I valori di sensitività, specificità, valore predittivo positivo e negativo dei 33 pazienti sono pari rispettivamente a 100%, 93%, 78% e 100%, mentre i valori ottenuti utilizzando solamente la tecnica ad elementi finiti sono pari rispettivamente a 100%, 74%, 39% e 100%. Anche le segmentazioni automatiche hanno

mostrato un miglioramento nella predizione del fattore di rischio ma non così buona come quella ottenuta con la segmentazione manuale. Per le metastasi blastiche, solo due pazienti su sei hanno mostrato l'andamento previsto. Entrambi i pazienti hanno in comune di avere lesioni molto diffuse sul femore, mentre gli altri quattro pazienti le lesioni risultano essere molto ridotte.

La tecnica ad elementi finiti combinata con la segmentazione manuale migliora la predizione del fattore di rischio delle metastasi ossee litiche nel femore, rispetto all'utilizzo della sola tecnica ad elementi finiti, invece per ottenere risultati simili con il deep learning, l'algoritmo deve essere migliorato. Nelle metastasi blastiche, la riduzione delle proprietà meccaniche nel modello ad elementi finiti influenza la forza di reazione solo in presenza di lesioni diffuse.

1. Introduzione

Il cancro, ad oggi, risulta essere una delle malattie più diffuse al mondo. Nel 2017, a più di 100.000 pazienti è stato diagnosticato il cancro nei Paesi Bassi [1]. Nel 2012, il numero di casi registrati ammontava a 14,1 milioni, mentre nel 2020 sono stati diagnosticati 20 milioni di casi in tutto il mondo e le previsioni future sono peggiori [2].

Il tessuto osseo è il terzo tessuto del corpo umano ad essere colpito da metastasi [3]. Queste si formano quando il processo di rimodellamento osseo subisce un'alterazione [4]. Le metastasi causano due tipologie di lesioni: le lesioni litiche, dovute ad un'eccessiva produzione di osteoclasti, e le lesioni blastiche, dovute ad un'eccessiva produzione di osteoblasti. L'eccessiva produzione di osteoclasti causa un riassorbimento del tessuto osseo locale. L'eccessiva produzione di osteoblasti, invece, causa un'eccessiva formazione di tessuto osseo locale priva della corretta struttura lamellare [5]. Questo comporta una minore resistenza del tessuto alle sollecitazioni. I pazienti che sviluppano metastasi ossee possono essere classificati in tre modi: prevalentemente litici, prevalentemente blastici o misti [6]. Le cellule cancerogene viaggiano attraverso il sistema circolatorio e quando trovano un "terreno" adatto, come il tessuto osseo riescono a riprodursi. Per questa ragione, le zone maggiormente colpite da metastasi sono quelle maggiormente vascolarizzate. Nel tessuto osseo, queste zone sono lo scheletro assiale e la parte distale e/o prossimale delle ossa lunghe [7].

Le metastasi ossee sono estremamente dolorose. I principali sintomi sono senso di malessere, stanchezza, dolore e sonnolenza [8]. Questi sintomi sono rilevati da più dell'80% dei pazienti. La peggiore complicazione delle metastasi ossee è che esse possono causare la frattura dell'osso stesso laddove si sviluppano. Nelle ossa lunghe, le fratture di un osso colpito da metastasi avvengono nel 10% dei casi [9]. Queste complicazioni causano nel paziente difficoltà nello svolgere le normali azioni di vita quotidiana, portando ad una ridotta qualità della vita [10]. Per il paziente, avere una frattura, significa essere sottoposto ad un intervento chirurgico molto complicato: esso può infatti causare molte complicazioni al paziente, che possono essere sistemiche come l'embolia polmonare o il fallimento del fegato, dovute ad infezioni o a problemi avuti durante l'intervento come la frattura di un mezzo di osteosintesi nelle vicinanze della frattura [11].

Per queste ragioni, la migliore soluzione è prevenire la frattura. Per fare ciò i medici utilizzano l'indice di rischio di frattura: un parametro utilizzato per valutare la probabilità che un osso del paziente si rompa. Basandosi sul rischio di frattura, viene scelta la terapia [12] [13]: nel caso in cui il paziente venga classificato ad alto rischio di frattura, egli verrà sottoposto ad un intervento chirurgico preventivo e, qualora il paziente non sia in grado di sostenere un intervento chirurgico, egli verrà trattato con sessioni multiple di radioterapia; nel caso in cui, invece, il paziente viene classificato come a basso rischio di frattura, egli verrà sottoposto ad una singola sessione di radioterapia [13]. La radioterapia, infatti, risulta essere molto efficace poiché con la sua azione stimola la re-mineralizzazione delle ossa [14].

Dato che i trattamenti chirurgici si basano sul rischio di frattura, è necessario che il calcolo sia affidabile. Nei Paesi Bassi, l'indice di rischio viene stimato utilizzando le radiografie convenzionali [13]. Il criterio con cui viene assegnato il rischio di frattura riguarda la dimensione delle metastasi: se vi è un coinvolgimento assiale maggiore di 30 mm, il paziente viene classificato ad alto rischio di frattura [14]. Questo metodo prevede correttamente la frattura del paziente solo nel 23% dei casi, implicando che il 77% dei pazienti subiscono un intervento senza averne effettivamente la necessità. Questo influisce negativamente sia sulla salute del paziente sia sull'ospedale da un punto di vista economico. L'obiettivo di molti gruppi di ricerca è quello di aumentare l'affidabilità della

previsione del rischio di frattura nelle ossa lunghe. Per raggiungere ciò uno strumento che sembra essere molto promettente è il metodo degli elementi finiti [15] [16] [17] [18].

Questo metodo migliora l'affidabilità dell'indice di rischio nei pazienti con metastasi prevalentemente litiche. Le metastasi blastiche causano un aumento locale della densità ossea, che però risulta in una resistenza inferiore dell'osso poiché manca la corretta struttura lamellare. Questo aumento della densità, invece, viene rilevato dal metodo degli elementi finiti come una aumento della resistenza del materiale [17].

Molti ricercatori hanno provato a dare una risposta su come implementare le proprietà meccaniche del tessuto osseo metastastatico. Kaneko et al. hanno dimostrato che la QCT (quantitative computer tomography) è in grado di fornire un'accurata e precisa stima dell'ash density anche nelle metastasi ossee [19] [20]. Per questa ragione, le immagini utilizzate in questo elaborato, per implementare le proprietà meccaniche del femore sono raccolte con la QCT. L'ash density ha un ruolo importante perché viene utilizzata per stimare le proprietà meccaniche del femore. Una forte relazione, infatti, è stata osservata tra l'ash density e il modulo elastico ed il carico di snervamento e di rottura. Nell'Hipp et al. si sono analizzate le proprietà meccaniche delle metastasi ossee nell'osso trabecolare delle vertebre [21]. I campioni sono stati sottoposti ad una compressione assiale fino a fallimento. I risultati non hanno rilevato nessuna differenza sostanziale tra le regioni litiche e le regioni blastiche, nonostante vi sia un'elevata differenza nella densità del tessuto. Per quanto riguarda il modulo elastico, allo stesso modo, non sono state riscontrate differenze significative. Lo studio ha presentato alcune limitazioni. Una delle principali è legata al fatto che molti campioni sono costituiti da una composizione mista di metastasi litiche e blastiche. Una seconda limitazione è che i campioni analizzati sono stati prelevati solo da due pazienti. Stadelman et al., hanno studiato le metastasi ossee situate nelle vertebre [22]. In questo caso le metastasi prevalentemente litiche e miste hanno mostrato di avere un modulo di indentazione, ovvero il modulo di Young ottenuto con prove di nano indentazione, senza differenze significative con il tessuto osseo sano. Nelle metastasi prevalentemente blastiche, i modulo di indentazione ottenuto è stato inferiore del 5,8% rispetto a quello dell'osso sano.

Per fare in modo che le proprietà meccaniche vengano modificate solo nelle metastasi è necessario che le metastasi siano identificate in maniera accurata. Per questo motivo, un algoritmo di deep learning viene utilizzato per riconoscere le metastasi direttamente nelle

immagini QCT. Metodi automatici di segmentazione sono stati utilizzati in passato per riconoscere le metastasi litiche [23] e le metastasi blastiche [24]. Per allenare l'algoritmo, le lesioni sono state segmentate manualmente. L'output dell'algoritmo è quindi dato dalle segmentazioni automatiche delle metastasi litiche e blastiche.

In questa trattazione si sono utilizzati entrambi gli strumenti: la tecnica degli elementi finiti ed il deep learning. L'obiettivo di questo lavoro è stato quello di verificare, nei pazienti con una prevalenza di metastasi litiche, se l'implementazione delle segmentazioni modifichi la classifica dei carichi di fallimento rispetto all'utilizzo della sola tecnica ad elementi finiti, se con l'implementazione delle segmentazioni vi è stato un miglioramento nell'affidabilità del fattore di rischio e se la segmentazione manuale e quella automatica portino a risultati simili. Nei pazienti con metastasi prevalentemente blastiche l'obiettivo, invece, è stato quello di trovare un modo per implementare le proprietà meccaniche.

2. Metodi

- Pazienti e CT-scan

Nello studio sono stati inclusi 8 pazienti con metastasi prevalentemente litiche (età media: 64,75; intervallo: 55-88 anni; 5 uomini, 3 donne) e sei pazienti con metastasi prevalentemente blastiche (età media: 73,67; intervallo: 59-95 anni; 5 uomini, 1 donna). I pazienti analizzati hanno avuto mieloma multiplo, cancro al seno, cancro al polmone, cancro alla prostata o cancro ai reni. Tutti hanno sviluppato metastasi al femore e sono stati sottoposti a QCT. Un phantom di calibrazione contenente quattro densità ossee note (50, 100, 150, 200 $\frac{mg}{cm^3}$) è stato scannerizzato insieme al paziente al livello del femore prossimale. La QCT è utilizzata con le seguenti impostazioni: 120kVp, 220 mA, spessore della sezione 3mm, passo 1,5 ricostruzione a spirale e standard, risoluzione del piano 0,9375 mm.

La densità ossea di ogni elemento è salvata in un calcium file, che è specifico per ogni paziente.

- Il modello ad elementi finiti

Il modello ad elementi finiti specifico (Fig. 1a) per il paziente viene generato dalle immagini QCT. Queste immagini sono state usate per segmentare i femori e per ottenere una mesh superficiale 3D utilizzando Mimics (version 11.0 and 14.0, Materialise, Leuven, Belgio). Al modello è stata poi applicata una mesh composta da elementi tetraedrici utilizzando Marc Mentat.

Le unità di Hounsfield delle immagini QCT sono state utilizzate per determinare le proprietà del materiale. A metà della diafisi è stata effettuata un'operazione di calibrazione che ha consentito di convertire le unità di Hounsfield con i valori di calcio equivalenti, ovvero una misura della densità ossea. La densità ossea viene di ogni elemento viene salvata nel calcium file che è specifico per ogni paziente [17]. La densità ossea viene utilizzata per calcolare l'ash density e le proprietà del materiale [25].

Il comportamento del materiale, dopo il fallimento, è stato descritto in tre fasi. La prima è una fase perfettamente plastica, la seconda è di "strain softening" ossia diminuzione dello sforzo all'aumentare della deformazione e la terza è, nuovamente, perfettamente plastica [25]. I modelli sono stati caricati spostando un afferraggio che è posizionato sulla testa del femore ed il modello è stato fissato distalmente al centro dell'articolazione del ginocchio da due fasci di molle ad alta rigidità ($2 \cdot 10^8$ N/m) (Figura 1). Questa configurazione è stata scelta in modo da imitare il più possibile la posizione eretta [16].
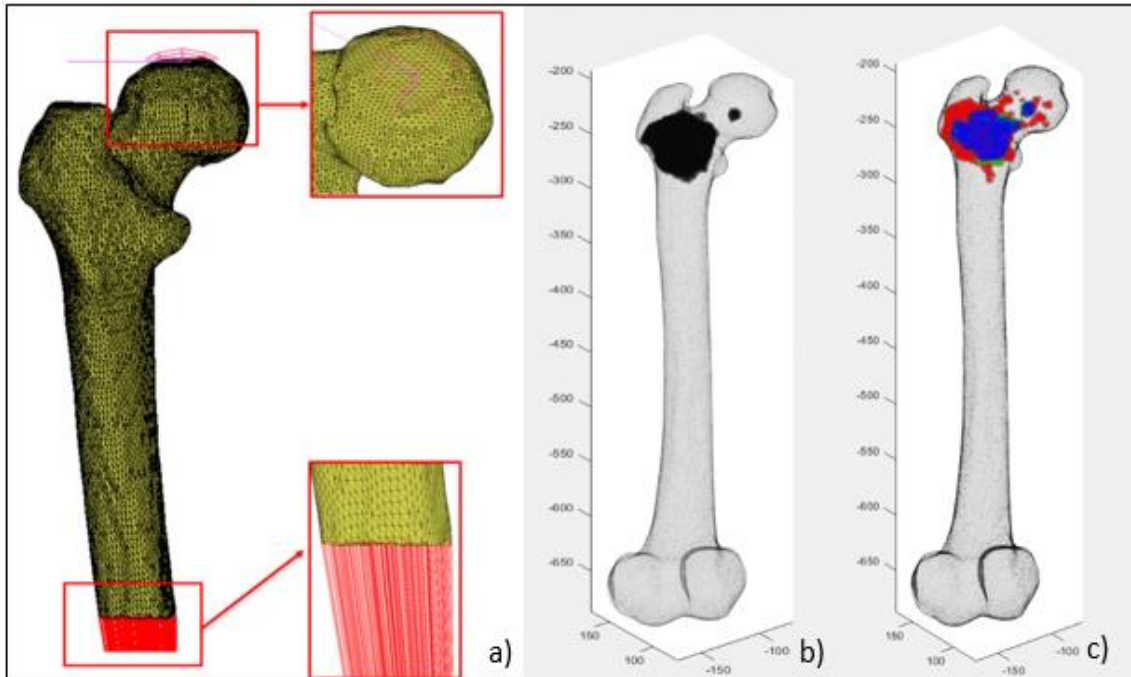
Figura 1: a) Esempio di un modello completo ad elementi finiti di un singolo paziente. b) Esempio di come le segmentazioni vengono implementati nel modello ad elementi finiti. c) Esempio di un confronto tra una segmentazione automatica e la segmentazione manuale. In verde sono rappresentate le metastasi trovate dalla segmentazione automatica, in rosso le metastasi trovate dalla segmentazione manuale ed in blu le metastasi trovate da entrambe le segmentazioni.

Durante la simulazione, il modello è stato caricato dell'afferraggio che si muove in direzione assiale. L'obiettivo della simulazione è quello di portare il femore alla frattura. Questa viene raggiunta in due casi: quando la curva forza-spostamento (output della simulazione) ha un evidente picco o quando la simulazione si interrompe perché non ha raggiunto convergenza (Figura 2a, Figura 2b). Il risultato è il carico di fallimento del femore. Questo è stato normalizzato con il peso corporeo ed è stato ottenuto il BOS score. Il BOS score è stato utilizzato per classificare i femori ad alto o a basso rischio di frattura [17].

Figura 2: Due esempi della curva forza-spostamento (l'output della simulazione) di due pazienti (K120L (a) e L342L (b)) delle segmenta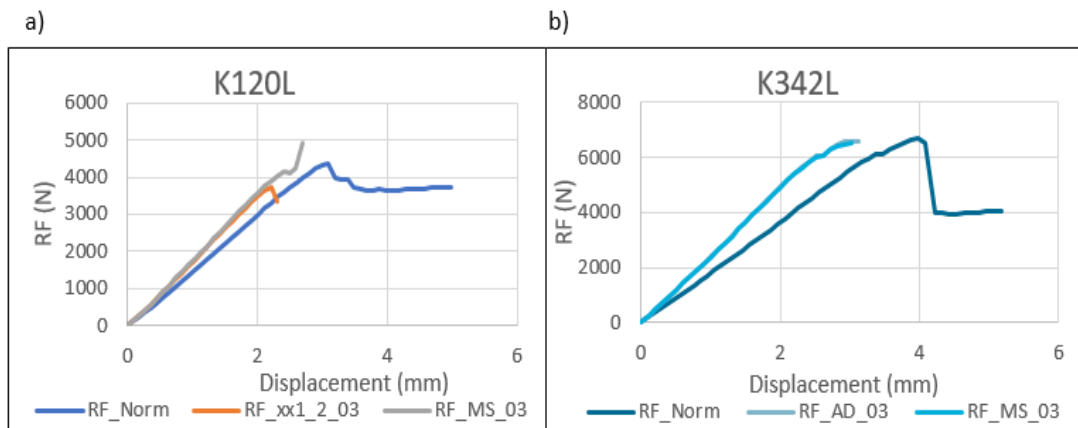zioni automatiche 1xx-2xx e AD e della segmentazione manuale (MS), confrontate con quelle ottenute dal modello standard (Norm).

- L'algoritmo di deep learning

Per trovare le metastasi litiche, sono state testate cinque segmentazioni delle stesse (quattro automatiche ed una manuale) sugli otto pazienti. Le segmentazioni automatiche sono state allenate con un set di immagini contenenti metastasi segmentate manualmente. Avere una perfetta corrispondenza tra le due segmentazioni è l'obiettivo dell'algoritmo di deep learning. La segmentazione ottenuta allenando l'algoritmo di deep learning con immagini QCT contenenti lesioni litiche è stata chiamata 1xx. La segmentazione ottenuta allenando l'algoritmo di deep learning con immagini QCT contenenti lesioni litiche e immagini QCT di ossa sane (senza metastasi) è stata chiamata 2xx. La segmentazione ottenuta combinando le due segmentazioni precedenti è stata chiamata 1xx-2xx. La segmentazione ottenuta allenando l'algoritmo di deep learning con immagini QCT contenenti lesioni litiche e lesioni blastiche è stata chiamata AD (all dataset).

Sulla base delle informazioni ottenute dalla segmentazione, le proprietà meccaniche del modello ad elementi finiti sono state modificate. Per fare ciò, è stato sviluppato uno script di Matlab che impone a zero la densità ossea negli elementi dove delle metastasi sono presenti. Il modello ad elementi finiti originale, senza alcuna modifica delle proprietà meccaniche è stato chiamato modello standard.

Per ottenere la mappature delle metastasi blastiche, è stata utilizzata la segmentazione di tipo AD. Per ridurre il modulo di Young, sono stati modificati i valori di densità

ossea negli elementi dove le metastasi sono state rilevate. Per fare ciò, uno script in Matlab che ha determinato la riduzione del modulo di Young dal 5.8% al 95% in intervalli pari a 5%. Questa operazione è stata effettuata su tutti i femori analizzati in modo da capire quale sia la percentuale di riduzione del modulo di Young corretta per non ottenere la sovrastima delle proprietà meccaniche ottenute nel modello ad elementi finiti standard.

- Analisi

Per determinare se i modelli implementati con le segmentazioni migliorino l'affidabilità del fattore di rischio, sono stati analizzati i seguenti parametri: il coefficiente di Dice è stato usato per confrontare le segmentazioni automatiche e la segmentazione manuale; la differenza tra il carico di fallimento del modello standard con quello implementato con le segmentazioni (manuale ed automatica); la densità ossea media è stata calcolata negli elementi dove le segmentazioni hanno rilevato una metastasi; il volume in percentuale della metastasi rispetto a tutto il volume osseo.

I carichi di fallimento sono stati classificati ed è stata analizzata la differenza nel ranking tra il modello standard e quelli con segmentazioni. È stata, poi, cercata una relazione tra il coefficiente di Dice e la percentuale di variazione del carico di fallimento. Il BOS score è stato calcolato per verificare se ci siano miglioramenti nell'affidabilità della predizione del fattore di rischio. Per verificare che la differenza tra i carichi di fallimento non è solo dovuta all'abbassamento delle proprietà del materiale, si è verificato se ci fosse o meno una relazione tra la densità ossea media e la differenza tra i carichi di fallimento, tra la percentuale di elementi che hanno metastasi e la differenza tra i carichi di fallimento.

Per le metastasi blastiche, è stata ricercata una relazione tra la riduzione del modulo di Young e la differenza tra la forza di reazione tra il modello standard e quello modificato. L'ipotesi è che con la riduzione del modulo di Young, si aumenti la differenza tra le forze di reazione dei due modelli.

3. Risultati

- Le metastasi litiche

Il coefficiente di Dice delle segmentazioni automatiche più elevato è stato quello della segmentazione, 2xx che è quella più simile alla segmentazione manuale. Il coefficiente di Dice medio è stato pari a 64,43%. Per le altre segmentazioni automatiche sono stati ottenuti i seguenti risultati: 49,67% per la 1xx, 39,17% per la 1xx-2xx e 57.02% per la AD.

La segmentazione AD ha avuto la più bassa differenza di carichi di fallimento media rispetto al carico di fallimento ottenuto dal modello standard. La differenza in percentuale media della segmentazione manuale rispetto al modello standard è stata la più elevata (24,41%) rispetto a tutte le segmentazioni. La segmentazione che in termini di carico di fallimento mostra i risultati più simili alla segmentazione manuale è la 1xx-2xx. I risultati, tra queste due segmentazioni, differiscono del 11,98%. Nelle altre segmentazioni, la differenza con la segmentazione manuale è pari a 14,88% per la 1xx, a 17,79% per la 2xx e per la 16,87% per la AD (Tabella 1).

		RF diff % AS_MS 00 mean
		03
Segmentations	1xx	14.88%
	2xx	17.79%
	1xx-2xx	11.98%
	All Dataset	16.89%

Tabella 1: Differenza nei carichi di fallimento tra la segmentazione manuale e quella automatica. La segmentazione 1xx è stata ottenuta allenando l'algoritmo con immagini QCT di lesioni litiche. La segmentazione 2xx è stata ottenuta allenando l'algoritmo con immagini QCT di lesioni litiche e ossa sane. La segmentazione 1xx-2xx è stata ottenuta tramite una combinazione delle due precedenti. La segmentazione AD è stata ottenuta allenando l'algoritmo con immagini QCT di lesioni litiche e lesioni blastiche.

Nell'analisi del ranking, i carichi di fallimento sono classificato dal più basso al più alto. Nella segmentazione manuale (Figura 3a) vi è stata una grande differenza rispetto al ranking ottenuto dai carichi di fallimento del modello standard. In tre segmentazioni automatiche (Figura 3c, Figura 3d, Figura 3e), ovvero le 2xx,1xx-2xx e AD, solo due carichi di fallimento si scambiano la posizione rispetto al ranking del modello standard. Il ranking della segmentazione automatica 1xx (Figura 3b) è stato uguale a quello del modello standard.
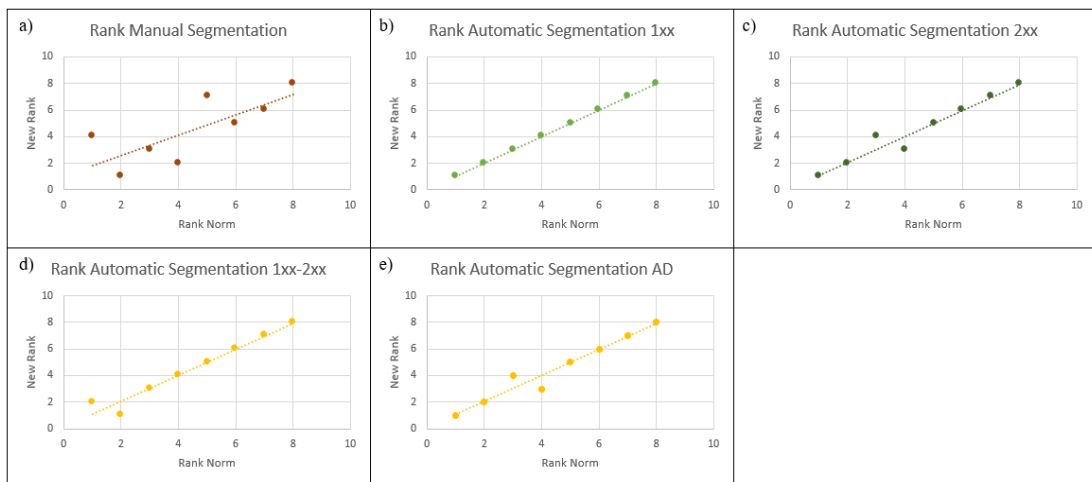

Figura 3: Confronto tra il ranking ottenuto dal modello modificato con la segmentazione manuale (a), con la segmentazione automatica 1xx (b), con la segmentazione automatica 2xx (c), con la segmentazione automatica 1xx-2xx (d) e con segmentazione automatica AD (e), rispetto a quello ottenuto con il modello standard.

È stato calcolato il BOS score di ogni paziente. Per il modello standard sono stati rilevati due falsi positivi (Figure 4). I carichi di fallimento ottenuti dal modello modificato con la segmentazione manuale hanno, invece, rilevato un solo falso positivo. Se si esclude questo paziente, la differenza tra il più alto BOS score tra i veri positivi più basso tra i veri negativi è risultato essere di 2,8 (Figura 5). Dato che i risultati sono stati promettenti, si è deciso di estendere l'analisi a 33 pazienti. Per analizzare i risultati sono stati scelti i valori di sensitività, specificità, valore predittivo positivo e valore predittivo negativo. La sensitività è la probabilità che, sapendo che il paziente sia ad alto rischio di frattura, il test dia il medesimo risultato, mentre la specificità è la probabilità che, sapendo che il paziente sia a basso rischio di frattura, il test dia il medesimo risultato. Il valore predittivo positivo ci dice la probabilità che

un paziente ad alto rischio di frattura sia effettivamente ad alto rischio di frattura, mentre il valore positivo negativo ci dice la probabilità che un a basso rischio di frattura sia effettivamente basso rischio di frattura. La sensitività, la specificità, il valore predittivo positivo e negativo sono stati rispettivamente 100%, 93%, 78% e 100%. I valori ottenuti con il modello standard sono stati rispettivamente 100%, 74%, 39% e 100%. Tra le segmentazioni automatiche, i risultati più simili alla segmentazione manuale sono derivati dal modello implementato con la segmentazione automatica 1xx. Anche in questa segmentazione, è presente solo un falso positivo. Escluso questo paziente, la differenza tra il più alto BOS score dei veri positivi ed il più basso dei pazienti tra i veri negativi è uguale a 0,6 (Figura 7a). Nelle segmentazioni 1xx-2xx e AD, ugualmente, un solo falso positivo è presente (Figura 7c e Figura 7d). Seguendo il ragionamento precedente, in questo caso la differenza tra i BOS score, escluso quel paziente è pari a 0,45 e 0,31 rispettivamente per 1xx-2xx e AD. Infine, nella segmentazione automatica 2xx sono stati rilevati due falsi positivi ed esclusi entrambi la differenza tra i due insiemi è di 0,43 (Figura 7b).
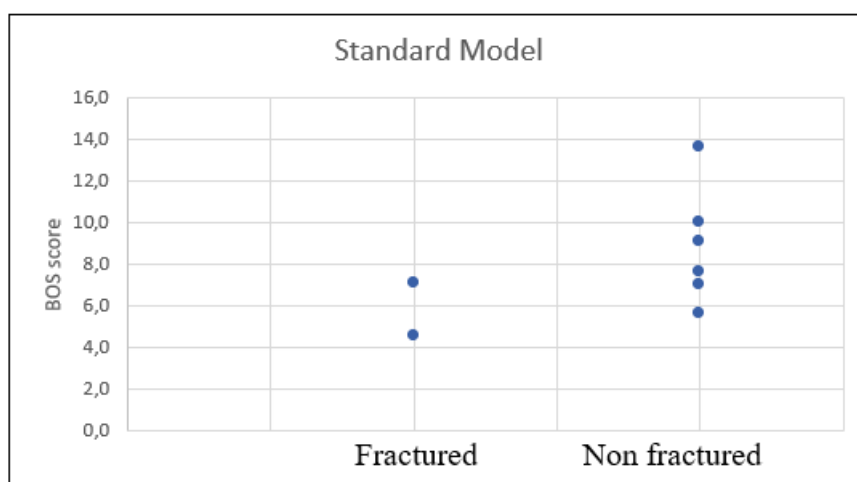

Figura 4: BOS scores del modello standard.
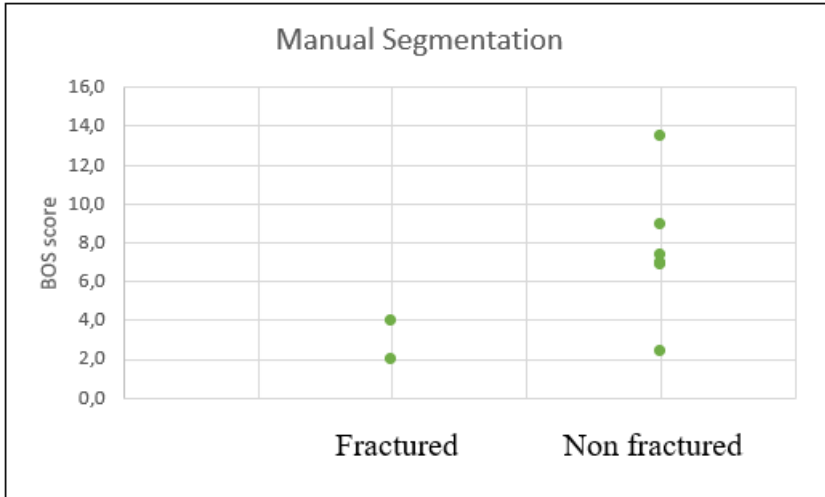
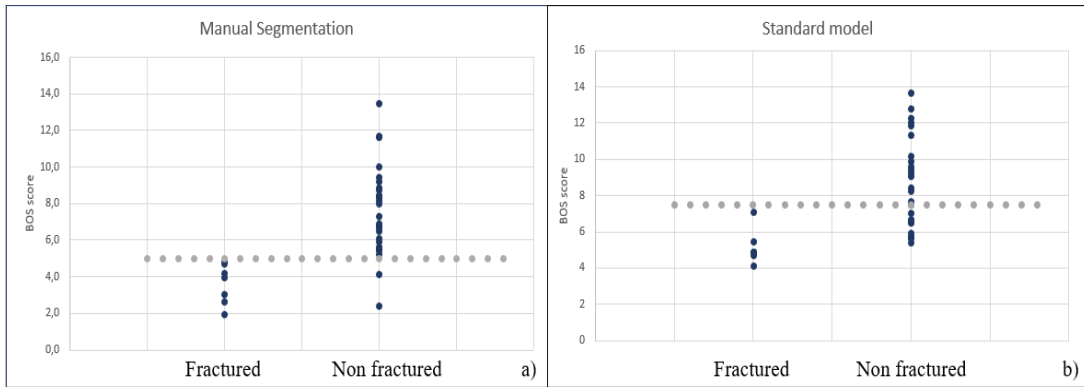**Figura 5:** BOS scores del modello ad elementi finiti modificato con la segmentazione manuale.

Figura 6: a) BOS scores ottenuti dal modello modificato con la segmnentazione manuale b) BOS scores ottenuti dal modello standard.
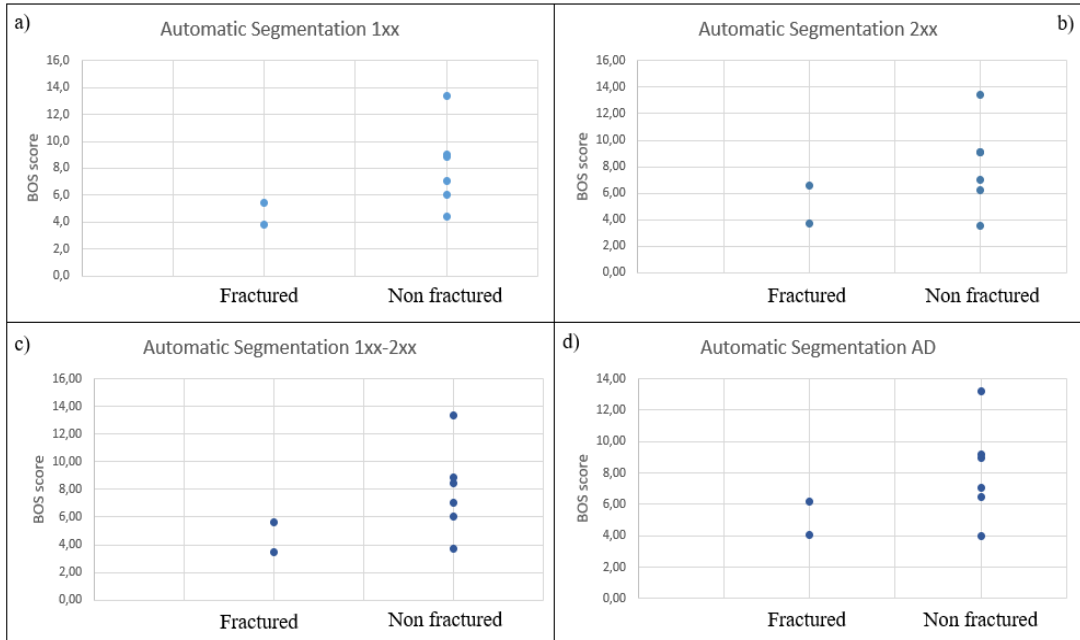
Figura 7: BOS scores del modello ad elementi finiti implementato con le segmentazioni automatiche.

Analizzando la relazione tra la media di densità ossea e la differenza in percentuale tra i carichi di fallimento, si evidenzia un andamento leggermente crescente: la differenza aumenta leggermente all'aumentare della media di densità ossea.

Una tendenza simile è stata osservata analizzando la relazione tra il volume delle metastasi e la differenza in percentuale dei carichi di fallimento.

Figura 8: La variazione della differenza in percentuale dei carichi di fallimento rispetto alla BMD media. Da sinistra a destra e dall'alto in basso c'è la relazione della segmentazione manuale, della segmentazione automatica 1xx, della segmentazione automatica 2xx, della segmentazione automatica 1xx-2xx, della segmentazione automatica AD.
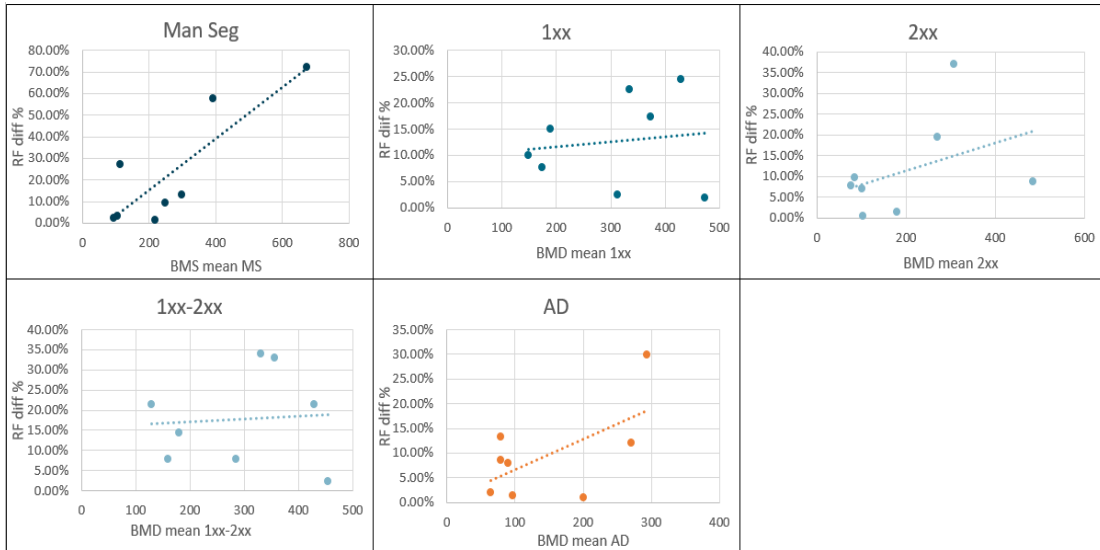

Figura 9: La variazione della differenza in percentuale dei carichi di fallimento rispetto al volume delle metastasi. Da sinistra a destra e dall'alto in basso c'è la relazione della segmentazione manuale, della segmentazione automatica 1xx, della segmentazione automatica 2xx, della segmentazione automatica 1xx-2xx, della segmentazione automatica AD.
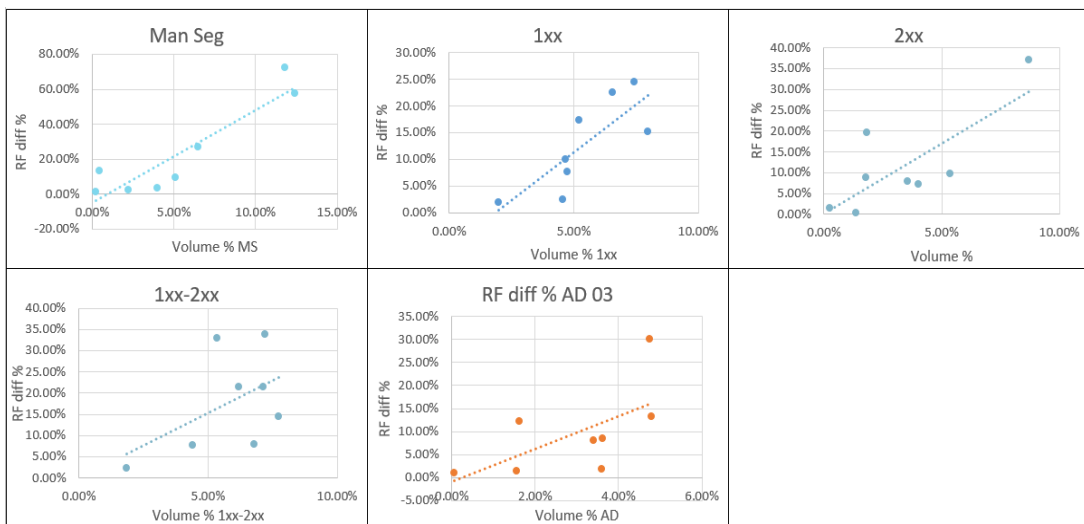
- le metastasi blastiche

Nei femori blastici, il paziente K352L ha mostrato l'andamento aspettato (Figura 10f). Questo paziente presenta lesioni metastatiche molto ampie e diffuse su tutto il femore. Il paziente 1151R ha mostrato un andamento simile quando la riduzione del modulo di Young è stata superiore al 60% (Figura 10c). In entrambi i casi la differenza tra le forze di reazione ha mostrato un aumento più netto quando il modulo di Young veniva ridotto per valori superiori al 60%. Negli altri femori, non è stato possibile definire alcuna relazione tra il modello standard e quello modificato (Figura 10a-b-d-e).
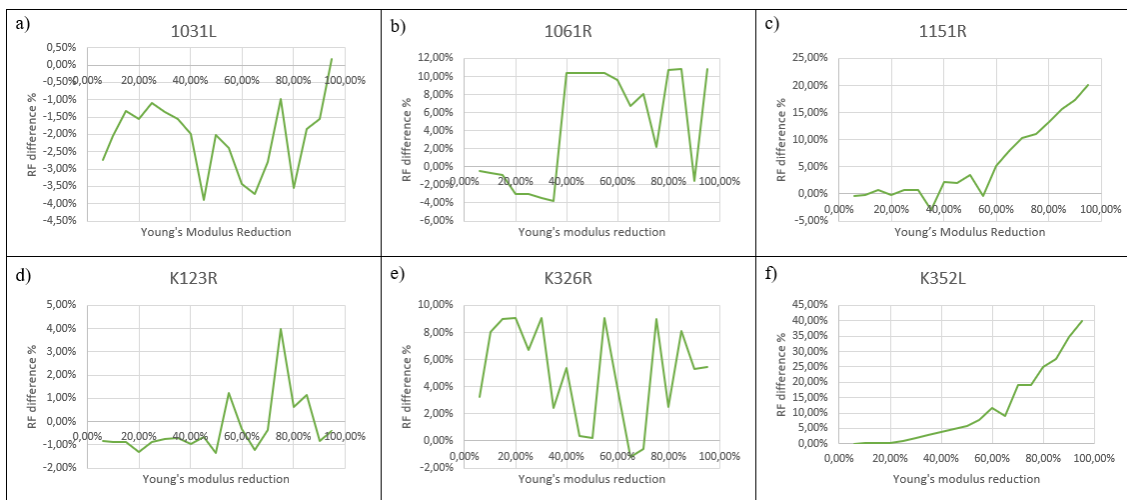
Figura 10: Relazione tra la riduzione del modulo di Young e la differenza tra le forze di reazione per tutti e sei i pazienti analizzati.

4. Discussione

In questa trattazione si sono utilizzati entrambi gli strumenti: la tecnica degli elementi finiti ed il deep learning. L'obiettivo di questo lavoro è stato quello di verificare, nei pazienti con una prevalenza di metastasi litiche, se l'implementazione delle segmentazioni modifichi la classifica dei carichi di fallimento, se con l'implementazione delle segmentazioni vi è stato un miglioramento nell'affidabilità del fattore di rischio e se la segmentazione manuale e quella automatica portino a risultati simili. Nei pazienti con metastasi prevalentemente blastiche l'obiettivo, invece, è stato quello di trovare un modo per implementare le proprietà meccaniche.

È stato rilevato che la modifica delle proprietà meccaniche ha variato maggiormente i modelli implementati con la segmentazione manuale rispetto a quelli implementati con le segmentazioni automatiche. Questo risulta evidente nei risultati della classifica dei carichi di fallimento. Nella segmentazione manuale, infatti, un elevato numero di pazienti modifica la loro posizione rispetto al modello standard.

Il confronto del coefficiente di Dice con la differenza nei carichi di fallimento tra le segmentazioni automatiche e la segmentazione manuale hanno mostrato dei risultati inaspettati. La segmentazione con il più elevato coefficiente di Dice ha ottenuto i carichi di fallimento più differenti rispetto alla segmentazione manuale. Al contrario, la segmentazione con il coefficiente di Dice più basso è quella che ha ottenuto i carichi di fallimento più simili a quelli della segmentazione manuale. Questo può essere spiegato dal fatto che la differenza nei carichi di fallimento tra i modelli modificati con le segmentazioni ed il modello standard sia dovuta ad una diminuzione delle proprietà meccaniche. Nelle segmentazioni con il coefficiente di Dice più basso, il tessuto osseo sano è stato considerato erroneamente come tessuto metastatico. In questo modo si sono indebolite le proprietà meccaniche dei modelli, ma senza ottenere una corretta mappatura delle metastasi. Per questa ragione, l'obiettivo dell'algoritmo è rimasto quello di ottenere segmentazioni con il coefficiente di Dice più alto possibile.

I BOS scores ottenuti dai modelli implementati con le segmentazioni hanno mostrato un miglioramento nel prevedere la frattura in un paziente rispetto a quelli ottenuti nel modello standard. In particolare, nella segmentazione manuale, la differenza nei BOS scores tra i veri negativi a ed i falsi positivi è la più elevata. Il miglioramento è stato confermato analizzando, con le stesse modalità, un numero di pazienti più elevato. Ottenere un fattore di rischio con il 100% di affidabilità rimane comunque impossibile con questa tecnica, poiché ci sono un numero elevato di fattori che non sono stati presi in considerazione. Un paziente, infatti, potrebbe avere una mobilità ridotta o essere costretto a letto a causa della malattia e dato che le fratture avvengono svolgendo attività quotidiane, i pazienti analizzati potrebbero non essere in grado di compierle. Un altro fattore, che non è stato considerato, è l'aspettativa di vita, alcuni pazienti sono deceduti poco dopo la raccolta delle immagini QCT, prima che la frattura potesse svilupparsi. In questo caso, anche le segmentazioni automatiche sembrano migliorare l'affidabilità dell'indice di rischio, ma non quanto la segmentazione manuale.

Nelle metastasi blastiche, quattro pazienti hanno mostrato un risultato che è stato contrario alle aspettative. La causa può essere dovuta al fatto che questi pazienti avevano lesioni molto ridotte, dove la modifica del loro modulo di Young ha comportato un piccolo cambiamento delle proprietà del materiale. Il risultato anomalo può essere dovuto al fatto che la simulazione è incrementale. Ciò ha portato al fatto che la frattura è avvenuta in un incremento leggermente diverso rispetto a quella del modello non modificato e quindi ottenendo un carico di fallimento leggermente diverso. Questo non implica, comunque, che il femore sia leggermente più debole o più forte ma i risultati possono essere dovuti a piccoli errori numerici verificatisi durante la simulazione. Quindi, il carico di fallimento nei pazienti blastici viene influenzato solamente quando si sono diminuire le proprietà meccaniche in femori con lesioni diffuse.

Lo studio ha dei punti di forza. Per prima cosa, la combinazione della tecnica degli elementi finiti e quella di deep learning propone un metodo oggettivo nell'ottenere l'indice di rischio. Per seconda cosa, vi è l'assenza di differenze tra i QCT-scanner, dovuta alla presenza del phantom di calibrazione. Questo studio ha, inoltre, delle limitazioni. Innanzitutto, il ridotto numero di pazienti inclusi nello studio. L'analisi della classifica e dei BOS scores sarebbe stata più completa con un numero di pazienti più elevato per le segmentazioni automatiche. Per questi motivi sono stati programmati studi su un campione più ampio per il futuro. Un altro aspetto da considerare è che ci possano essere casi di sensitività della mesh principalmente dovuta alla fase di diminuzione dello stress ed all'aumentare della deformazione. La dimensione della mesh, in questo caso, è stata scelta dopo un'analisi di sensitività della stessa in modo da ridurre il più possibile la differenza tra i modelli. Infine, non ci sono dati sullo stato di salute del paziente, dunque non è stato possibile integrare questi dati nello studio (allettato o meno, la sua aspettativa di vita ecc.). Questo ha portato all'impossibilità di dare un'interpretazione più precisa ai dati ottenuti.

5. Conclusione

La combinazione del modello ad elementi finiti specifico per il paziente con il deep learning sono uno strumento che potenzialmente riesce a migliorare la predizione e l'affidabilità del fattore di rischio. Sono comunque necessarie ulteriori analisi su un

numero di pazienti più elevato, in modo da avere un risultato ed un'analisi più completa ed affidabile. In futuro la combinazione di queste due tecniche potrebbe avere un ruolo molto importante nell'aiutare i medici ed i pazienti a decidere il trattamento più appropriato per le metastasi ossee nel femore.

Per le metastasi blastiche di piccole dimensioni, l'analisi ha mostrato che le modifiche alle proprietà dei materiali hanno un effetto marginale sulle forze di reazione, mentre per le metastasi di grandi dimensioni vi è un'influenza importante. Come implementare le proprietà dei materiali per le lesioni blastiche dovrà essere sviluppato in futuro.

Summary

Abstract

The purpose of this work is to determine if patient-specific finite element models (FEM) with adapted material properties in the lesions segmented by a deep learning metastatic or a manual segmentation are better at assessing fracture risk for femoral bone metastasis compared to the original patient-specific FEMs. Additionally, we aimed to find a way to adapt the material properties of the blastic metastasis in the FEMs to diminish the overestimation of the strength in these femurs.

Material properties of eight lytic patients and six blastic patients were adapted based on five segmentations and one manual segmentation respectively. Patient-specific FEMs were constructed based on the geometry and the bone density obtained from the baseline CT scans used for radiotherapy planning. The analysis of the lytic patients consisted in the calculation of the Dice coefficients (DC), the BOne strength (BOS) score (the reaction force (RF) normalized by body weights) and the ranking of the RFs. Since the BOS scores obtained by the FEMs modified with the manual segmentation were very promising, a larger number of patients (33) was tested and the diagnostic accuracy values (sensitivity, specificity and positive (PPV) and negative predictive values (NPV)) were calculated. For the blastic metastasis, the relation between the reduction in Young's modulus and the difference in RF between the standard and the modified model was determined, expecting a progressive decreasing of the reaction force of the femurs.

The automatic segmentation that the most like the manual segmentation had a DC equal to 64.43%. The manual segmentation had a completely different ranking in comparison to the standard FEM, whereas the ranking of all the automatic segmentations were very similar to the standard FEM. The automatic segmentations showed an improvement on the assessment on the fracture risk but not as good as the manual segmentations. The sensitivity, the specificity, the PPV and the NPV obtained studying 33 patients were

respectively 100%, 93%, 78% and 100%, whereas the values obtained by using the standard FEM were respectively 100%, 74%, 39% and 100%. For the blastic metastasis only two out of six patients showed the expected trend. This can be explained by the fact that these two patients had large lesions spread throughout the femurs, whereas in the other four femurs the metastatic lesions were small and had less effect on the strength of the femur.

The patient-specific FEMs combine with the manual segmentation improved the fracture risk assessments of femoral bone metastasis in cancer patients compared to the original patient-specific FEM. However, to reach the same goal with the automatic segmentations the algorithm must be improved. In the blastic metastasis, decreasing the material properties in the FEM only influenced the RF if the patient had larger metastatic lesions.

1.Introduction

Cancer is a disease that affects a large number of patients. In 2017, more than 100.000 patients were diagnosed with cancer in the Netherlands [1]. Worldwide in 2012, 20 million new cases were registered, and the incidence is increasing [2].

Bone is the third most common tissue affected with metastases [3]. In case of bone metastasis, the bone remodeling process is distorted [4]. There are two different kinds of metastatic lesions: lytic lesions, which are caused by an excessive activity of osteoclasts, and blastic lesions, which are caused by an excessive proliferation of osteoblastic cells. Excessive activity of osteoclast cells cause resorption of bone, whereas excessive production of osteoblasts cause formation of bone but without the correct architectural structure [5]. This leads to the weakening of the bone. Patients can also have metastases classified as mixed when both types of lesions are present [6]. Since cancer cells travel through the blood and then cause metastases, they are often seen in the most vascularized part of the skeleton, i.e., the axial skeleton and in the proximal ends of the long bones [7]. Bone metastases are very painful, and the most prevalent symptoms are four as poor sense of well-being, fatigue, pain and drowsiness [8]. These symptoms are detected in more than 80% of the patients [8]. However, the worst complication of metastatic bone disease are the pathological fractures. Fractures of long bones occur in approximately 10% of patients with bone metastases [9] and cause impaired mobility and a reduced quality of

life. Additionally, pathological fractures have shown to have a significant bad impact on survival [10]. The surgical treatment after such fractures is very complex with the risk of many complications. Depend on the type of surgery complications can be systemic such as lung embolism or liver failure, due to infections or surgical such as breaking of a nail or a fracture next to the implant [11].

For these reasons, it is very important to prevent a fracture of the femur in patients with bone metastases. The kind of treatment is based on the fracture risk of the femur [12] [13]. If the patient has a high fracture risk, the subject will undergo surgery. However, if the patient is unable to undergo surgery, for example because of limited condition, or refuses to undergo surgery the subject will be treated with multiple fractions of radiotherapy. If the patient has a low fracture risk, the subject will be treated with a single fraction of radiotherapy [13]. The radiotherapy is very helpful because most patients declare to have pain relief [14]. Additionally, radiotherapy is said to reduce the risk of fracture by inducing remineralization of bone [14].

Since one of the factors the treatment plans are based on is the fracture risk, it is important that the fracture risk assessment is reliable. There are several guidelines that are currently used to assess the fracture risk. In the Netherlands the current method to estimate the fracture risk is by using conventional radiographs [13]. If there is an axial involvement greater than 30 mm, the patient is classified as high risk [14]. However, this method is not perfect, it has been demonstrated that only 23% of the high-risk femur will develop a fracture.[14] This often leads to overtreatment which affects the health of the patient and raises an economic burden. This can also lead to undertreatment when the patients are classified as low-risk of fracture, but they undergo to a fracture.

The goal of many research groups is to improve the reliability of the fracture risk assessment. For this, a very important tool is patient-specific finite element (FE) modeling. FE models have been shown to be very promising for femurs affected with lytic lesions [15] [16] [17] [18].

The blastic metastasis have a higher density on CT scans, but the bone has an insufficient architectural structure and therefore a reduced strength. However, in finite element models this higher density leads to an overestimation of the mechanical properties in FE model, resulting in an overestimation of the bone strength and the RF [17]. Many researchers tried to give an answer on how to implement the mechanical properties of

blastic metastases in the FE models but the results that come out are conflicting. Kaneko et al. showed that quantitative computer tomography (QCT) can provide an accurate and precise estimate of the ash density (ρ_{ash}) also in metastatic bone [19] [20]. For that reason, they used QCT images to compute the material properties of the femur. The ash density is very important because it can be used to estimate the mechanical properties of the bone. Kaneko et al. found a strong relationship between the Young's modulus and the ash density, between the yield and the ultimate strength and the ash density, and between the QCT density and the ash density [19] [20]. In the work of Hipp et al. they analyzed the mechanical properties of metastases in trabecular bone of vertebrae by testing the specimens to failure in uniaxial compression [21]. The results showed that there was not a substantial difference in strength between lytic and blastic regions, despite of their difference in density. Also, the Young's moduli of lytic and blastic metastases were similar and both lower than in healthy bone. The principal limitations of Hipp's study are that many specimens contained a mixed composition of lytic and blastic lesions and that they came from only two patients [21]. In Stadelmann et al., vertebral bone metastasis has been tested [22]. In this case the results highlighted those lytic and mixed metastases had an indentation modulus (E_{it}), which is the Young's modulus obtained by nanoindentation tests, very similar to the intact bone. The indentation modulus is the Young's modulus obtained by nanoindentation measurements, very similar to intact bone, whereas blastic metastases had an indentation modulus lower than 5.8% [22].

To enable adaptation of material properties of blastic lesions in FE models, the metastases need to be indicated exactly. For this, a deep learning algorithm can be used to detect metastasis.

Deep neural networks use training sets to be able to recognize the abnormalities (in our case bone metastases), and test sets to evaluate the performance of the training. Training sets are usually obtained by manual segmentation, which is considered as golden standard. The quality of the segmentations as well as the size of the training set are of the most important contributing factors in the neural network training. Methods to segment the metastasis were used in the past to detect lytic metastasis [23] and blastic metastasis [24]. In our case, the output of the deep learning algorithm would be an automatic segmentation of both lytic and blastic metastases.

In this work, we combined the FE and lesions segmentations obtained by the deep learning. In previous works, patient-specific FE models were tested for patients with lytic metastasis without the use of the lesion segmentations [16] [17]. The patients with predominantly blastic metastases were excluded because of the overestimation of the strength of femurs affected by blastic metastases [26]. The aim of this work was to check if the implementation of the lesion segmentations modified the ranking between of the strength determined by the FE models, if there is an improvement on the assessment of the fracture risk and if the manual segmentations and the automatic segmentations were similar in terms of topography and results. For the patients affected with blastic metastases, the aim was to determine a way to adapt the material properties of the bone, without obtain the overestimation of the strength of the femurs.

2. Methods

- Patient and CT scans

Eight patients with lytic metastasis were included in this study (mean age: 64.75 years, range: 55-88; 5 males, 3 females) and six patients with blastic metastasis (mean age: 73.67 years, range: 59-95; 5 males, 1 female). The patients analyzed had multiple myeloma tumor, breast, lung, prostate and kidney cancer. Every patient underwent to QCT. A solid calibration phantom containing four known calcium equivalent densities (50, 100, 150, 200 $\frac{mg}{cm^3}$) was scanned along with the patient at the level of the proximal femur. The QCT had the following settings: 120 kVp, 220 mA, slice thickness of 3 mm, pitch 1.5, spiral and standard reconstruction, in-plane resolution 0.9375 mm.

- Finite element model

The patient-specific finite element models (Figure 1a) were generated from the QCT images. These images were used to segment the femur resulting to a 3D surface mesh using Mimics (version 11.0 and 14.0, Materialise, Leuven, Belgium) which was converted to a solid mesh of tetrahedral elements (Marc Mentat). The Hounsfield units of the CT scan were used to determine the patient specific material properties. A mean

diaphyseal slice calibration was performed to convert the Hounsfield units (HU) to calcium equivalent densities, which was a measure of bone mineral density. The bone mineral density of each element was written in a calcium file that was specific for each patient [17]. The calcium equivalent densities were used to calculate the ash densities and the isotropic non-linear material properties of the bone [25].

The material behavior was implemented as non-linear isotropic where the post-failure material behavior for each element was represented by an initial perfectly plasticity phase, followed by a strain softening phase and finally an indefinite perfectly plastic phase [25]. For the FE models a cup was placed on the head of the femur and the model was distally fixed at the knee joint center by two bundles of high-stiffness ($2 \cdot 10^8 \frac{N}{m}$) springs (Figure 11a). This alignment was chosen to mimic the stance position [16] [17].
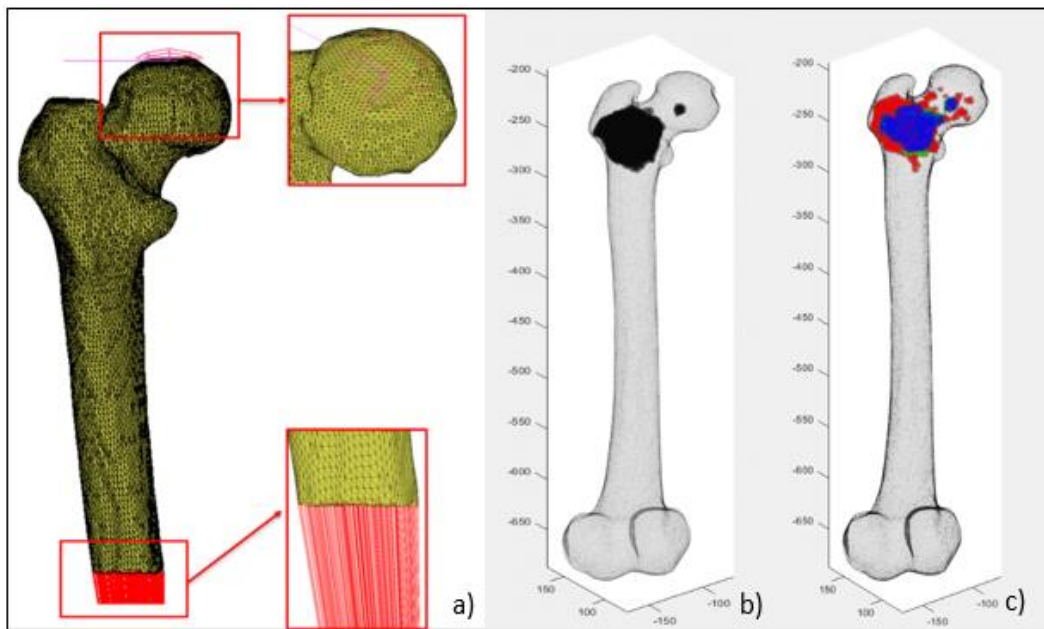
Figure 11: (a) An example of the patient specific finite element model with the boundary conditions. (b) A representation of the combination of the finite element model and the lesion segmentation. (c) A representation of the comparison between one of the automatic segmentations and the manual lesions segmentation. In blue the elements that were identified as metastases by both the segmentations are shown, in red the elements only detected by the manual segmentation and in green the elements only detected by the automatic segmentation.

During the simulation, the model was loaded by displacing the cup on the head of the femur in the axial direction. The goal was to bring the femur to fracture. Failure was

reached when the force displacement curve (Figure 12a; Figure 12b) had a clear peak or when the simulation did not converge any further. The result was the RF of the femur. The RF was corrected for the body weight, resulting in the Bone Strength score (BOS score). The BOS score can be used to classify the femur high-risk or low risk of fracture [17].
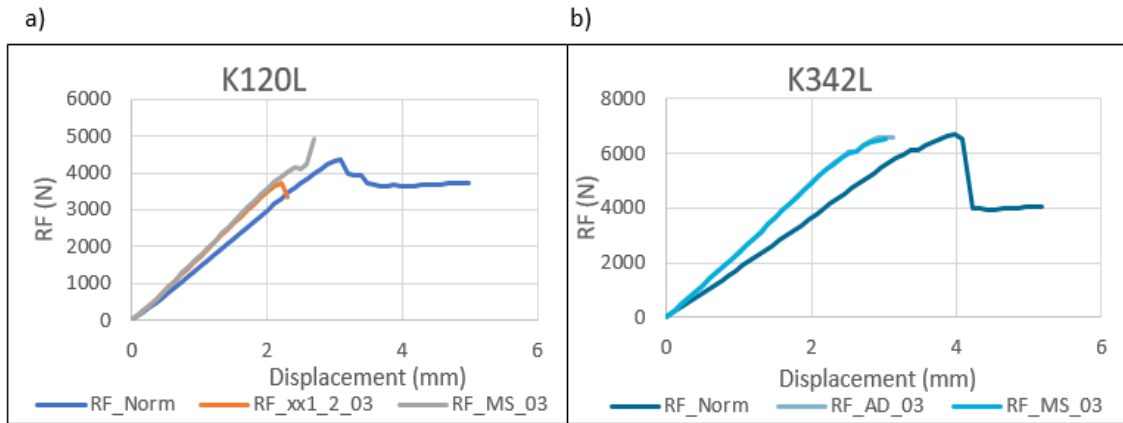

Figure 12: Two examples of the force displacement curve of two patient (K120L (a) and K342L (b)) of two segmentations (AD and 1xx-2xx). RF_Norm was the force displacement curve obtained by the standard FE simulation. The RF_AD_03 was the force displacement curve obtained by model implemented with the AD segmentation. The RF_MS_03 was the force displacement curve obtained by model implemented with the manual segmentation. The RF_xx1_2_03 was the force displacement curve obtained by model implemented with the 1xx_2xx segmentation.

- The deep learning algorithm

To detect the lytic metastasis, several different lesion segmentations were done for all 8 patients (Figure 1b): one manual segmentation and four automatic segmentations. The deep learning segmentations (also called automatic segmentation) were trained having a set of training images (manual segmentation) which in this study had been considered as golden standard. The segmentation obtained by training the deep learning algorithm with lytic metastasis was named "1xx". The segmentation obtained by training the deep learning algorithm using slices with lytic metastatic lesion and slices without any metastasis lytic was named "2xx". The segmentation obtained by a combination of the previous two was named "1xx-2xx". The segmentation obtained by training the deep learning algorithm with both lytic and blastic metastasis was named "all dataset" (AD).

With a Matlab script, the BMD (or calcium equivalent values) of the elements containing the metastases were set to 0.

Based on the segmentations, the material properties of the FE models were modified, resulting in the modified FE models. For this, in a Matlab script, the BMD of the elements containing the metastases were set to 0. The original FE model, without any adaptations in material properties, was defined as the standard model.

To detect the blastic metastasis the AD segmentation was used. To reduce the Young's modulus, we changed the bone mineral density in our finite element model, because from that the ash density was calculated and from that the elastic modulus was computed. A Matlab's script that determined the reduction of the bone mineral density in the exact amount to reduce the Young's modulus from 5.8% to 95% in 5% steps was written. This operation was carried on for each femur to understand which the right percentage was to decrease the Young's modulus to correct for the overestimation of the strength of the blastic tissue in the FE model.

- Analysis

To determine if the modified model for lytic metastasis improved the calculation of the fracture risk of the patients, several output values were analyzed. The DC was used to compare the automatic segmentations to the manual segmentation. The difference between the RF of the standard model and the RF of each modified model was determined relative to the RF of the standard model. The difference in RFs were compared between the different lesion segmentations (manual and automatic). Moreover, the mean BMD of the metastatic elements and the percentage of metastatic elements with respect to all the elements were calculated.

Furthermore, the RFs of the standard models and the modified models were ranked, and the difference in ranking was analyzed. It was determined whether there was a relation between the DC and the difference in RF. Six months after the CT scan, the patients were divided in a fracture set and in a non-fracture set. Next, the BOS score was calculated to assess any changes in the prediction of the fracture risk between the different models. To verify that the difference was not only due to weakening of the material properties of the FE model, the relationship between the bone mineral density of the metastatic elements

and the difference in RF, and between the volume of metastatic elements and the difference in RF were investigated.

For the blastic metastasis, a relation between the Young's modulus reduction and the difference in reaction force between the standard and the modified model was searched. We hypnotize that the reducing the Young's modulus, would increase the difference in reaction force.

3. Results

- Lytic metastasis

The DC of the four automatic segmentations showed that the automatic segmentation 2xx was the most like manual segmentation. The mean DC of all the patients for this segmentation was 64.43%, whereas the DC of 1xx, 1xx-2xx and AD were 49.67%, 39.17% and 57.02%, respectively.

The AD segmentation had the lowest mean difference in RF (9.83%). The mean difference in RF between the manual segmentation and the standard model was the highest (24.41%) of all the segmentations. The mean difference in RF of the 1xx-2xx segmentation was closest to the manual segmentation (11.98%). The difference in RFs in comparison to the manual segmentations were 14.88%, 17.79% and 16.89%, respectively (Table 2).

		RF diff % AS_MS 00 mean
		03
Segmentations	1xx	14.88%
	2xx	17.79%
	1xx-2xx	11.98%
	All Dataset	16.89%

Table 2: Difference between the automatic segmentations and the manual segmentation in terms of RF. The segmentation 1xx was obtained from the network trained only by the slices with lytic metastasis. The segmentation 2xx was obtained from the network trained by the slices with and without lytic metastasis. The segmentation 1xx-2xx was a combination of the previous two

segmentations. The segmentation All Dataset was obtained from the network trained by the slices with lytic and blastic metastasis.

In the ranking analysis, the RFs of the eight patients were ranked from the lowest to the highest. The ranking of the manual segmentation was the one that differed most the standard model (Figure 13a). In the ranking of the three automatic segmentations (Figure 3c; Figure 13d; Figure 13e) just two RFs close to each other were switched. The ranking of the segmentations 1xx (Figure 13b) matched the ranking of the standard FE model perfectly.
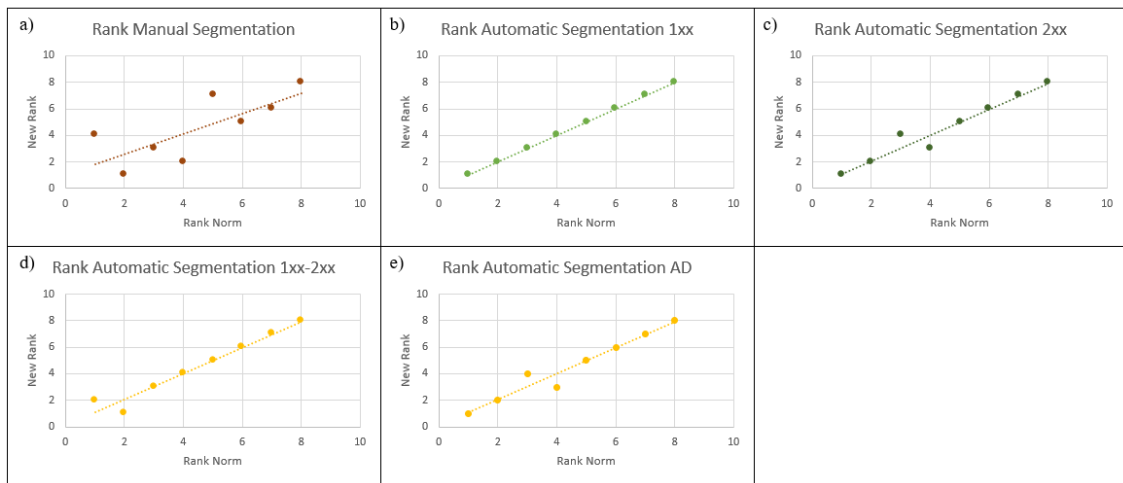
Figure 13: The ranking of the RFs obtained with the standard FE model (x-axis) compared with the ranking of the modified FE models (y-axis) for (a) the manual segmentation, (b) the automatic segmentation 1xx, (c) the automatic segmentation 2xx, (d) the automatic segmentation 1xx-2xx, (e) the automatic segmentation AD.

No relationship was found between the DC and the difference in RF. The results differed largely between the various segmentations. For segmentation the manual segmentation and 1xx, there seemed to be a trend showing an increase of the reaction for difference percentage with the increase of the DC. For segmentation AD and 2xx the trend seemed to show a decrease of the reaction for difference percentage with the increase of the DC. For the segmentation 1xx-2xx, there seemed to be a steady trend. As said previously, a clear correlation was no clear in any simulation.

Additionally, the BOS scores for each patient were determined. For the standard model, there were two false positives (Figure 14). In the standard model, the threshold was set to 7.5. Since the lesion segmentations were implemented, the BOS scores decreased

massively, the threshold was set to the highest BOS score values in the fracture set. The BOS scores obtained by the manual segmentation models showed that only one false positive was present. Not considering him, the difference between the highest true positive and the lowest true negative was 2.8 (Figure 15). Since the results were promising, we decided to extend the analysis to 33 patients (Figure 16). The sensitivity, the specificity, the positive (PPV) and the negative predictive (NPV) value were respectively 100%, 93%, 78% and 100%. The values obtained using only the FE model were respectively 100%, 74%, 39% and 100%. Among the automatic segmentations, the BOS scores results of automatic segmentation 1xx were closest to the results of the manual segmentations. In this segmentation, there was just one false positive. Excluding this patient, the gap between the highest true positive and the true negative equal to 0.6 (Figure 17a). Also, in the segmentations 1xx-2xx and AD only one false positive. In these cases, excluding these patients, the difference in BOS scores were 0.45 and 0.31 for the 1xx-2xx (Figure 17c) and the AD (Figure 17d), respectively. In the automatic segmentation 2xx, two false positives were present and the difference in BOS scores, excluding these two patients was 0.43 (Figure 17b).
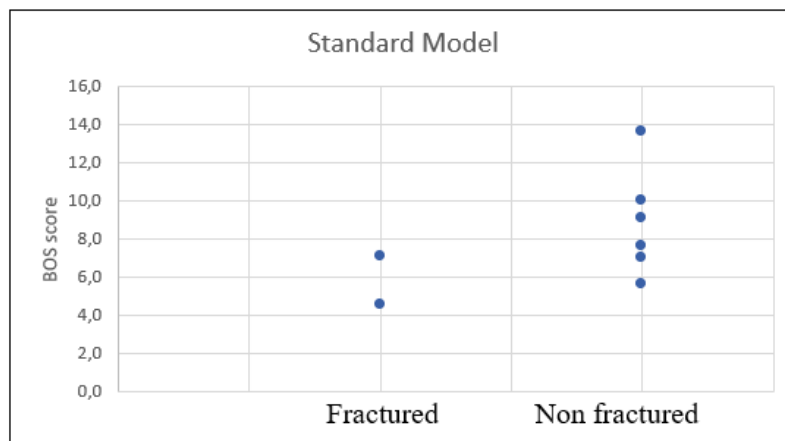
Figure 14: B0S score of the standard FE model.

Figure 15: BOS scores of the FE model modified based on the manual segmentation.

Figure 16: a) BOS scores obtained by the model with the manual segmentations, b) BOS scores obtained by the standard model.
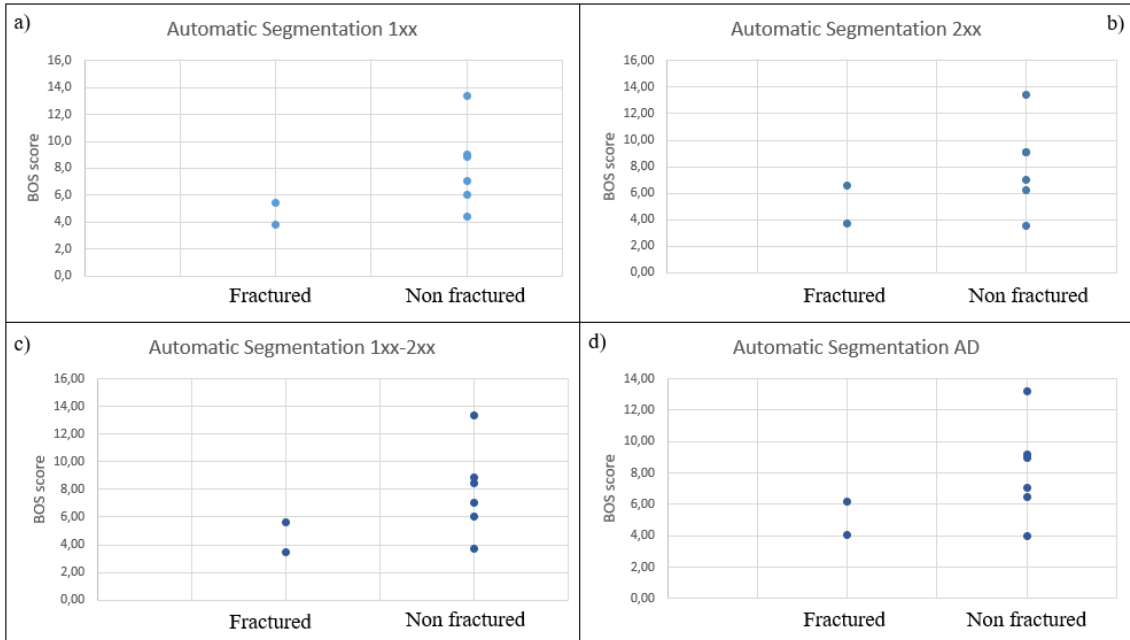
Figure 17: BOS score of the FE models modifies based on automatic segmentation 1xx (a), 2xx (b), 1xx-2xx (c) and AD (d) respectively.

There was a slight trend showing an increase in difference in RF percentage when the mean BMD increased in all the segmentations. A similar trend was seen between the difference in RF and the percentage of metastatic elements in all the segmentations.
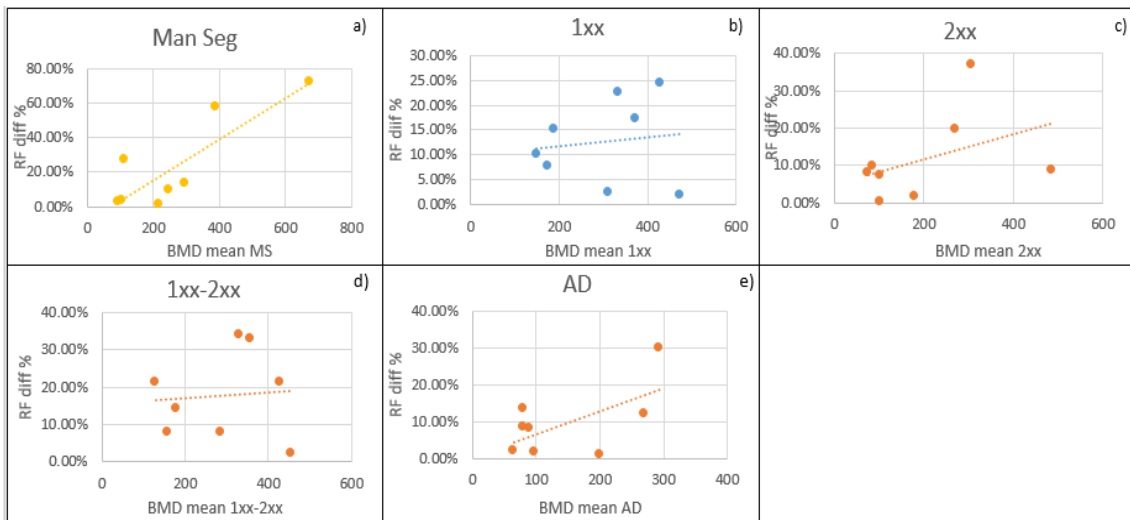
Figure 18: The mean BMD With respect to the difference in RF obtained from the FE models modified based on the manual segmentation (a), automatic segmentation 1xx (b), automatic segmentation 2xx (c), automatic segmentation 1xx-2xx (d), automatic segmentation AD (e) respectively.
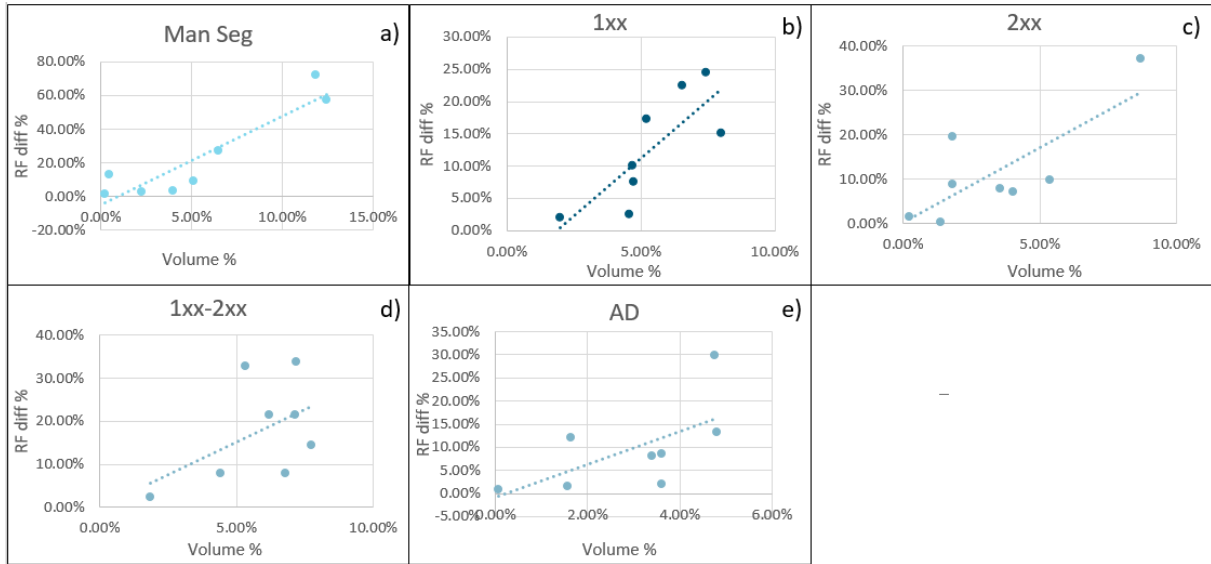
Figure 19: The volume percentage of the elements set to zero with respect to the difference in RF percentage of the RFs obtained from the manual segmentation models of the manual segmentation (a), automatic segmentation 1xx (b), automatic segmentation 2xx (c), automatic segmentation 1xx-2xx (d), automatic segmentation AD (e).

- Blastic metastasis

In the blastic femurs, patient K352L mostly showed the trend we expected (Figure 20f). This patient had large metastatic lesions spread throughout the femur. Patient 1151R showed a similar behavior when the reduction of the Young's modulus was lower than 60% of the original Young's modulus (Figure 20c). In both cases the difference in reaction force showed a large increase when the Young's modulus was lower than 60% of the original Young's modulus. In the other femur, there was no a clear trend between the reduction of the Young's modulus and the difference in reaction force between the standard and the modified model (Figure 20a; Figure 20b; Figure 20d; Figure 20e).
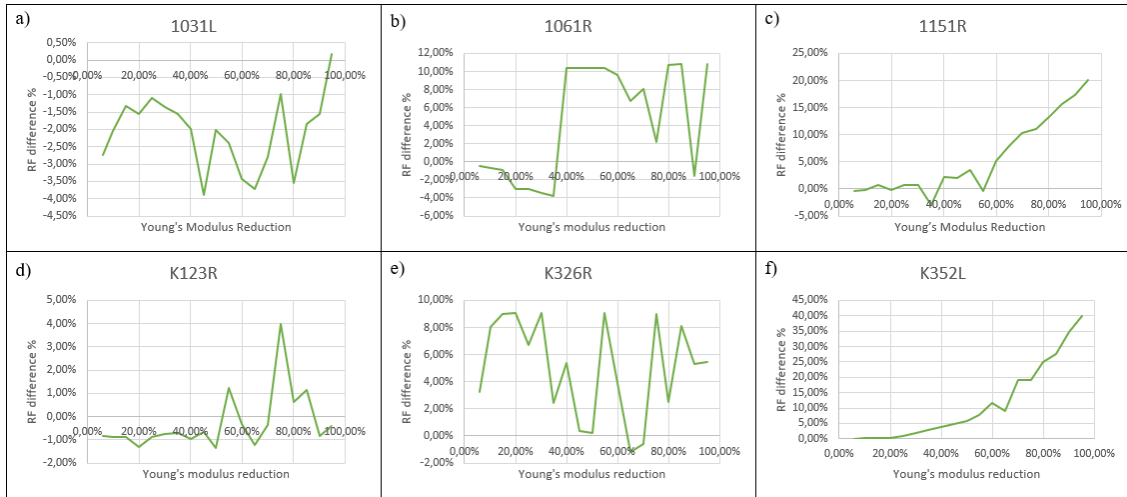
Figure 20: Relation between the reduction of the Young's modulus for the six patients.

4. Discussion

In this work, we aimed to combine the FE and the deep learning algorithm tool to check if the implementation of the lesion segmentations modified the ranking between of the strength determined by the FE models and if the manual segmentations and the automatic segmentations were similar in terms of topography and results. For the patients affected with blastic metastases, the aim was to determine a way to adapt the material properties of the bone which prevents overestimation of the bone strength.

The impact of the segmentations on the material properties was greater in the manual segmentation models than the automatic segmentations models. This became clear from the ranking of the RFs, where in the manual lesion's segmentation, more patients changed their positions. However, this did not happen in the automatic lesion's segmentations, where the ranking was barely modified the material properties with respect to the standard model.

The DCs and the difference in the RFs between the manual and the automatic segmentations showed an inconsistency. The segmentations with the highest DC was also the one that obtained the results that differed most from the manual segmentations. This worked also in the opposite way: the segmentations with the lowest DC were the ones with RFs more like the manual segmentation. This can be explained by the fact that the difference in RFs was due to a weakening of the material properties since the BMD of the metastatic elements was set to zero. So, if in the segmentation considered wrongly some

healthy as metastatic tissue, the result was a weakening of the material properties of healthy bone but a low DC. This leaded to obtain more similar results in the segmentation that have lower DC. For these reasons, The aim remained to obtain an automatic lesion segmentation with a DC as high as possible.

Furthermore, the BOS scores obtained by all FE models modified by manual or automatic segmentations seemed to improve in comparison to the BOS scores obtained by the standard model. In the manual segmentation the gap between the fracture set and the non-fracture set was largest except for one patient. This trend was confirmed from the analysis of a larger number of patients. However, to obtain a 100% reliability was impossible because there were too many factors that were not considered. For instance, patients could be less active or even bedridden due to pain, and since the fractures usually happened during daily activity, these patients possibly did not load their femurs enough to develop a fracture. Another factor was that some patients died after the QCT scan before they could develop a fracture. In this case, also the automatic segmentations results improved the results of the standard model, even if the results were not as good as in the manual segmentation.

In the blastic femurs, four patients showed a trend that was not expected. The cause could be these femurs had metastatic lesions that were not large. This led slight changes in the material properties, but apparently not enough to get the outcome as we expected. This could be due to the fact the simulation was incremental, which could lead to the fracture occurring in a slightly different increment, resulting in a slightly different reaction force. However, this does not necessarily mean that the femur was indeed slightly weaker or stronger but could also be due to a small numerical error during the simulation. So, decreasing the material properties of the blastic metastases in the finite element model only influenced the reaction force if the patient had larger metastatic lesions.

The strength of this study is that the combination of the FE method and the deep learning is an objective method on the prediction of the fracture risk. A second strength is the absence of inter-scanner differences due to the presence of a phantom scanned with the patient. This means that the human error is going to be reduced with this method. This study had also some limitations. First, the low number of lytic-patients included. The ranking of RFs and the BOS scores would have been more complete with a higher number of patients. For these reasons further studies to a larger sample were planned. Second, a

mesh sensitivity can occur due to the use of a strain softening material. This size was selected after a mesh sensitivity analysis and then was maintained to reduce as much as possible the difference between the bones. Thirdly, there is no data of the quality of life of the patients. There is no information if the patients were bedridden or die immediately after the QCT-scan. This leads to the impossibility to give an interpretation the data obtained. For instance, the patient that was wrongly predicted from the manual segmentation may live longer or engage in activities which would bring its leg to fracture.

5. Conclusion

The combination of the patient-specific FE model with deep learning algorithms to detect bone metastases and subsequently adapt material properties of the metastases, was a potential tool that can improve the reliability of the fracture risk prediction. The results showed an improvement on the fracture risk assessment if the model was modified with the manual segmentations. For the automatic segmentations the improvement seemed less clear and the algorithm needed to be improved. However, further analysis in a larger patient population should be carried out, to verify if the models in which lesions are manually segmented are a real improvement on the prediction of the fracture risk. In the future, the combination of these tools may have a very important role to help clinicians and patients to choose the most appropriate treatment for femoral bone metastases.

For small blastic lesions, the analysis showed that they have a small effect on the RF, whereas larger blastic lesions apparently do influence the RF. How to adapt the material properties of the blastic lesions to enable to calculate reliable RFs needs to be researched in the future.

Chapter 1:

Anatomy, disease and treatment of the metastatic femur

General excursus on anatomy, disease and treatments
of metastatic femur and the method current used

1.1 Anatomy of the femur

The femur is a bone with many particularities. It is the only bone of the tight and it is the longest bone of the body. To describe its anatomy, it is usually divided in three parts, which are the proximal, the distal and the shaft.

The proximal part is the one that articulates with the pelvis to form the hip joint. The main component of the proximal part are the head of the femur, the neck and two bony processes, which are called the greater and the lesser trochanters. There are two bony ridges that put in contact these two trochanters, called the intertrochanteric line anteriorly and the trochanteric crest posteriorly. The head has a smooth surface and covered by cartilage tissue except for a small part, called fovea, where the ligamentum teres attaches. The neck is the part that connects the femoral head with the shaft. It has a cylindrical shape had it forms an angle of around 135 degrees with the shaft. This angle allows to have a wider range of movement. The greater trochanter is the most lateral palpable projection of the femur. From this bony process many muscles develop. The most important muscles that use the great trochanter as site of attachment are the gluteus region and the vastus lateralis. Also, the lesser trochanter, despite of it is smaller than the greater trochanter has many muscles that develop from this site of attachment. The most important is the iliopsoas. There is also the intertrochanteric line, that after it is passing the lesser trochanter is also known as the pectineal line. The intertrochanteric line is a site of attachment of the iliofemoral ligament, which is the strongest ligament of the hip joint and for the joint capsule.
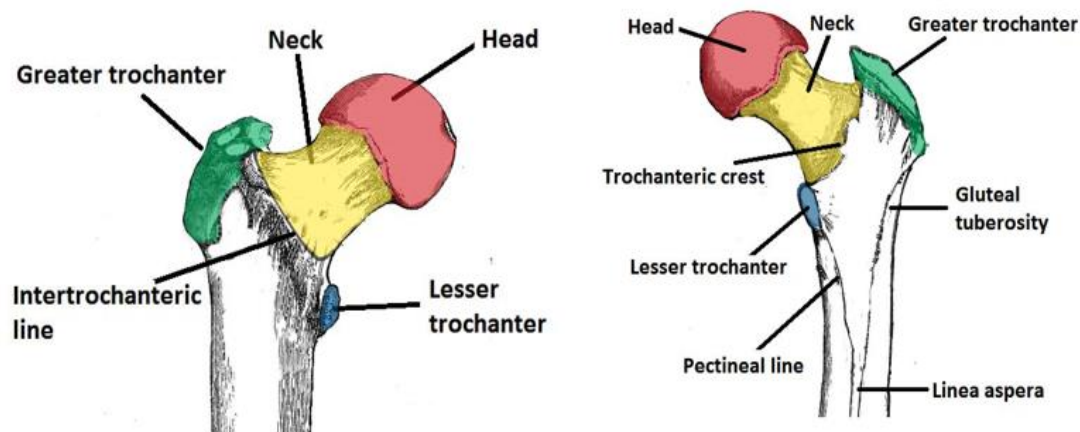
Figure 1.1: The representation of upper part of the femur. The head of the femur is the part that articulated with the iliac bone forming the hip. In yellow the neck that is the part that connect the head with the rest of the femur. In green and in blue the greater and the lesser trochanter, respectively.

The second part is the shaft. This part descends to the knee into a slight medial direction. Its cross section is almost circular: the posterior part is slightly flattened. In the posterior part some roughened ridges are present, called the linea aspera. This ridge split in the distal part of the shaft, and it will form the medial and the lateral condyle. In the proximal part of the shaft, the medial border of the linea aspera became the pectineal line and the distal part become the gluteal tuberosity. It is in this point where the gluteus maximum attaches. In the end, distally, the linea aspera became wider and it going to form the popliteal fossa.

The distal part of the femur is characterized by the presence of the medial and the lateral condyle. They are covered by a layer of cartilage tissue, and they are going to form the knee joint, articulating with the tibia and the patella. In this part, the medial and the lateral epicondyles are present, that are bony elevations situated on the non-articular areas of the condyles. The medial and the collateral ligaments have, respectively, these site of attachment. In the end, there is the intercondylar fossa. It is a deep notch on the posterior surface of the femur that places between the two condyles. It contains two facets where the anterior cruciate ligament and the posterior cruciate ligament can attach respectively.
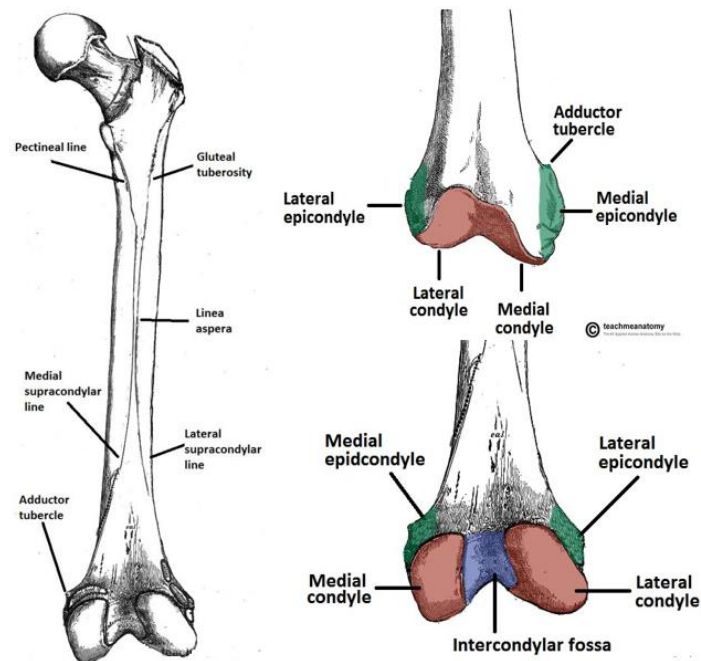
Figure 1: The most important anatomic part in the shaft. The frontal view of the distal part of the femur where the condyle and the epicondyle are highlighted in red and in green respectively. The back view of the distal part of the femur where the condyle and the epicondyle are highlighted in red and in green respectively and the intercondylar fossa which is represented in blue.

1.2 Bone metastasis

The metastasize process have many factors involved: the loss of intercellular cohesion, the cell migration, the angiogenesis, the access to systemic circulation, the evasion of local immune response and the growth in different organs [27]. Cancers of the breast, prostate, lung, kidney, and thyroid can metastasize to bone [28]. These metastases can cause pain and, when left untreated, carry a risk of developing complications such as pathological fractures or, in case of vertebral metastases, spinal cord compression [29]. Cancer is a disease that affects a huge number of patients. In fact, in 2017 more than 100.000 patients were diagnosed with the cancer in the Netherlands [26].

1.2.1 The bone

The bone is a unique organ of the body. Its main function is to provide support to the body and to protect the most important organs, like the cerebrum, the spinal cord, the

heart and the lungs. The bone has other jobs as the regulation the level of calcium in blood [30].

There are two different type of bone that is the cortical bone and the trabecular bone [31]. The cortical bone has a higher density and commonly it is placed in the outer layers. Approximately, at this typology of bone correspond the 80% of the bone mass [31]. Trabecular bone has a large surface exposed to the bone marrow and blood flow, and the turnover is higher than in cortical bone [32].

In the skeleton, the bones are also classified for their shape: the long bones, the short bones, the flat bones and the irregular bones [33]. Short bones have a shape that can be approximated to a cube. Usually, they can be found in the wrist or in the ankle. Flat bones are plates of bone that usually have a curvy shape. Some examples of this typology are the skull, the mandible. The irregular bone, instead, do not have a uniform shape. In the end, the long bone has a shape that excess in one dimension with respect the other two. This type of bones supports the limbs of the body [5].

Since the bone is extremely metabolic active, it is constantly in a remodeled process. This remodeling is due to three typologies of cells, that are the osteocytes, the osteoblasts and the osteoclasts [34]. The osteoblasts have the role of mineralization and synthetization of new bone tissue. The osteoclasts, instead, are the responsible for the bone reabsorption process [5]. In the end, the osteocytes, that are the greater percentage of the cells in the bones, are the ones that detect the mechanical force and stresses that the bones receives, and they regulate the activity of the absorption or the mineralization of the bone [35]. For a healthy bone is necessary that the mineralization process and the reabsorption process are strictly balanced. The essence of this phenomenon is repetitive, with consequent reconstruction of bone matrix.

1.2.2 The bone metastases characteristic

The equilibrium between osteoblasts and osteocytes can be broken in particular situations, as infections, chronic inflammations or cancer. The bone tissue is favorable for the growing and develop of the metastatic cells [4]. For this reason, a high percentage of metastases develop in the bone. In particular, the osteoblasts and the osteoclasts, that are the cells of the bone responsible on remodeling, have a very important role on the develop of the metastases [5]. These metastases, after their seedings in the bone, are going to grow

until they arrive to cause macroscopic lesions. This is due to a massive colonization of bone by the tumor cells. The result is a quality of life impaired [36].

This colonization can be described in three stages: early disease, disease progression and advanced stage. In the early stage, the tumor cells that enter the bone can be considered, mainly, as a single cells. Due to the very few spaces they occupy, they would be probably undetectable by the technology's method. Cancer cell dormancy could also occur. In the second stage, the disease progression, these cells will colonize the bone and they are going to occupy always more room. Patients can undergo to treatments able to reduce the speed of the colonization of the tumor cells. However, in the end, macro lesions will form in the patients. Patients may have various symptoms as severe bone pain, hypercalcemia or bone fracture [5].

It has been estimated that a patient with breast cancer out of three will develop metastasis [37] and these metastases are bone metastasis in the 15% of the case [38]. If the bone metastasis derives from a breast cancer, they are predominantly osteolytic [39]. The formation of the lytic metastasis is because the bone resorption happens to a higher rate with respect to the bone deposition. This is since the osteoblasts located close to the cell cancers undergo to apoptosis. This means that the number of osteoblasts in that part of the bone is decreased [5]. This leads to the bone resorption. Usually, these kinds of patients are treated with drugs that have the goal to reduce the osteoclasts action. Also, biphosphate therapies that alter the osteoclast formation are used like denosumab, ibandronate [40], and zoledronic acid [41]. This is not a heal for the patients, but it is just a postponing.

Multiple myeloma cancer metastasizes the bone very often [42]. Also, in this case the metastasis that are going to develop are predominately lytic [43]. For the prostate cancer, instead, the metastasis that usually develop can be either lytic, mixed and blastic, but the blastic lesions happens in most of the cases [44]. These kinds of lesions, in CT-scan images and X-rays images, appears as zone with a higher density [45]. However, this does not mean that the strength of the bone is increased. In fact, there is no more an organized matrix because the bone layers are misalignment. This means that the bone will have a spongeous structure instead of a compact one. The consequences are a reduced bone strength the overall bone function impaired [46].

All this situation has something in common. In fact, in all the cases the strict balance between the bone formation and bone resorption in altered. This leads to a vicious cycle. When the metastasis starts to colonize the bone, it alters in a very light way the balance between growing and resorption of the bone. The tumor cells, indeed, connects with the osteoblast and the pre-osteoclasts cells. With these connections they can alter the equilibrium and they can proliferate. This leads to more tumoral cells in the bone that can alter the growing-resorption balance with greater action [5].
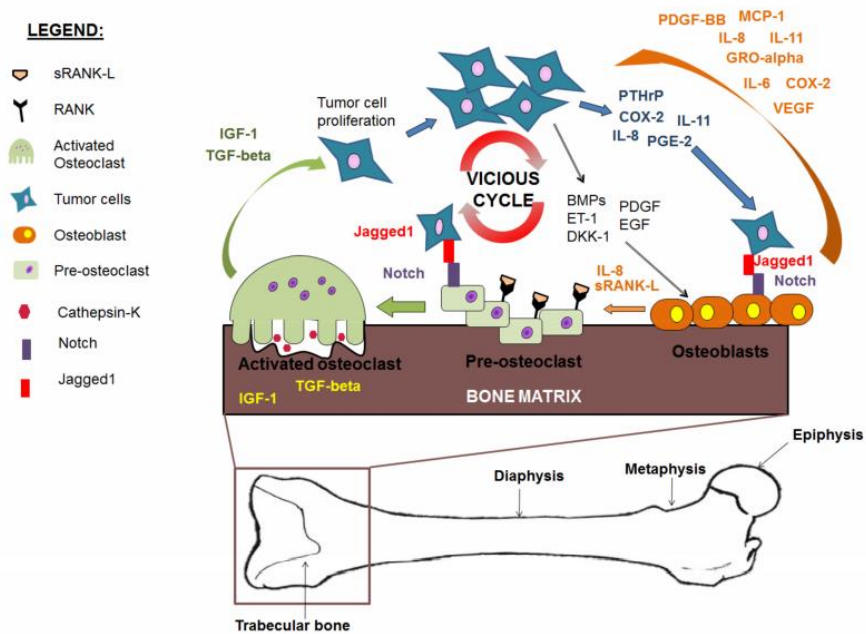
Figure 2: Representation of the vicious cycle

1.2.3 The clinical aspects

The mean time left for a patient who develop the bone metastasis is 20 months [47]. However, this factor depends principally on two factors: the performance status of the patient and the tumor from where the metastasis came from. In prostate cancer, if the patient is in a good performance status and if the bone disease affects predominately the axial skeleton, the time left to the patient increases up to 53 months. However, if the patient is in a good performance status but with visceral disease, this time decreases to 30 months. If the patient has a bad performance status and visceral disease, the patient has 12 months of life expectancy [48].

One of the most complication of bone metastasis is the hypercalcemia [49]. The hypercalcemia is a metabolic disease that if it is not treated properly can lead to cardiac arrhythmias and acute renal failure [50].

In patients with bone metastasis, pathologic fractures occur in the 30% of the cases. This pathologic fracture happens in the proximal parts of the long bones in more than 50% of the cases [28]. The second and the third most common sites are the ribs and the vertebrae [51]. The most impending consequence is the spreading of the tumor into the spinal cord [50]. The first aspect that the patient complain is the pain. However, the patient has some difficult to localize it and it is usually worst at night. The inhibition of the bone reabsorption thanks to specific drugs as bisphosphonates and denosumab leads to the reducing of the pain [52]. In the worst-case scenario (the spreading of the tumor in the spinal cord), the diagnosis must be fast. The treatment is based on a high dose of corticosteroids, a rapid assessment and an urgent referral for both decompression and spinal stabilization. The compression must be solved within two days, otherwise the neurological recovery will be complicated [49].

When a patient complains these symptoms, a protocol must be performed. The data analyzed regards the blood (looking for anemia or hypercalcemia) and imaging data [53]. The imaging data can be collected in various ways that have their pros and their drawbacks. Bone scintigraphy is highly sensitivity, but it has also characterized by a low specificity. The fastest and cheapest method available are radiographs [3]. The radiographs are very specific, but they have a low sensitivity. Metastasis smaller than one centimeter may not be detected. Moreover, the medullary lesions in cortical bone are very difficult to be detected [54]. Osteolytic metastasis hole appears as a darker hole in the bone, meanwhile osteoblastic metastasis appears as a whiter area. The sensitivity of the CT-scan is high [55] and for this reason is highly used for the localization of lesions for biopsy [53]. A very interesting tool is the positron emission tomography that it can detect the presence of the tumor studying the metabolic activity of the patient.

1.2.4 The medical treatments

Several parameters can be involved on a medical decision. The doctor usually evaluates the spread of the bone metastasis and if some extra skeletal metastases are detected in the

patient. The kind of cancer is also a parameter that must be kept into account as the treatment history of the patient, the disease response, the symptoms and the general state of health [49]. However, all the treatments known up to now, do not solve the problem, they impair the spreading of the metastasis.

The standard treatment for this typology of patients is bisphosphonates. They are effective in reducing hypercalcemia [56]. The bisphosphonates are usually well tolerated. The most common contraindication symptoms are flu-like symptoms, anemia, nausea and peripheral edema. However, it is extremely rare that these pathologies affect the patients with hard symptoms [28]. The most serious symptoms that can occur to the patient is the osteonecrosis of the jaw. However, this symptom is very rare. A patient with renal impairment should not receive the treatment because the bisphosphonates undergo to renal clearance [57]. The bisphosphonates work hampering the vicious cycle and they may stimulate innate antitumor mechanism, so to have effector memory-like that can improve the immune system to face against malignant cells [58].

A second solution is the denosumab. The denosumab is a human monoclonal antibody that prevent the develop of osteoclasts. Preventing the developing of osteoclasts, it is possible to delay fractures. Differently from bisphosphonates, denosumab does not accumulate in the bone. This means that its effect can be reversers if the doctors decide, for any reason, to stop the treatment [59]. The side effects of this drug are very similar to the ones of bisphosphonates [60]. As mentioned before, one benefits of denosumab is reversibility, but there are other benefits. Indeed, this drug can be used in patient who had renal failure because its clearance it is independent of renal function [61]. However, drawbacks are also present. An increased infection rate has been found in osteoporotic patients [62], a worse survival percentage have been seen in patients affected with multiple myeloma [63] and it is more expensive.

A third treatment is the external radiotherapy which seems to be very helpful for localized metastatic bone pain. [64] A positive side of this technique is that the pain relief is quick, in 1-2 weeks [53]. Doctors can prescribe this kind of therapy in three typologies: local-field radiation, wide-field radiation and radionuclide. The treatment that usually doctors prescribe is the local-field radiation therapy. This treatment has a very high pain relief rate [65]. The wide-field radiation therapy is prescribed when bone metastases are really spread or to have an extra-action to the local-field radiation [66]. In the end, the

radionuclide therapy uses radioisotopes to remove the pain [49]. They are most effective for a patient that have prevalently blastic metastasis [67].

A fourth technique is ablation. The ablation is a medical procedure that consists in inducing heat, cold or a chemical agent into the tumor using a needle. The most common ablation is the one called radiofrequency ablation where an electric current is used to destroy the cancer cells. The main said effect of radiofrequency ablation is the impossibility to visualize the ablation margins through a CT-monitoring. This is possible, instead with cryoablation. This is not the only advantage of cryoablation, in fact the patient does not feel an increased pain during the treatment and in the immediate post-operative period [68]. The complications rate that can derive from this kind of treatment is low, however neurologic injuries, neuropathic pain and infection have been reported [69]. Another treatment is the surgery, but the doctors consider that only when there is a fracture of long bones or if it involves a spinal cord compression [30].

The bone metastases have an important impact on patient's quality of life. New strategies are necessary to reduce as much as possible diseases for the patients. To do that a multidisciplinary approach is necessary.

Chapter 2:

The finite element tool and the deep learning in bone metastasis

General excursus on the techniques used in the literature for metastatic bone and an introduction of the machine learning algorithms

2.1 The fracture risk

Long bones are the most common sites affected by metastasis [70]. Usually, if metastatic tissue develop on of a segment of a long bone, it induces a regional mechanical weakening, that leads on a reduction of the overall strength of the bone. Being the femur a load-bearing bone, it has a higher risk of fracture in case of segmental involvement and loss of bone integrity than other long bones. When a pathologic fracture occurs, it leads to a reduced life quality of patients, that have already a limited life expectancy. It is very important to predict correctly the probability that a patient, affected by bone metastasis, will have a pathological fracture. This probability is called fracture risk. Clinicians calculate the fracture risk of the patient and divide them in high-risk patients and low risk patients. Depending on the fracture risk, the treatment changes.

Usually, the most suitable treatment consists in a preventive prophylactic surgery and/or in conservative treatments, as radiation therapy [71]. Patients with an expected low fracture risk are treated with radiotherapy, usually a single fraction of 8 Gy, to relieve pain, whereas patients with an expected high fracture risk are considered firstly for preventive stabilizing surgery. In case of an expected high fracture risk and the refusing by the patient to undergo surgery, radiotherapy in multiple fractions will be given, with the goal to prevent a pathological fracture by inducing remineralization [13].

The current assessment of the fracture risk assessment does not have a high accuracy. There are two methods currently used to predict the fracture risk. In the Netherlands, if lesions with an axial cortical involvement 30mm were found, the risk of fracture is estimated at 23%. The patient is classified as a high-risk patient and he has to undergo to a prophylactic surgery. However, this system leads to overtreatment and so a patient does not necessitate a surgery will undergo to that. This is uncomfortable for the patient and it is also a waste of resources for the hospital [13].

The second one is the Mirels' system. Mirels' system classifies the risk of pathologic fractures related to many features as metastatic bone disease, pain, location and size of the lesions. Clinicians assign to these feature a progressive score ranging from 1 to 3. These scores are then summed and if the patients have a score above 8 are at high fracture risk and usually, they must undergo to surgery. This classification has been shown to be reproducible, valid and more sensitive than clinical judgment [72]. However, it's a low

specificity method that may result in unnecessary surgery in two thirds of the patients [71]. So, in both case we have many patients that will undergo to a prevent surgery without the real necessity.

2.2 The finite element tool

It is necessary find methods that can improve the reliability of the prediction of the fracture risk. A very important tool that can improve the reliability of the fracture risk it is the finite element model [73].

In the literature, there are many examples of the use of this tool to predict the fracture risk. In Eggermont et al. [16] [17] there is the construction of the patient-specific finite element model based on the CT-scan images. The CT-scan images and the phantom allow to obtain the geometry and the bone density. To convert from the grey values to the calcium equivalent densities, ash density and non-linear isotropic material behavior a slice calibration have been performed. The material model of Keyak et al. [25] have been used. In this material model, the post failure material behavior is constituted by three phases for each element. The first phase consists of a perfectly plasticity behave, the second phase on a strain softening behave and the third phase on an indefinite perfectly plastic behave. The finite element model was loaded by a cup that hits the femur in the axial direction. The femur was fixed in distally position (at the knee joint) by two bundles of high-stiffness springs. From the force displacement curve the reaction force have been extrapolated. This finite element model was validated with experimental tests [15]. The fracture risk was computed mediating the reaction force by the body weight. The fracture risk is calculated normalizing the reaction force with the body weight. A threshold where set to 7.5 x body weight. If the patient was below this threshold it is classified as a high fracture risk patient. It was proved that the finite element model tool calculate with more reliability the fracture risk then expert clinician and the Mirels' score [16] [17].

In the Sternheim et al., [74] [75] the topic has been treated in a different way. Their aim was also to evaluate how the CT-based finite element analysis can be used to accurately predict the strength in metastatic femur. To do that they performed the analysis to fifty patients. The patients were divided in two groups. The first group was composed by the patients that have already developed a fracture. To create the finite element model, it was

necessary to manipulate the CT- images and inhomogeneous isotropic material properties were assigned to all points within the femur based on the HU. In the FE model, a load used to mimic the stance position was applied on the femoral head. The load was directed along the line which connected the center of the femoral head and the intercondylar region. The median tensile or compressive principal strain was calculated in four regions of the femur. These regions where the neck, the proximal shaft, the middle shaft and the distal shaft. The fracture risk was given by the typical strain fold ration. The typical strain fold ratio was the ration between the absolute maximum principal strain obtained close to the metastasis area and the typical median strain in the same anatomical femur. A second feature named contralateral strain fold ration was also evaluated. This feature was obtained by the division of the maximum tensile and compressive strains in the vicinity of the tumor and the strain in the contralateral disease-free femur of the same region. [76] In the end, studying the group 1, the researcher evaluated a threshold of strain fold ratio. This threshold was used to classify the patients as high-risk of fracture or low risk of fracture. They analyzed that almost the half of the patient (44%) that were indicated for prophylactic surgery were classified as a low risk. However, this study has several limitations. In fact, selection bias can be present, the strain fold ratio have been calculated basing only on five patients, the study control was composed only by patients that declined surgery and CT scan were not optimized to finite element analysis.

However, a limitation of the finite element model is that there was the involving of a lot of manual work since the use of specific software and engineering knowledge are necessary [18]. For this reason, a voxels-based mesh models was analyzed. The voxels mesh model resulted more affordable for everyone and can be generate in less time and in a simpler way. The drawback is that the mesh is more jagged, and some sensitivities points can be generated. However, the results on the calculation of the yield results similar for the two meshes in microscale models [77]. Made these premise the aim of this work was to reduce the difference between the results of the tetrahedral and voxels approaches on a macroscale level. To validate this model, the data obtained from the tests made in Derikx et Al. were used [18]. In this case, linear cubical voxels that were converted in hexahedral mesh were used. The Hounsfield unit were converted into bone mineral density with the use of a calibration phantom as a reference. A nonlinear isotropic material behavior was defined [15]. During the compression test in the simulation, when the bone

enter in the plastic phase, the Young's modulus changed. This means that an adaptation of the Young's moduli was required. To do that, a step size was set considering the accuracy of the results and the computational time. Decreasing the step size leaded to a results more accurate but also more computational effort [15]. The results show a very good correspondence in the force-displacement curve except for a small overshot placed in the passage from the elastic to the plastic behavior. However, this overshoot decreased with the reduction of the step size [18].

In the Falcinelli et al. [76] a female patient with lytic metastasis in the femur was analyzed using the finite element tool. The model was reconstructed using the CT images and the metastasis were segmented manually. The mesh is constituted by a second order tetrahedral element. In this paper the bone is treated as a biphasic material where there is a fluid present in the porous matrix, [78] the local stress are assumed partially distributed between the solid phase and the liquid phase [79]. The failure mechanism was assumed as strain based, but to have a comparison also a stress based failure mechanism was computed. To do that, the maximum principal strain criterion and the maximum principal stress criterion were assumed. Then, when the failure criterion was satisfied, a local constitution degradation of the bone was implemented. To arrive at these results, the stiffness tensor was reduced. The simulation was performed with a quasi-static displacement-driven incremental approach. The load was applied with the displacement of a surface on the top of the femur. The femur was fully constrained in the distal part. During the simulation, the values of displacements, stresses and strains were computed. Then at every step, the model verified if the failure conditions were reached or not. If they are not reached, the values of displacements, stresses and strains were updated to each element. If they are reached the material properties for those elements followed the degradation rule. The simulation stopped when the procedure did not converge any further. In that case, the maximum reaction force values were extrapolated, and it was considered the reaction force of the femur.

Another paper that proved the great utility of the CT-scan finite element method tool on the prediction of the fracture risk is the Kawabata et al. [23] In this case, 14 elements were analyzed. The mesh was constituted by two typology of elements that were a tetrahedral element for the trabecular bone and the inner cortical bone and a shell element (with a thickness of 0.4) for the outer surface. Also in this case, the mechanical property of the

model was detected starting from the CT density value and obtaining the bone mineral density values through the equations of Keyak et al [25]. The model was loaded until the fracture occurred and next, the reaction force was computed and mediated by body weight. The threshold between a high-risk patient and a low risk patient was set to 7 times the body weight because this is the force that the femur must bear during the sit-to-stand daily activity.

2.3 The convolutional neural network

A convolutional neural network, or CNN, is a deep learning neural network designed for processing structured arrays of data such as images. Convolutional neural networks are widely used in computer vision and have become the state of the art for many visual applications such as image classification, and have also found success in natural language processing for text classification.

2.3.1 The convolutional neural network on detecting bone metastasis

In the literature the convolutional neural network has been used for detecting both lytic and blastic (or sclerotic) bone metastases. The reason why this technique is becoming always more important is that the radiologist images are becoming more complex. A tool that can improve the radiologist reading efficiency and so helps with diagnosis is the computer aided detection and diagnosis [23]. This tool can be used also for the detection of the bone metastasis. In Yao et al. [23] the detection focuses on the axial skeleton that is the most common place where metastasis can develop [80]. To reach goal, the first step was to identify the spine. To do that a thresholding operation was performed. Since the study analyzed lytic bone metastasis, the vertebrae had holes in the bone. To close those holes, a mathematical morphology operation was conducted. Next, it was necessary to separate the bone from the spinal canal, which is characterized by a lower by a low-density region. To do that, a watershed algorithm was used [81]. However, this problem leads to an over segmentation. This problem was partially solved merging neighboring basins [23]. The final step was to segment the vertebrae. This means to extract the bone

and separate it from the surrounding structures. To reach this aim, the vertebrae was considered as the sum of four parts: vertebral body, spinous process, right transverse process and left transverse process. The detection of the metastasis is evaluated by 26 different features that can be grouped in three categories: location, shape and density. The metastasis appears as a low-density region which is surrounded by a high density bone tissue. In the end, there was a control points to reduce the number of false positives. The results obtained proved a very high sensitivity of the algorithm on the detection on metastasis. However, a number of false positives was present. Their source was due to four different cases: veins, disk volume averaging, osteopenia and some surveys were outside the vertebrae bone.

A study that focusses on the detection of the blastic metastasis in CT-scan images with the use of the convolutional neural network is the Burns et Al. [80] To start, the images in Dicom format were analyzed by three radiologists. A 3D manual segmentation operation was performed for each lesion. Next, a software was used to generate quantitative data starting from the manual segmentations obtained. The quantitative data regards the lesion's location, the lesions volume and the attenuation for comparison with the computer-aided detection. These lesions segmented with the manual segmentation were considered as the golden standard. Also in this case, the first step is the segmentation of the bone part, using a thresholding level of Hounsfield unit. Next, first the spine was divided in 3D vertebral models and then the vertebrae were separated in region of interest. Then, the algorithm (the watershed algorithm) checked the CT-images and, as in the previous paper, it divided the vertebrae in many subregions. Then, there are two merging phases: the merging of two similar subregions in a 2D detections and the merging of the 2D detections in a 3D detection. For each detections a set of 25 features was computed that were used to identify the location and the morphologic characteristic. Next, there is another passage that was used to reduce the false positive as much as possible. Also, in this case the sensitivity was very high and the results really promising. However, a number of false positives was still present also for this typology of metastasis.

2.4 The blastic metastasis in the finite element model

In the literature, the CT-scan finite element model tool on patients who develop bone metastasis is always analyzed on patients that have developed mainly lytic or mixed metastasis. The patients with predominately blastic metastasis are often excluded. This is since in the blastic metastasis there is a bone strength diminished [82]. This is not reelevated by the finite element model, that translates this higher density in an overestimation of the bone strength [26]. One of the first publication that analyzed the mechanical properties of the metastatic tissue was Hipp et al. [21] In this study, the metastatic bone tissue specimens derived from vertebrae was analyzed. These specimens (cubes) were tested along the craniocaudal axis to the 5% strain. From this data, the ultimate stress and the yield stress were calculated. Then, the density of each specimen were determined. The results of the tests showed that all the specimens had a linear region before failure and a define ultimate stress. However, the average moduli for lytic and blastic specimens were not statistically different.

Two other studies that focus on the trabecular bone surrounded by bone metastasis is the Kaneko et al.. In the Kaneko et al., the focus was put on the trabecular bone [19] [20]. To do that the collect three categories of femoral bone samples, the first category was the patient who developed lytic, blastic or mixed metastasis, the second category was from patient who developed cancer but did not develop bone metastasis and the third from healthy patient. First, the QCT density of each sample was computed. Next, the Young's moduli of each sample were calculated with mechanical tests. The mechanical test consisted of a non-destructive test in each anatomical direction. After the testing, the samples were ashed to determine the ash density of the bone. However, the relationship searched between Young's modulus and ash density and between strength and ash density were found but they did not depend on the categories the sample belonged. In Kaneko et al. 2003 the focus was on the cortical bone. The procedures were very similar. The samples were divided on the three categories analyzed before [19]. The feature analyzed showed similar results that did not depend on the categories. A linear relation was present between the QCT density and the compression Young's modulus.

A very recent study on the mechanical properties of the blastic metastasis in the Stadelman et al. [22] The goal of this study was to estimate the effect of the bone

metastasis on the bone structure and to test the capability of the bone mineral content measurements and the standard finite element model on predict the strength of the metastatic bone. In this study, the vertebrae were scan with μCT-scan. The images, after a thresholding operation, were reviewed by three clinicians, so to classify the metastasis as lytic, blastic or mixed. For the experimental part, indentation measurements were performed. The feature of each measurement were the indentation modulus, the elastic, the plastic and the total indentation work. Instead, on the finite element parts, two typology of finite element models were created: a linear μ-FE model and a non-linear homogenized finite element model that reproduced the experimental test conditions. The mechanical test highlighted no difference between the lytic metastasis, the mixed metastases and the healthy bone in terms of indentation modulus and in terms of the ratio of plastic to total work. Instead, for the blastic metastasis, the tissue showed an indentation modulus lower than 5.8% and a ratio of plastic to total work lower than 3.3%. The answer to the second research question was that the variation bone mineral content was moderately associated to the variation to the strength of the material. Also, the μ-FE model, the variation the strength of the material were moderately associated to the variation of the stiffness tensor. In the end in the non-linear homogenized finite element model the predicted strength of the model were strongly associated with the strength of the material.

Chapter 3:
Workflow of the simulation

Description of the combination of the finite element model and the deep learning algorithm

3.1 The finite element model

The workflow of the standard FE model can be described in five steps.

3.1.1 Mimics

The first step was the segmentation. The segmentation was done using the program Mimics (version 11.0 and 14.0, Materialise, Leuven, Belgium). In this program, the CT scan images in Dicom format were imported. Subsequently, a thresholding operation was done to generate a first mask. To make the mask, the voxels with a HU between the threshold 226 and 1926 were selected, to select the bone. Next, the mask was refined to create a mask of only the femur (Figure 3.1).
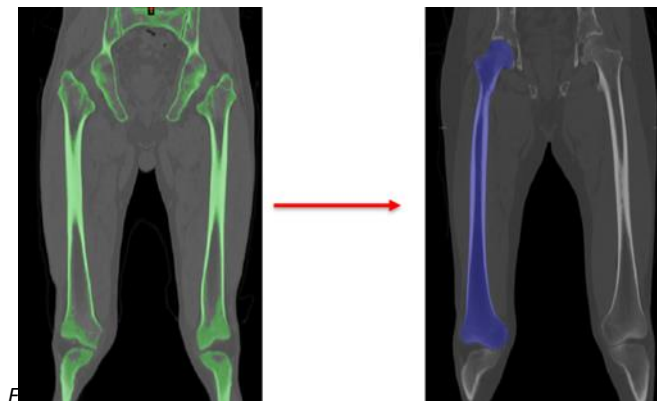
Figure 3.1: On the left: the situation after the first thresholding. On the right the result.

First it was necessary to isolate the femur from the iliac bone and the tibia by erasing the voxels that connect the femur to the pelvis and the tibia. Then all edges of the femur were closed, to create a continue outer surface. The results were the femur voxels and the inner voxels.

Subsequently, a surface mesh was created from the final mask. This 3D object was imported into 3-matic (version 11.0 and 14.0, Materialise, Leuven, Belgium). In this program, the 3D object was smoothed three times, preserving the sharp edges and not preserving the bad edges. In the end, the STL file was exported.

3.1.2 The volume mesh

The file STL was imported in Marc Mentat (MSC.MARC 2007r1 and 2013.1, MSC SoftwareCorporation, Santa Ana, CA, USA), where a volume mesh was created using the Patran mesher, based on the surface mesh previously created (Figure 3.2).
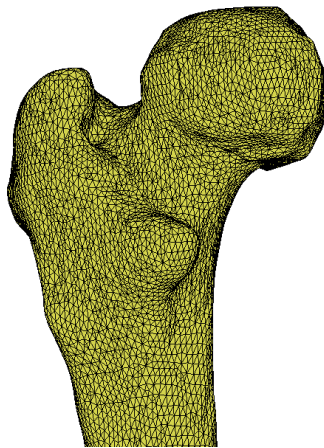
Figure 3.2: The surface mesh.

The volume mesh consisted of linear tetrahedral elements. In the end, the dat file, containing the description of the patient-specific finite element model of the femur, was exported.

3.1.3 The calcium file

Then, a Matlab (Matlab R2020a) script was run with the goal to calibrate the Hounsfield units of the CT scan to bone mineral density, which was later used to assign the material properties to every element. The script calculated a weighted average bone mineral density for each element and it saved these data in the calcium file. To do that the script asked to import the dat file and the CT images. At first, the scripts asked the user to select 9 slices where only the two legs of the patient had to be present. Then, the script asked to indicate the tubes of the phantom that correspond to $200 \frac{mg}{cm^3}$ and $50 \frac{mg}{cm^3}$. Basing on the indication of these two rods, the script calculated the average HU of the other two rods. Then, it calculated the average HU in the 9 slices selected previously. Next, a calibration

function was determined by linearly fitting the HU in the rods to the known of the bone mineral density in the rods. This function was applied to the whole scan to convert the HU to the bone mineral density. In the end, the weighted average bone mineral density for each element was calculated. The result of this script was a calcium file where at each element was assigned its correspondent value of bone mineral density.

The material was modeled with three phases. Until the material reached the yield stress (σ_y) the material was considered as a perfectly elastic. After that point there was a perfectly plastic phase which terminated when a precise strain (ε_{AB}) was reached. This phase was followed by a strain softening phase, with a different Young's modulus with respect to the elastic modulus in the first phase. This phase terminated when a precise stress (σ_{min}) was reached. After that point the material was indefinitely perfectly plastic (Figure 3.3) [25].
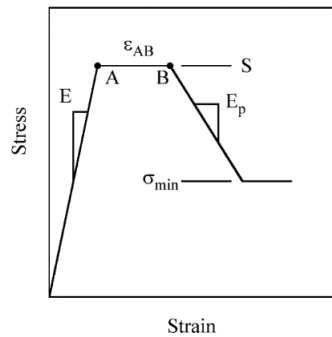
Figure 3.3: Representation in a stress-strain diagram the material properties of the bone.

To obtain al the material properties as Young moduli and yield stress, the operation computed was the following:

$$\rho_{ash} = a * bmd^b + c; \quad a = 0.8770 \ , b = \ 1.00 \ , c = 0.06330.$$

$$E \ = a * \rho_{ash}^{\ b} + c; \quad a = 14900.0 \ , b = \ 1.86 \ , c = 0.$$

$$S_{max} \ = a * \rho_{ash}^{\ b} + c; \quad a = 102.0 \ , b = \ 1.80 \ , c = 0.$$

$$S_{min} \ = a * \rho_{ash}^{\ b} + c; \quad a = 43.1 \ , b = \ 1.810 \ , c = 0.$$

These formulas had been included in the material file.

3.1.4: The complete model

Then, a second Matlab script was run, which was divided in two steps. The first step was to align the mesh to mimic stance. For this, the hip joint center and knee joint centers were aligned. The knee joint center was defined as the origin of the FE model. The hip joint center was determined by a sphere-fit through the femoral head. The hip joint center was defined as the center of the sphere. For the knee joint center, the two condylar centers were detected by fitting two cylinders through both condyles. The knee joint center was defined as the center of the transepicondylar axis (given by the connection of the two condylar centers). A rotation matrix was calculated to align the hip joint center and the knee joint center in z-direction. The rotation matrix was applied to all element coordinates, to align the mesh.

Then a proc file was created and the matlab script stopped. This proc file was run in Marc Mentat. The proc file contained Mentat's command that allowed Mentat to load the model of the femur and the model of a cup that was used to later apply the load to the model were loaded. Next, it was necessary to manually translate the cup along the z-axis to place it on top of the femoral head but without each other (Figure 3.4).
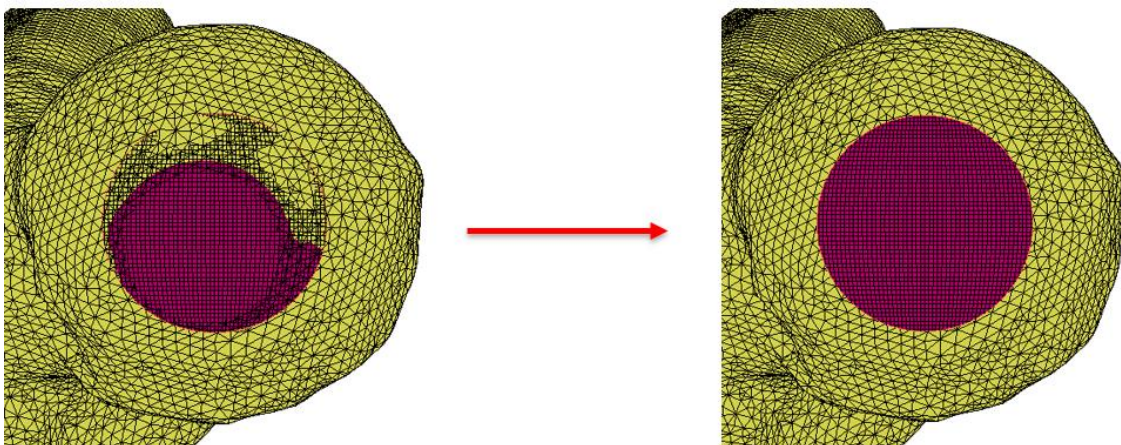
Figure 3.4: The displacement operation that the script asks to the user.

When this was done, the Matlab's script continued, and created a second proc file. This second proc file was run in Mentat to obtain the complete model with the boundary

conditions. The femur was fixed at the knee joint center by two bundles of high-stiffness $(2 \cdot 10^8 \frac{N}{m})$ springs that were attached on on the distal part of the shaft.

 A dat file with the final model was exported (Figure 3.5).
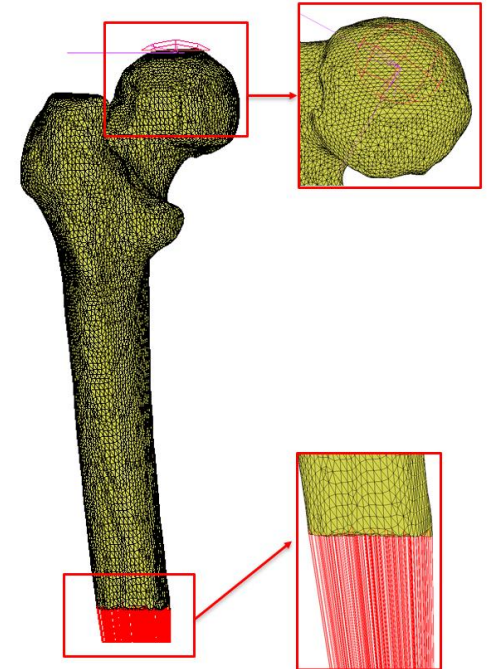
Figure 3.5: Representation on the complete model with a zoom on the boundary conditions.

3.1.5 Run the simulation

Before running the simulations, a reference node was added to the material file and the z-displacement of the cup in the dat file it was set to -5.0 mm. The reference node was used to determine the displacement of the cup and was defined as the femoral node closest to the center of the cup.

The simulation was run on the workstation which was assessed using an SSHclient. To run the simulation four files were needed: the calcium file, the material file, the dat file, and the subroutine. In the subroutine there were functions that allowed the program to run the simulation.

During the simulation, the model was loaded by displacing the cup on the head of the femur in the axial direction. The goal was to bring the femur to fracture. Failure was

reached when the force displacement curve had a clear peak or when the simulation did not converge any further (Figure 3.6).
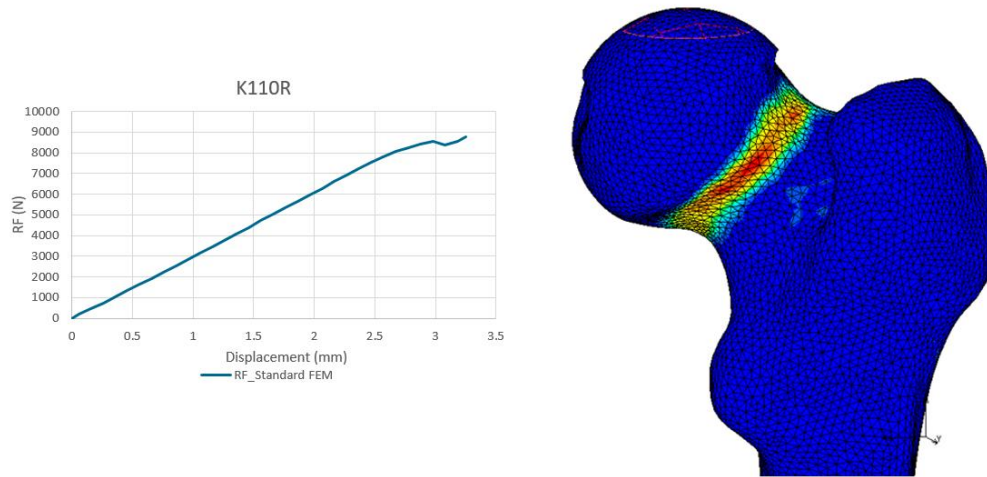
Figure 3.6: On the curve: the force-displacement curve of the patient K110R obtained by the standard FE model. On the left: the plastic energy of the model at the end of simulation in the standard FE model.

3.2 Implementation of the segmentations in the standard FE model

The aim of this study was the one to combine the deep learning technique with the finite element tool. In the predominantly lytic patients the values of the bone mineral density, in the area where the lytic metastases were detected from the segmentations, were set to zero. So, the only parameter modified was the material properties of the bone.

3.2.1 The automatic and manual segmentation

To verify the difference in the results between the standard simulation (without no modifications of the material properties), the deep learning segmentation and the manual segmentation both quantitative and qualitative features were analyzed. For the deep learning segmentation (also called automatic segmentations) the file was in nifti format. For the manual segmentation the file was in mha format. In these files there were just two

number: the 0 where the metastasis in no present. One where the metastasis was present. The visualization of the files was represented by a black and white image (Figure 3.7).
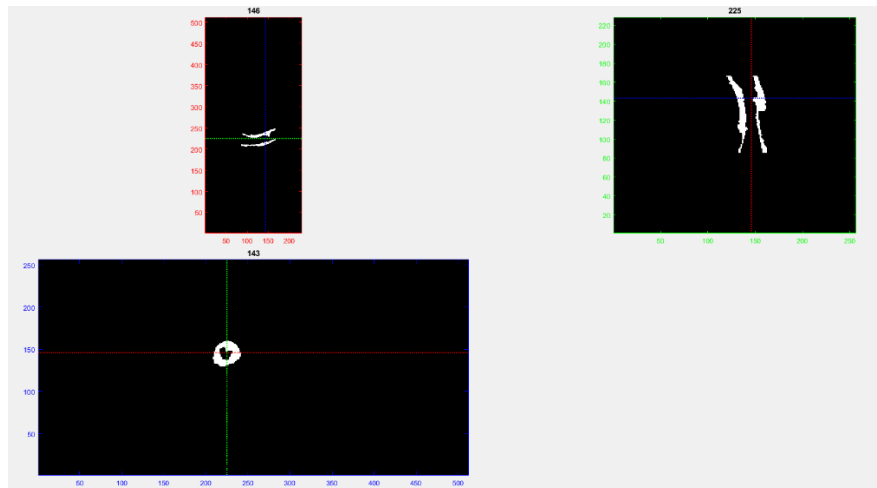
Figure 3.7: Example of the visualization of one of the segmentation file.

To modify the material properties including the data derived from the segmentations, two scripts in Matlab were written. The script used for the deep learning segmentation required the implementation of the dat file (the ones exported by Marc Mentat) and the nifti file (the automatic segmentation file). Then, the script visualized the femur of the patient in 3D with the metastasis represented in black. The script generated a vector with the same length of the calcium file and that contained with values between zero and one. Every unit of the vector corresponded to an element of the model. If in that unit there was a value different from zero, in the corresponding element was a metastatic element. This means that the segmentation detected the presence of a metastasis on that element. An

output of the script was a qualitative image of the distribution of the metastasis on the femur (Figure 3.8).
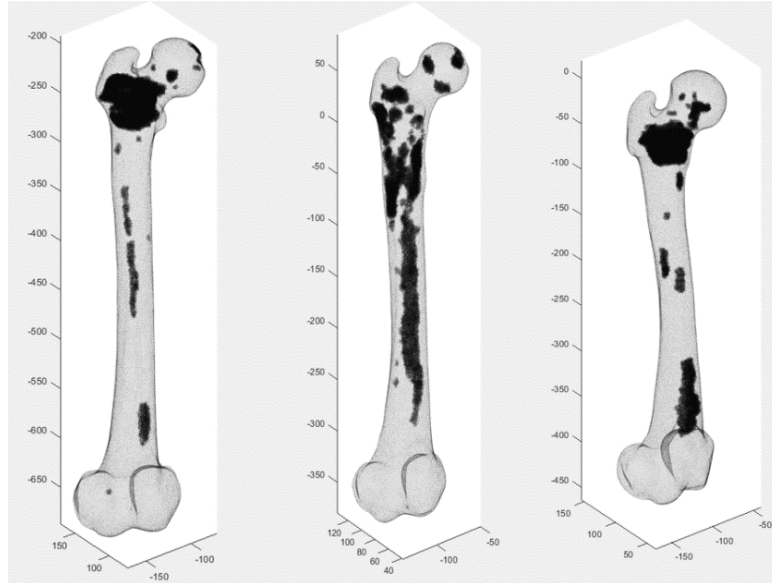
Figure 3.8: Three examples of metastasis detected by the automatic segmentations.

The script also calculated three quantitative features. These features were the mean of the bone mineral density mean of the metastatic elements, the number of elements set to zero and their percentage with respect to all the elements.

Then second script was mha version of the first script so to follow the same workflow for the manual segmentation's files.

When the automatic segmentation and the CT-scan were scan in two different reference systems, an aligner tool was used (Figure 3.9).
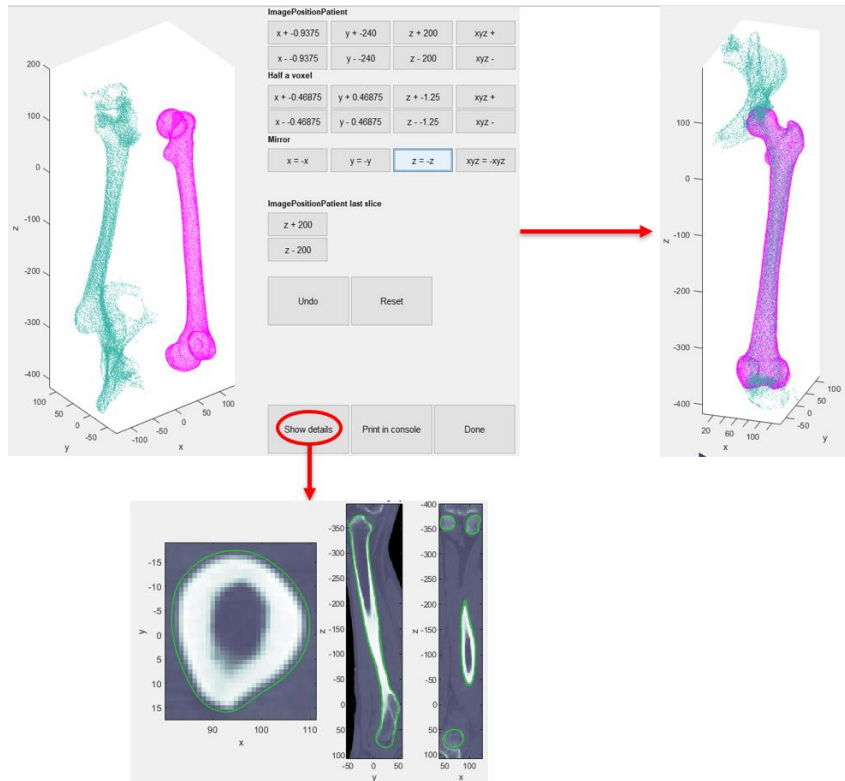
Figure 3.9: From the commands in the table, it was possible to pass from the initial situation from the left to the final situation on the right. To be sure to have a perfect match we can use the "show details" option.

Four automatic segmentations and one manual segmentation were tested. The automatic segmentations tested were four and they were named 1xx, 2xx, 1xx-2xx and all dataset (AD). The algorithm was trained with some manual segmentation's images. The training images were classified in six typologies: if they were lytic or blastic and if they were easy, hard or medium difficult to detect basing on their dimension. Every segmentation was trained with different training images. The segmentation 1xx was obtained trained the algorithm with lytic metastasis CT-image classified as easy, medium and hard. The 2xx segmentation was obtained trained the algorithm with lytic metastasis CT-images classified as easy, medium and hard and intact bone CT-images. The 1xx-2xx was obtained by the combination of the automatic segmentation 1xx and the automatic segmentation 2xx. The AD segmentation was obtained training the algorithm with the lytic metastasis CT-imaged classified as easy, medium and hard and with blastic metastasis CT-images classified as easy, medium and hard.

3.2.2 The Dice coefficient

In the end, a third script was written where we can face the automatic segmentations and the manual segmentation in qualitative and in quantitative way. About the qualitative feature the script obtained a representation of the confrontation of both the segmentations in 2D (Figure 3.10a) and in 3D (Figure 3.10b).
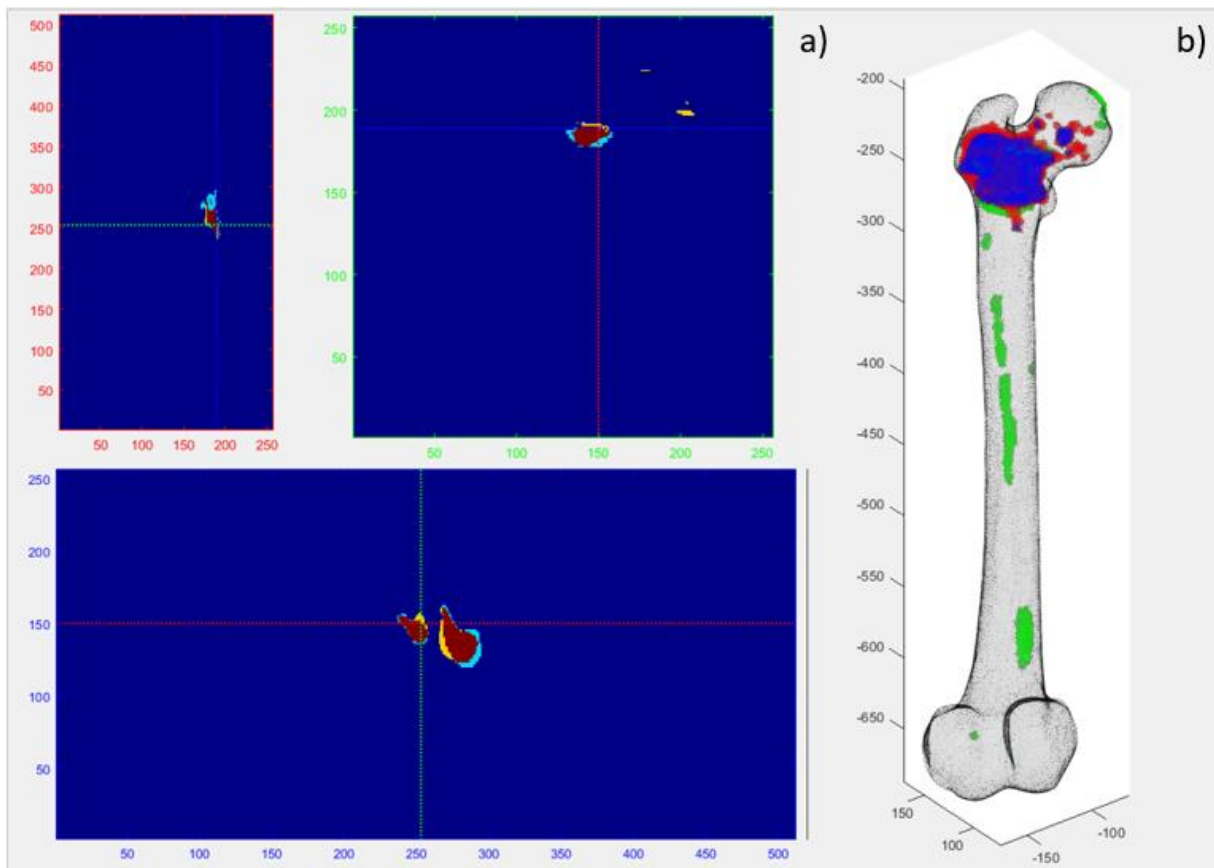
Figure 3.10: a) The three plans of the 2D images where the light blue represent the manual segmentation, the yellow the automatic segmentation and the dark red the overlapping of the two segmentations. b) The representation of the segmentation in 3D where the red color represents the manual segmentation, the green color represents the automatic segmentation and the blue color the overlapping of the two segmentations.

For the quantitative features the Dice coefficient of the two configurations was calculated. The Dice coefficient was used to quantify how much the two segmentations overlap. It was obtained in the following manner:

$$\text{Dice} = \frac{2*|ManSeg \cap AutSeg|}{|ManSeg|+|AutSeg|}.$$

In this case, the script calculated two Dice coefficients, one basing on the voxels (the black-and-white image) and the other one basing on the elements (the metastatic vector). The first Dice coefficient was named $Dice_{2D}$ and the second one was named $Dice_{3D}$.

3.3 After the simulation: Analysis of the results

Once run the simulation, some other quantitative features were extract from the force-displacement curve: the reaction force, the difference in RF percentage, the difference between the difference in RF percentage of the automatic segmentation and the difference in RF percentage of the manual segmentation. The reaction force was the highest value found of RF found in the force-displacement curve. The difference in RF percentage was the difference between the reaction force of the standard FE model and the reaction force of the automatic segmentation, mediated by the reaction force of the standard FE model:

$$\frac{RF_{Standard\ FE}-RF_{Aut\_Seg}}{RF_{Standard\ FE}}.$$

The reaction forces in the model with the segmentation was ranked and compared to the ranking obtained in the standard finite element model. A relation between the Dice coefficient and the difference in RF percentage was analyzed. In the calculation of the fracture risk with the finite element tool, two set were created: the fractured femur set, and the non-fractured femur set. The reaction force was mediated with the body weight and the BOS score obtained. Basing on the BOS the patient was classified as high-risk fracture or as low-risk fracture. The difference between the standard model and the model implanted with the segmentations was discussed.

The relation between the bone mineral density means and the difference in RF percentage was analyzed. The relation between the volume of the metastasis with respect the all femur (percentage) and the difference in RF percentage was analyzed. In this way, it was possible to verify if the difference in RF depended only on how much the material was weaken or if other factors were also involved.

Eight lytic patients were analyzed: 1811L, K110R, K117R, K120L, K304R, K342L, K353R, K411L.

Chapter 4:

The manual segmentation and the automatic segmentation 1xx

Analysis of the results with the segmentation trained with lytic metastatic bone (easy-medium and hard)

4.1: Force-displacement curve and Dice coefficient analysis

4.1.1 Patient 1181L
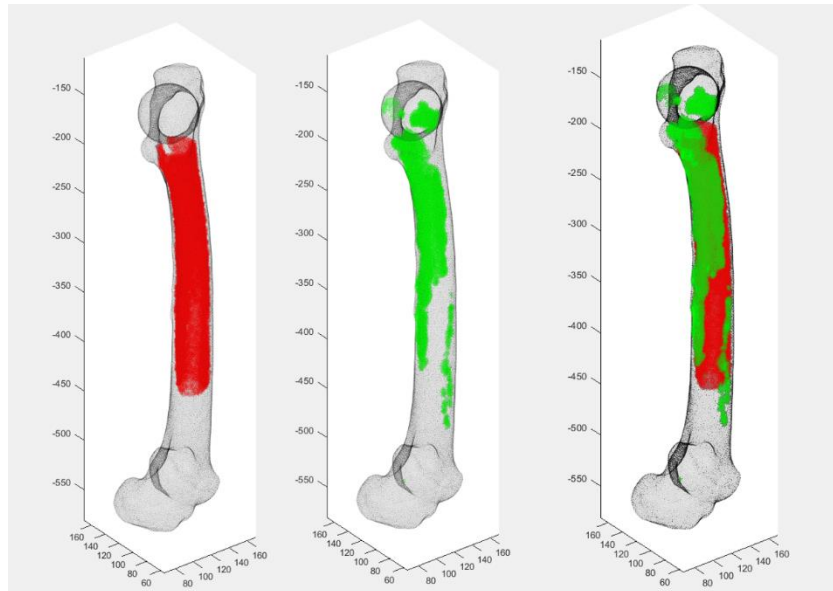
Figure 3: ■ Automatic segmentation ■ Manual segmentation ■ Overlap between manual segmentation and automatic segmentation

The 2D and 3D Dice coefficients were 39.74% and 51.72%, respectively.

For the automatic segmentation, the volume of the metastatic elements was 10.69% and the mean BMD of the metastatic elements was 449.33 $\frac{g}{cm^3}$. For the manual segmentation, the volume of the metastatic elements was 16.52% and the mean BMD of the metastatic elements was 657.02 $\frac{g}{cm^3}$.
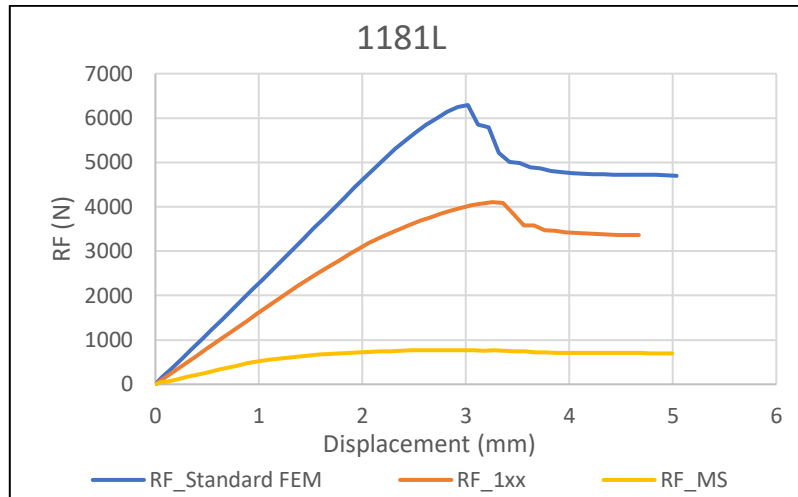
Figure 4.2: Force-displacement curves of patient 1181L. RF_Standard FEM = Standard finite element model. RF_1xx = automatic segmentation 1xx. RF_MS = manual segmentation.

The reaction force differences were 34.77% for segmentation 1xx was and 87,86% for the manual segmentation.

In this patient there was a very high difference between the results of the reaction forces between the automatic and manual segmentation. In fact, in the manual segmentation 6% more elements were involved in the metastases than in the automatic segmentation. The difference in mean bone mineral density of the metastatic elements was much higher in the manual segmentations compared to the automatic segmentation.

Additionally, the comparison between the segmentation models and the standard finite element model was also important because this could modify the fracture risk prediction of the patient. The Dice coefficient showed that the manual segmentation and the automatic segmentation overlapped for about 50%. This means that the deep learning algorithm was not able to detect all the metastasis in this patient. This probably caused the differences between the manual and automatic segmentations and could also cause a difference on the prediction of the fracture risk.
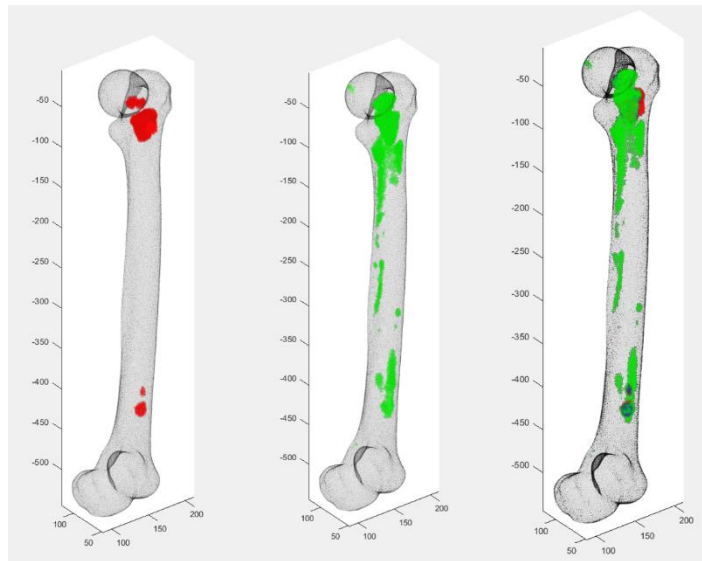
4.1.2 Patient K110R
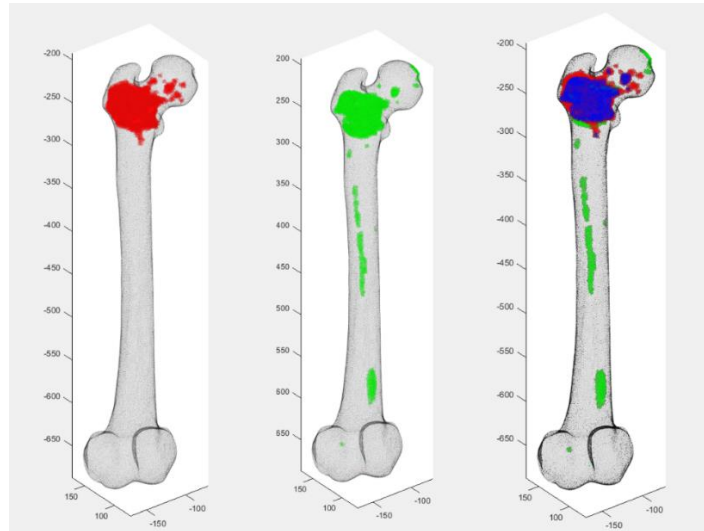
Figure 1: ■ Automatic segmentation   ■ Manual segmentation   ■ Overlap between manual segmentation and automatic segmentation

The 2D and 3D Dice coefficients were 51.49% and to 66.2% respectively.

For the automatic segmentation, the volume of the metastatic elements was 6.67% and the mean BMD of the metastatic elements was 195.96 $\frac{g}{cm^3}$. For the manual segmentation, the volume of the metastatic elements was 8.14% and the mean BMD of the metastatic elements was 155.88 $\frac{g}{cm^3}$.
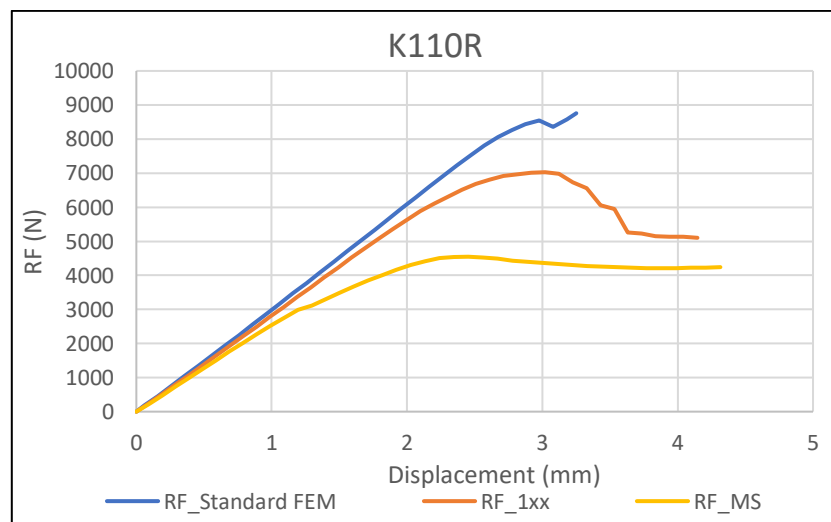
Figure 2: Force-displacement curves of patient 1181L. RF_Standard FEM = Standard finite element model. RF_1xx = automatic segmentation 1xx. RF_MS = manual segmentation.

The reaction force differences were 19.75% for segmentation 1xx was and 48.08% for the manual segmentation.

In this patient there was a high difference between the results of the reaction forces between the automatic and manual segmentation. In fact, in the manual segmentation 2% more elements were involved in the metastases than in the automatic segmentation. The difference in mean bone mineral density of the metastatic elements was slightly lower in the manual segmentations compared to the automatic segmentation.

Additionally, the comparison between the segmentation models and the standard finite element model was also important because this could modify the fracture risk prediction of the patient. The Dice coefficient showed that the manual segmentation and the automatic segmentation overlapped for about 65%. This means that the deep learning algorithm was not able to detect all the metastasis in this patient. This probably caused the differences between the manual and automatic segmentations and could also cause a difference on the prediction of the fracture risk.
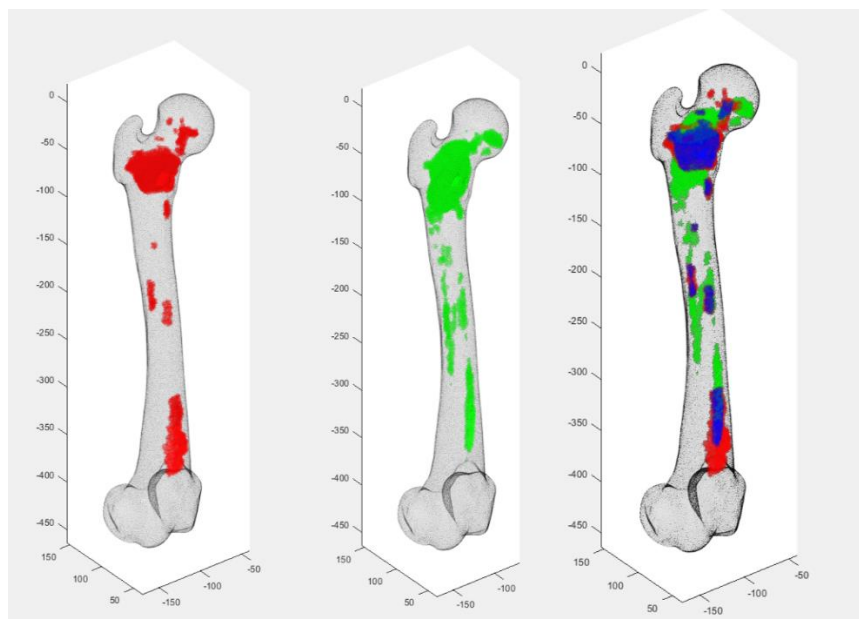
4.1.3 Patient K117R
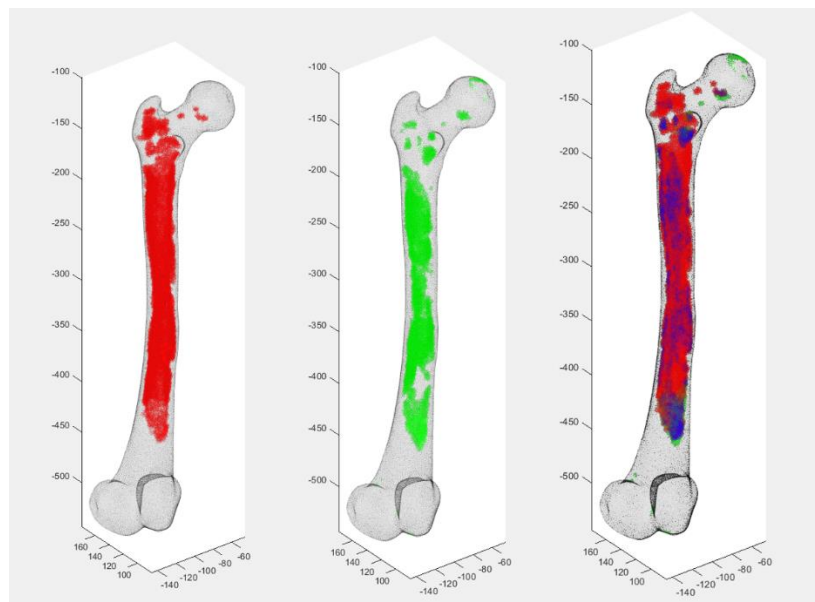
Figure 35: ■ Automatic segmentation ■ Manual segmentation ■ Overlap between MS and AS

The 2D and 3D Dice coefficients were 44.07% and 66.80%, respectively.

For the automatic segmentation, the volume of the metastatic elements was 11.12% and the mean BMD of the metastatic elements was 391.33 $\frac{g}{cm^3}$. For the manual segmentation, the volume of the metastatic elements was 18.76% and the mean BMD of the metastatic elements was 446.58 $\frac{g}{cm^3}$.
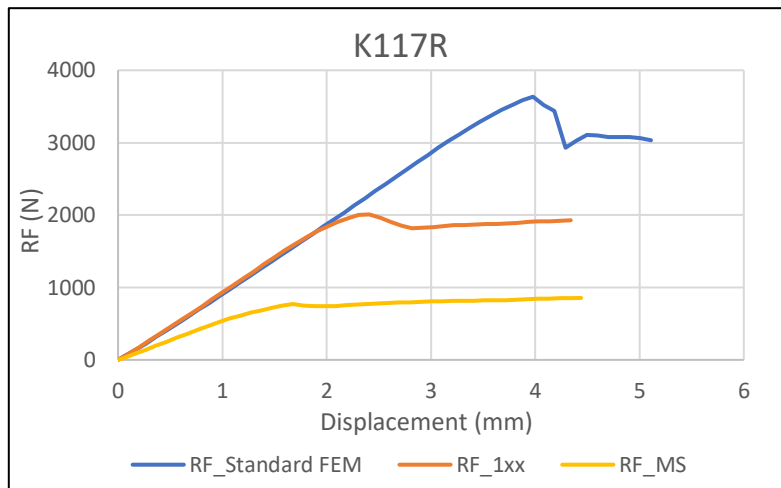
Figure 46: Force displacement curve of the patient K117R where RF_1xx stays automatic segmentation 1xx and RF_MS stays manual segmentation.

The reaction force differences were 44.73% for segmentation 1xx was and 78.81% for the manual segmentation.

In this patient there was a very high difference between the results of the reaction forces between the automatic and manual segmentation. In fact, in the manual segmentation 7% more elements were involved in the metastases than in the automatic segmentation. The difference in mean bone mineral density of the metastatic elements was much higher in the manual segmentations compared to the automatic segmentation.

Additionally, the comparison between the segmentation models and the standard finite element model was also important because this could modify the fracture risk prediction of the patient. The Dice coefficient showed that the manual segmentation and the automatic segmentation overlapped for about 65%. This means that the deep learning algorithm was not able to detect all the metastasis in this patient. This probably caused

the differences between the manual and automatic segmentations and could also cause a difference on the prediction of the fracture risk.
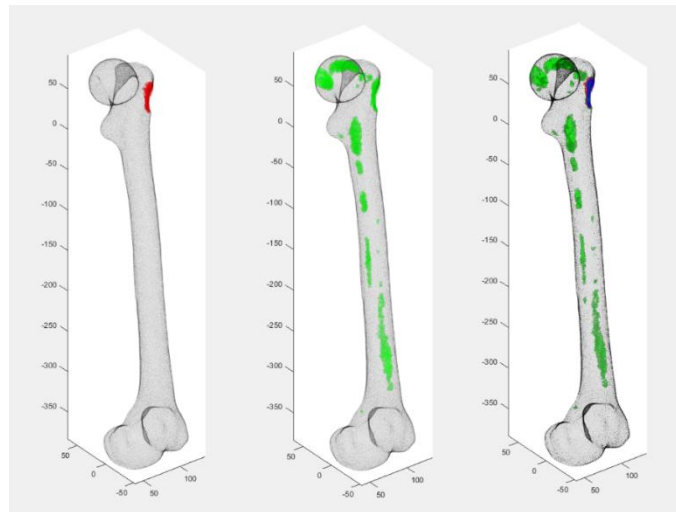
4.1.4 Patient K120L
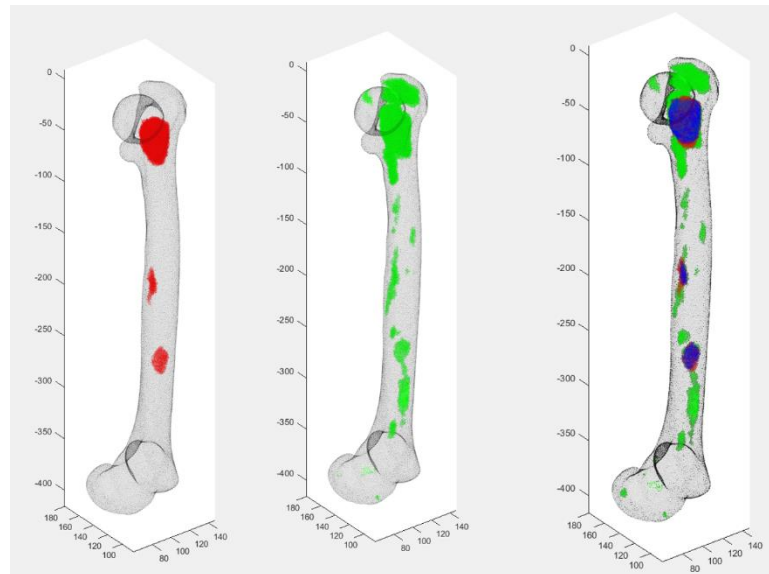
Figure 57: ■ Automatic segmentation ■ Manual segmentation ■ Overlap between MS and AS

The 2D and 3D Dice coefficients were 40.99% and 60.61%, respectively.

For the automatic segmentation, the volume of the metastatic elements was 11.31% and the mean BMD of the metastatic elements was $263.75 \frac{g}{cm^3}$. For the manual segmentation, the volume of the metastatic elements was 5.18% and the mean BMD of the metastatic elements was $168.75 \frac{g}{cm^3}$.
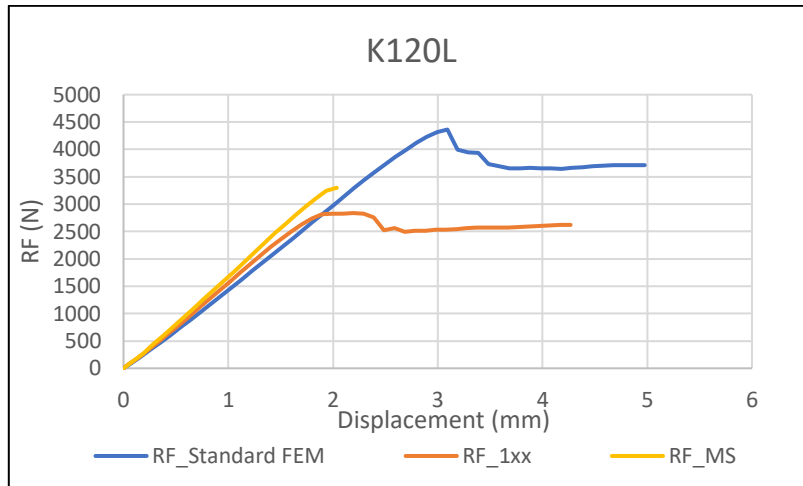
Figure 68: Force-displacement curves of patient 1181L. RF_Standard FEM = Standard finite element model. RF_1xx = automatic segmentation 1xx. RF_MS = manual segmentation.

The reaction force differences were 34.98% for segmentation 1xx was and 24.39% for the manual segmentation.

In this patient there was a difference between the results of the reaction forces between the automatic and manual segmentation. In fact, in the automatic segmentation 6% more elements were involved in the metastases than in the manual segmentation. The difference in mean bone mineral density of the metastatic elements was much higher in the automatic segmentations compared to the manual segmentation.

Additionally, the comparison between the segmentation models and the standard finite element model was also important because this could modify the fracture risk prediction of the patient. The Dice coefficient showed that the manual segmentation and the automatic segmentation overlapped for about 60%. In this case, the algorithm confused some healthy bone tissue with metastatic bone tissue. This probably caused the differences between the manual and automatic segmentations and could also cause a difference on the prediction of the fracture risk.

4.1.5 Patient K304R
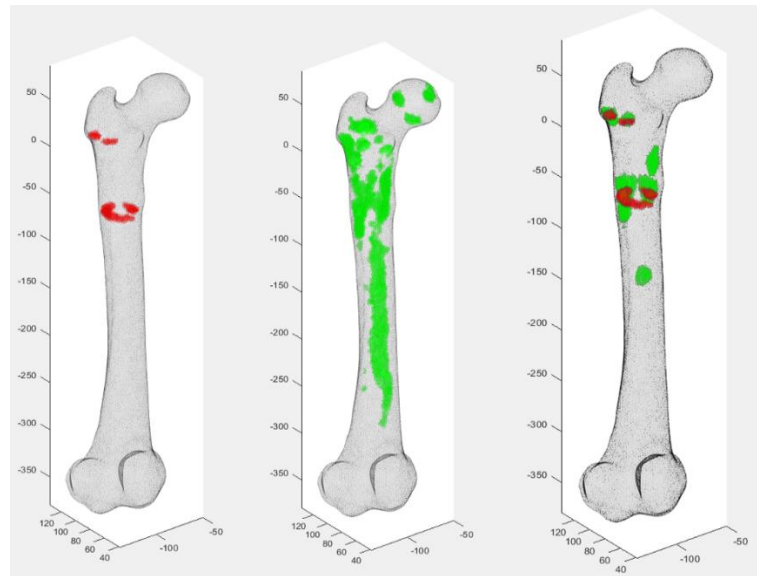
Figure 79: ■ Automatic segmentation ■ Manual segmentation ■ Overlap between MS and AS

The 2D and 3D Dice coefficients were 8.11% and 12.22%, respectively.

For the automatic segmentation, the volume of the metastatic elements was 8.63% and the mean BMD of the metastatic elements was 395.75 $\frac{g}{cm^3}$. For the manual segmentation, the volume of the metastatic elements was 0.78% and the mean BMD of the metastatic elements was 324.87 $\frac{g}{cm^3}$.
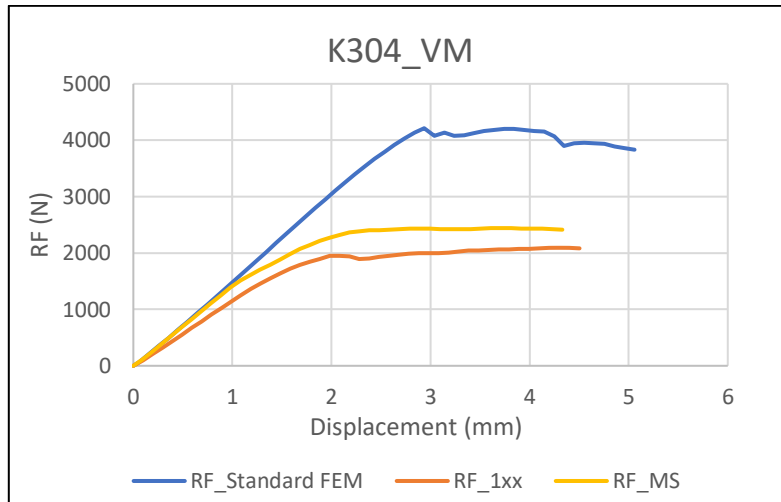
Figure 810: Force-displacement curves of patient 1181L. RF_Standard FEM = Standard finite element model. RF_1xx = automatic segmentation 1xx. RF_MS = manual segmentation.

The reaction force differences were 52.90% for segmentation 1xx was and 41.12% for the manual segmentation.

In this patient there was a difference between the results of the reaction forces between the automatic and manual segmentation. In fact, in the automatic segmentation 8% more elements were involved in the metastases than in the manual segmentation. The difference in mean bone mineral density of the metastatic elements was higher in the automatic segmentations compared to the manual segmentation.

Additionally, the comparison between the segmentation models and the standard finite element model was also important because this could modify the fracture risk prediction of the patient. The Dice coefficient showed that the manual segmentation and the automatic segmentation overlapped for about 12%. In this case, the algorithm confused some healthy bone tissue with metastatic bone tissue. This probably caused the differences between the manual and automatic segmentations and could also cause a difference on the prediction of the fracture risk.

4.1.6 Patient K342L

Figure 91: ■ Automatic segmentation ■ Manual segmentation ■ Overlap between MS and AS

The 2D and 3D Dice coefficients were 24.41% and 46.32%, respectively.

For the automatic segmentation, the volume of the metastatic elements was 6.88% and the mean BMD of the metastatic elements was 379.39 $\frac{g}{cm^3}$. For the manual segmentation, the volume of the metastatic elements was 2.91% and the mean BMD of the metastatic elements was 128.87 $\frac{g}{cm^3}$.
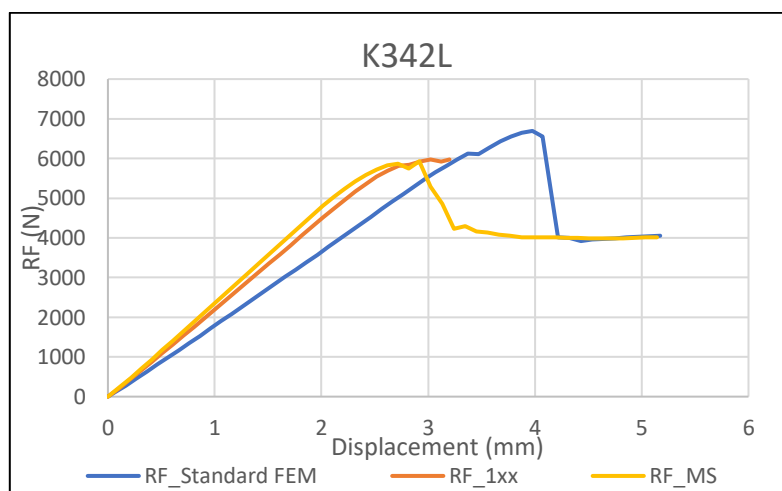
Figure 102: Force-displacement curves of patient 1181L. RF_Standard FEM = Standard finite element model. RF_1xx = automatic segmentation 1xx. RF_MS = manual segmentation.

The reaction force differences were 10.75% for segmentation 1xx was and 11.42% for the manual segmentation.

In this patient there was a very low difference between the results of the reaction forces between the automatic and manual segmentation. However, the automatic segmentation 4% more elements were involved in the metastases than in the manual segmentation. The difference in mean bone mineral density of the metastatic elements was much higher in the automatic segmentations compared to the manual segmentation.

Additionally, the comparison between the segmentation models and the standard finite element model was also important because this could modify the fracture risk prediction of the patient. The Dice coefficient showed that the manual segmentation and the automatic segmentation overlapped for about 45%. In this case, the algorithm confused some healthy bone tissue with metastatic bone tissue. This probably caused the differences between the manual and automatic segmentations, but it was improbable that could also cause a difference on the prediction of the fracture risk.

4.1.7 Patient K353R

Figure 113: ■ Automatic segmentation ■ Manual segmentation ■ Overlap between MS and AS

The 2D and 3D Dice coefficients were 37.44% and 50.56%, respectively.

For the automatic segmentation, the volume of the metastatic elements was 9.00% and the mean BMD of the metastatic elements was 239.11 $\frac{g}{cm^3}$. For the manual segmentation, the volume of the metastatic elements was 7.04% and the mean BMD of the metastatic elements was 276.81 $\frac{g}{cm^3}$.
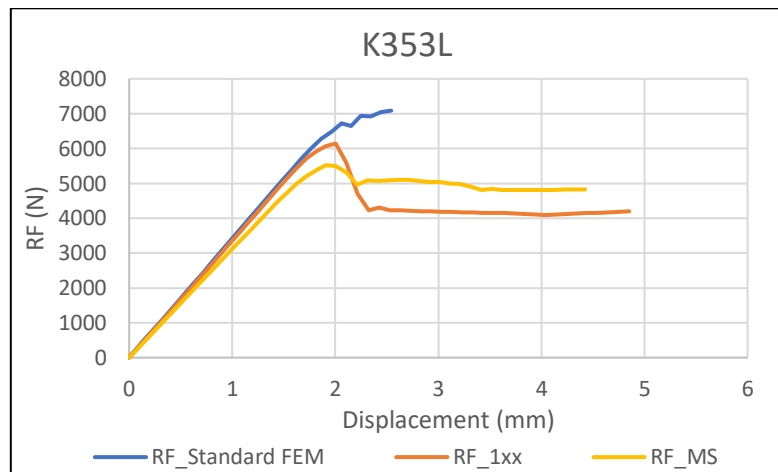
Figure 4.14: Force-displacement curves of patient 1181L. RF_Standard FEM = Standard finite element model. RF_1xx = automatic segmentation 1xx. RF_MS = manual segmentation.

The reaction force differences were 13.22% for segmentation 1xx was and 22.13% for the manual segmentation.

In this patient there was a difference between the results of the reaction forces between the automatic and manual segmentation. In fact, in the automatic segmentation 2% more elements were involved in the metastases than in the manual segmentation. The difference in mean bone mineral density of the metastatic elements was slightly higher in the manual segmentations compared to the automatic segmentation.

Additionally, the comparison between the segmentation models and the standard finite element model was also important because this could modify the fracture risk prediction of the patient. The Dice coefficient showed that the manual segmentation and the automatic segmentation overlapped for about 50%. In this case, the algorithm confused some healthy bone tissue with metastatic bone tissue. This probably caused the differences between the manual and automatic segmentations and could also cause a difference on the prediction of the fracture risk.

4.1.8 Patient K411L

Figure 4.1512: ■ Automatic segmentation ■ Manual segmentation ■ Overlap between MS and AS

The 2D and 3D Dice coefficients were 19.61% and 14.58%, respectively.

For the automatic segmentation, the volume of the metastatic elements was 3.55% and the mean BMD of the metastatic elements was 500.15 $\frac{g}{cm^3}$. For the manual segmentation, the volume of the metastatic elements was 0.38% and the mean BMD of the metastatic elements was 230.68 $\frac{g}{cm^3}$.
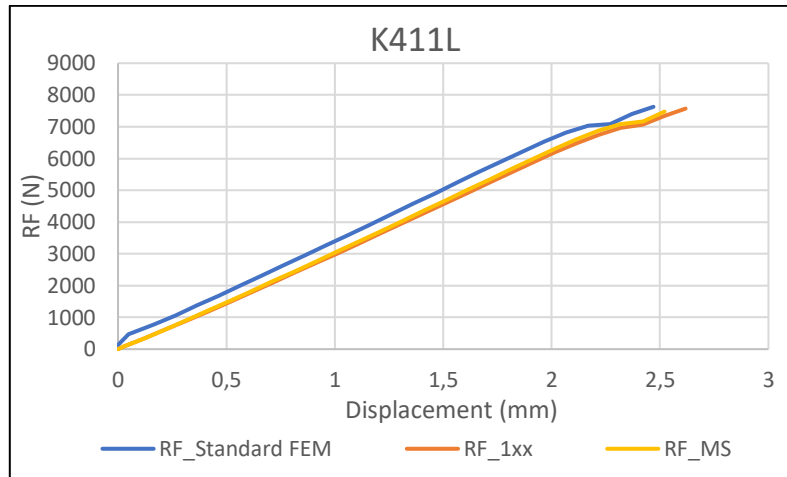
Figure 4.16: Force-displacement curves of patient 1181L. RF_Standard FEM = Standard finite element model. RF_1xx = automatic segmentation 1xx. RF_MS = manual segmentation.

The reaction force differences were 3.80% for segmentation 1xx was and 1.87% for the manual segmentation.

In this patient there was a very small difference between the results of the reaction forces between the automatic and manual segmentation. In fact, in the automatic segmentation 2% more elements were involved in the metastases than in the manual segmentation. The difference in mean bone mineral density of the metastatic elements was much higher in the manual segmentations compared to the automatic segmentation.

Additionally, the comparison between the segmentation models and the standard finite element model was also important because this could modify the fracture risk prediction of the patient. The Dice coefficient showed that the manual segmentation and the automatic segmentation overlapped for about 15%. In this case, the algorithm confused some healthy bone tissue with metastatic bone tissue. This was unprobeable that would cause a difference on the prediction of the fracture risk.

4.1.9 Summary

The results of the reaction difference percentage were briefly reported in this table.

RF diff percentage	Automatic Segmentation 1xx	Manual Segmentation
1881L	35%	88%
K110R	20%	48%
K117R	44%	76%
K120L	35%	24%
K304R	54%	42%
K342L	9%	11%
K353R	14%	22%
K411L	5%	1%

Table 4.1: Difference in reaction force between the standard finite element model and the model implemented with the automatic segmentation 1xx and the manual segmentation.

Dice coefficient	Dice 2D	Dice 3D
1881L	39.74%	51.72%
K110R	51.49%	66.20%
K117R	44.07%	66.80%
K120L	40.99%	60.61%
K304R	8.11%	12.22%
K342L	24.41%	46.32%
K353R	37.44%	50.56%
K411L	19.61%	14.58%

Table 4.2: The Dice coefficient obtained from the voxels (2D) and from the element (3D) of the all eight patients

BMD mean	Automatic Segmentation 1xx	Manual Segmentation
1881L	449	657
K110R	195	155
K117R	391	446
K120L	263	168
K304R	395	324
K342L	379	128
K353R	239	276
K411L	500	230

Table 4.3: Bone mineral density between the standard finite element model and the model implemented with the automatic segmentation 1xx and the manual segmentation.

Volume percentage	Automatic Segmentation 1xx	Manual Segmentation
1881L	10.69%	16.52%
K110R	6.67%	8.14%
K117R	11.12%	18.76%
K120L	11.31%	5.18%
K304R	8.63%	0.78%
K342L	6.88%	2.91%
K353R	9.00%	7.04%
K411L	3.55%	0.38%

Table 4.4: Volume percentage between the standard finite element model and the model implemented with the automatic segmentation 1xx and the manual segmentation.

4.2   Analysis of the results: Improvement on the implementation

This high difference between the models implemented with segmentations and the standard finite element model was not expected, even if a weakening of the material was applicated. However, despite the weakening the procedure consisted of set to zero the element where lytic metastasis were present. So, the bone mineral density in those elements should be very low, but analyzing the bone mineral density mean data, it was clear that the values were much higher than zero.

4.2.1 Two different new way of implementation

For this reason, it was hypnotized that something was wrong on the way the metastasis was implemented to the finite element model. So, two new methods to implement the metastasis were tested. Further studies were made, and two modalities were attempted. The first consisted of to set the bone mineral density placed in the metastasis zone to the 50%. The second consisted of to set a threshold value and set to zero the value of bone mineral density that were below than the threshold and set to the half the value of bone mineral density that were greater than the threshold. This was to simulate better the difference between trabecular bone and compact bone. Since in the literature it was not present a threshold value that separate the compact bone to the trabecular bone because this value can vary by many factors as the gender, the age and the constitution of the patient, the threshold value was computed by the mean of the bone mineral density of all the elements.

In this case it was decided to analyze just three patients to save time. The three patients who were evaluated also with the new modalities usually showed a decrease of this difference for the threshold modality and a higher decrease for the half modality. The patient that has been analyzed have been the K110R, K117R and K120L

The results were shown in the three tables below:

K110R	Max difference in RF (N)	Max difference in RF percentage (%)
1xx_0	1729	19.75%
1xx_T	1487	16.98%
1xx_50%	907	10.36%
MS_0	4210	48.08%
MS_T	3112	35.54%
MS_50%	1964	22.43%

Table 4.5: 1xx_0 means the model implemented with the automatic segmentation 1xx and with the bone mineral density of all the element set to zero. 1xx_T means the model implemented with the automatic segmentation 1xx and with the bone mineral density of the element set with the threshold method. 1xx_50% means the model implemented with the automatic segmentation 1xx and with the bone mineral density of all the element set to 50%. MS_0 means the model implemented with the manual segmentation and with the bone mineral density of all the element set to zero. MS_T means the model implemented with the manual segmentation and with the bone mineral density of the element set with the threshold method.MS_50% means the model implemented with the manual segmentation and with the bone mineral density of all the element set to 50%.

K117R	Max difference in RF (N)	Max difference in RF percentage (%)
AS_0	1625	19.75%
AS_T	1163	16.98%
AS_50%	1075	10.36%
MS_0	2753	75.76%
MS_T	1937	53.30%
MS_50%	1954	53.77%

Table 4.6: 1xx_0 means the model implemented with the automatic segmentation 1xx and with the bone mineral density of all the element set to zero. 1xx_T means the model implemented with the automatic segmentation 1xx and with the bone mineral density of the element set with the threshold method. 1xx_50% means the model implemented with the automatic segmentation 1xx and with the bone mineral density of all the element set to 50%. MS_0 means the model implemented with the manual segmentation and with the bone mineral density of all the element set to zero. MS_T means the model implemented with the manual segmentation and with the bone mineral density of the element set with the threshold method. MS_50% means the model implemented with the manual segmentation and with the bone mineral density of all the element set to 50%.

K120L	Max difference in RF (N)	Max difference in RF percentage (%)
AS_0	1525	34.98%
AS_T	1120	25.68%
AS_50%	923	21.17%
MS_0	1020	23.59%
MS_T	793	18.19%
MS_50%	507	11.63%

Table 4.7: 1xx_0 means the model implemented with the automatic segmentation 1xx and with the bone mineral density of all the element set to zero. 1xx_T means the model implemented with the automatic segmentation 1xx and with the bone mineral density of the element set with the threshold method. 1xx_50% means the model implemented with the automatic segmentation 1xx and with the bone mineral density of all the element set to 50%. MS_0 means the model implemented with the manual segmentation and with the bone mineral density of all the element set to zero. MS_T means the model implemented with the manual segmentation and with the bone mineral density of the element set with the threshold method. MS_50% means the model implemented with the manual segmentation and with the bone mineral density of all the element set to 50%.

The results seemed to become more like the standard finite element model, but this could not be due to the implementation method but just because the material was weakened less. For this reason, further studies to better implement the metastasis was carried on.

4.2.2 Analysis of the threshold value

Up to know, all the value greater than zero in the metastatic vector were set to zero in the calcium file. The hypothesis was that this condition could not be realistic because in this way the elements that were barely touched by the metastasis were set to zero. So, it was hypothesized that this condition was not realistic. The patients analyzed were the following: the K110R, the K117R and the K120L with both the segmentations (1xx and manual segmentation) and then if the results were promising, the method would be extended to the other patients. Ten simulations for each segmentation were performed. The threshold value was changed between 0 to 0.9 with 0.1 increments. The features computed were various. The reaction force difference and the difference in reaction force, to quantify the difference between the simulations. The bone mineral density means to verify if it would decrease with the increase of the threshold because if it would decrease

this means that the metastasis were detected better. The third feature was the number of elements involved.

The results showed always a very huge difference between the threshold 0 and 0.1 in terms of difference in reaction force. Then this difference was always less in the next ranges.
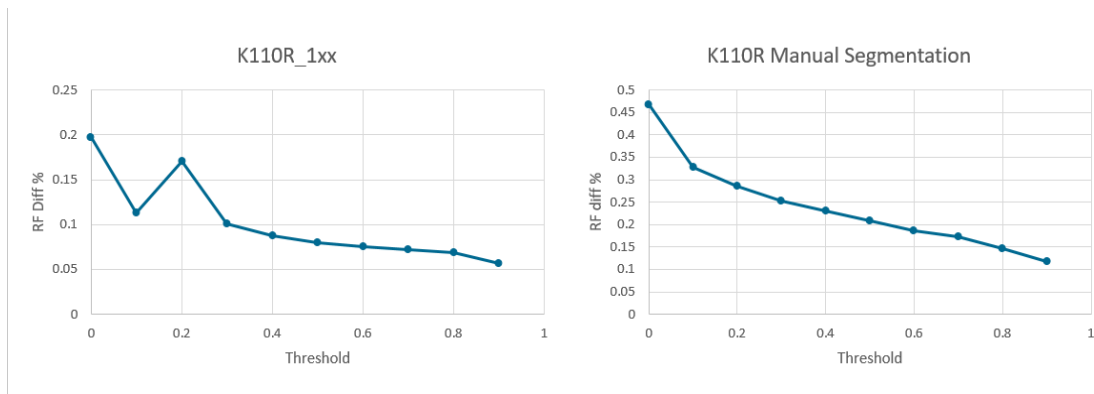
Figure 4.17: These graphs show how the reaction force difference change increasing the threshold for the patient K110R for the automatic segmentation 1xx and the manual segmentation.
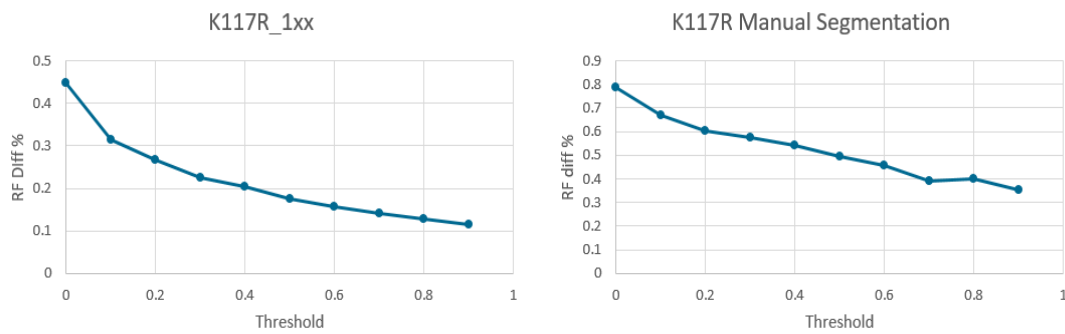
Figure 4.18: These graphs show how the reaction force difference change increasing the threshold for the patient K117R for the automatic segmentation 1xx and the manual segmentation.
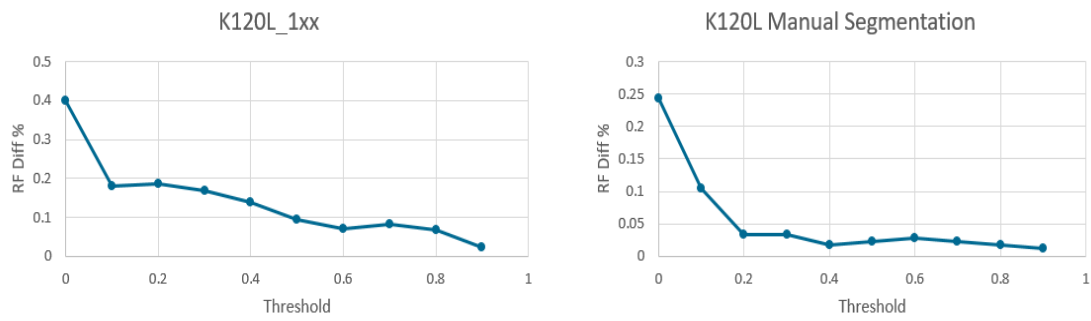
Figure 4.19: These graphs show how the reaction force difference change increasing the threshold for the patient K120L for the automatic segmentation 1xx and the manual segmentation.

The results showed that there was always a huge difference between the threshold 0 and 0.1 and between 0.1 and 0.2. The bone mineral density mean decreased, so the metastasis were caught better with the increase of the threshold. Since the fact between the threshold 0.3 and 0.4 there was a difference lower than 3.2%, a threshold of 0.3 was set. The results changed with respect to the previous implementation. They were showed in the tables below:

Pat/RF diff %	Aut_Seg_1xx_0	Aut_Seg_1xx_0.3	Man_Seg_0	Man_Seg_0.3
1181L	34.77%	24.41%	87.86%	72.14%
K110R	19.75%	10.05%	48.08%	27.15%
K117R	44.73%	22.48%	78.81%	57.49%
K120L	34.98%	15.10%	24.39%	3.38%
K304R	52.90%	17.29%	41.12%	13.13%
K342L	10.75%	2.51%	11.42%	2.59%
K353L	30.25%	7.6%	22.13%	9.35%
K411L	3.80%	2.03%	1.97%	1.38%

Table 4.8: The difference in reaction force difference between the threshold 0 and 0.3 for all the 8 patients. Aut_Seg_1xx_0 means that the model was implemented with an automatic segmentations 1xx with threshold 0. Aut_Seg_1xx_0.3 means that the model was implemented with an automatic segmentations 1xx with threshold 0.3. Man_Seg_0 means that the model was implemented with a manual segmentation with threshold 0. Man_Seg_0.3 means that the model was implemented with a manual segmentation with threshold 0.3.

The results now were closer to reality. In the following segmentations, the models have been implemented with the value of threshold of 0.3.

RF diff %	K110R_1xx	K110R_MS	K117R_1xx	K117R_MS	K120L_1xx	K120L_MS
0.0	19.75%	48.08%	44.73%	78.81%	34.98%	24.39%
0.1	11.29%	32.82%	31.43%	66.76%	17.93%	10.4%
0.2	17.01%	28.64%	26.67%	60.45%	18.72%	3.38%
0.3	10.05%	25.29%	22.48%	57.49%	16.75%	3.38%
0.4	8.70%	23.13%	20.40%	54.34%	13.93%	1.82%
0.5	7.95%	20.75%	17.63%	49.60%	9.48%	2.31%
0.6	7.54%	18.60%	15.75%	45.92%	7.00%	2.84%
0.7	7.19%	17.33%	14.03%	39.31%	8.38%	2.25%
0.8	6.85%	14.66%	12.81%	39.81%	6.65%	1.74%
0.9	5.66%	11.80	11.63%	35.24%	2.34%	1.23

Table 1: The different reaction force of all the model for all the threshold selected. Every time there was MS after the code of a patient means that those patients were implemented with the manual segmentation. Every time there was 1xx after the code of a patient means that those patients were implemented with the automatic segmentation 1xx.

BMD mean	K110R_1xx	K110R_MS	K117R_1xx	K117R_MS	K120L_1xx	K120L_MS
0.0	195	155	391	446	263	168
0.1	164	134	355	432	216	125
0.2	155	127	344	425	202	113
0.3	149	122	334	420	190	105
0.4	143	118	326	415	181	98
0.5	137	114	318	410	172	93
0.6	131	110	311	406	163	87
0.7	125	106	304	401	153	81
0.8	118	102	294	394	141	74
0.9	109	97	283	385	127	67

Table 4.10: The bone mineral density mean of all the model for all the threshold selected. Every time there was MS after the code of a patient means that those patients were implemented with the manual segmentation. Every time there was 1xx after the code of a patient means that those patients were implemented with the automatic segmentation 1xx.

Vol %	K110R_1xx	K110R_MS	K117R_1xx	K117R_MS	K120L_1xx	K120L_MS
0.0	6.67%	8.14%	11.12%	18.75%	11.31%	5.18%
0.1	5.31%	7.08%	8.00%	14.51%	9.03%	4.35%
0.2	4.95%	6.79%	7.17%	13.30%	8.42%	4.14%
0.3	4.69%	6.57%	6.56%	12.41%	7.99%	3.98%
0.4	4.48%	6.39%	6.03%	11.66%	6.39%	3.84%
0.5	4.28%	6.21%	5.55%	10.95%	7.30%	3.72%
0.6	4.09%	6.06%	5.08%	10.21%	6.98%	3.60%
0.7	3.90%	5.89%	4.59%	9.47%	6.65%	3.47%
0.8	3.67%	5.71%	4.05%	8.59%	5.98%	3.32%
0.9	3.38%	5.47%	3.36%	7.43%	5.81%	3.13%

Table 2: The percentage of elements sets to zero of all the model for all the thresholds selected. Every time there was MS after the code of a patient means that those patients were implemented with the manual segmentation. Every time there was 1xx after the code of a patient means that those patients were implemented with the automatic segmentation 1xx.

4.3   Analysis of the results

4.3.1 Ranking analysis

The first feature was analyzed was the ranking. A focus was posted on the difference in the raking between the standard finite element model and the models implemented with the segmentations.
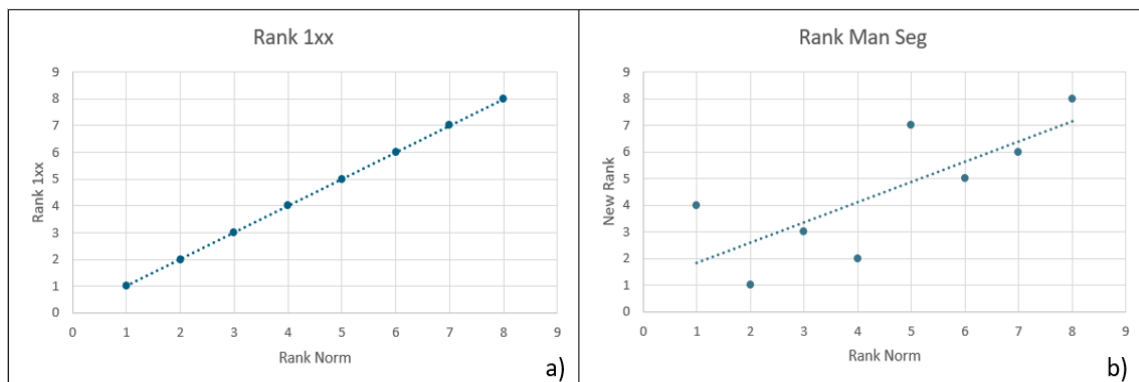
Figure 4.20: a) how the ranking change between the rank of the standard FE model and the model implemented with the automatic segmentation 1xx. b) how the ranking change between the rank of the standard FE model and the model implemented with the manual segmentation.

Meanwhile in the manual segmentation there was many samples that change their position, in the automatic segmentation a perfect matching was found. This means that despite the changing of the material properties of the bone, this segmentation seemed far to reproduce the same results of the manual segmentation.

4.3.2 Dice coefficient and difference in reaction force

The second feature analyzed was the correlation between the Dice coefficient and the difference in reaction force. The trendline showed a growing trend. However, since there were many spots that were not even close to the trendline, the conclusion was that to relation was found.
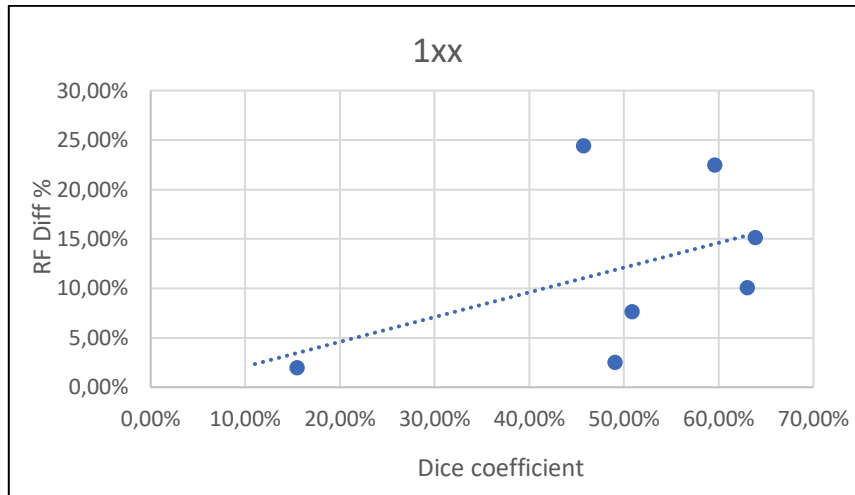
Figure 4.21: The relation between the difference in reaction force and the Dice coefficient

4.3.3 BOS score

Then, the reaction force mediated by body weight was analyzed starting from the results obtained by the standard model. In this sample (made of 8 patient), there were two patients that underwent to fracture. The higher fracture risk obtained in the fracture set was equal to 7.1. In the non-fracture set two sample were present with a fracture risk equal or lower 7.1 and the fracture risk of the patient immediately higher was equal to 7.6. So, in this group of patients two patients would be classified as high fractured risk patients and underwent to surgery without the real necessity. Then, excluding the two false positives, the gap between the high risk patient and the low risk patient was 0.5.
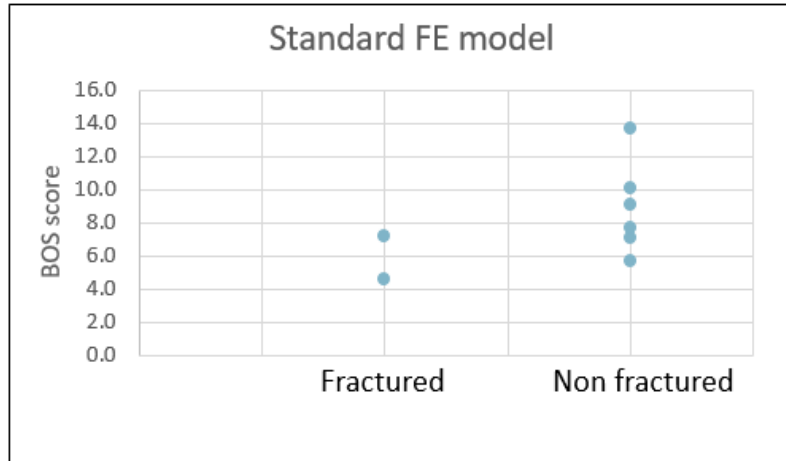
Figure 4.22: The graph shows the coefficient obtained between the ratio and body weight obtained with the simulations of the standard model.

The use of the automatic segmentations and the manual segmentation leaded to different results. Below the results obtained by the models implemented with the manual segmentations:
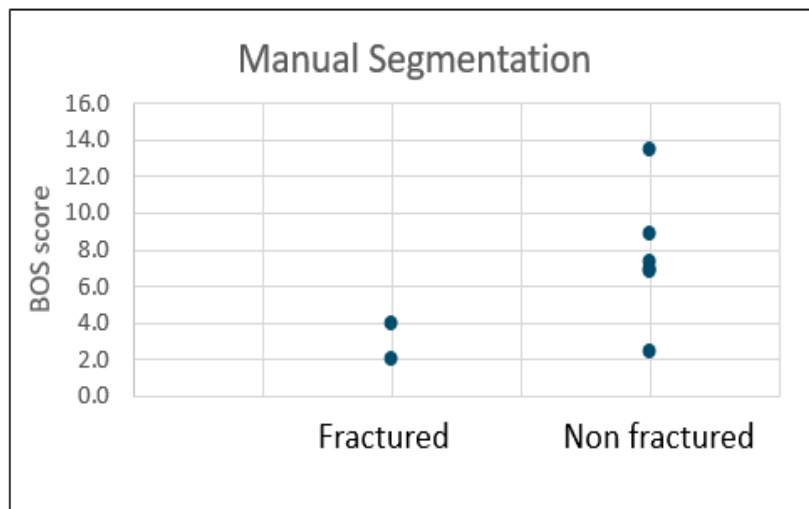
Figure 4.23: The graph show the coefficient obtained between the ration and body weight obtained with the manual segmentation simulations model.

In the manual segmentation, the highest fracture risk obtained in the fractured set was 4.0, much lower than before. Moreover, the results show just one patient would have been wrongly classified as a high fracture risk. That patient would have been classified as a high fracture risk and he would have undergone to surgery when it was not necessary.

Excluded this patient, the fracture risk of the patient who was in non-fracture set and he was classified correctly was equal to 6.8. In this situation there was just one false positive and there was much more gap between the non-fracture and the fracture patients. This behave was confirmed partially in the automatic segmentations. In fact, the results obtained in the automatic segmentations 1xx with threshold 0.3 were very similar to the ones obtained in the manual segmentations.
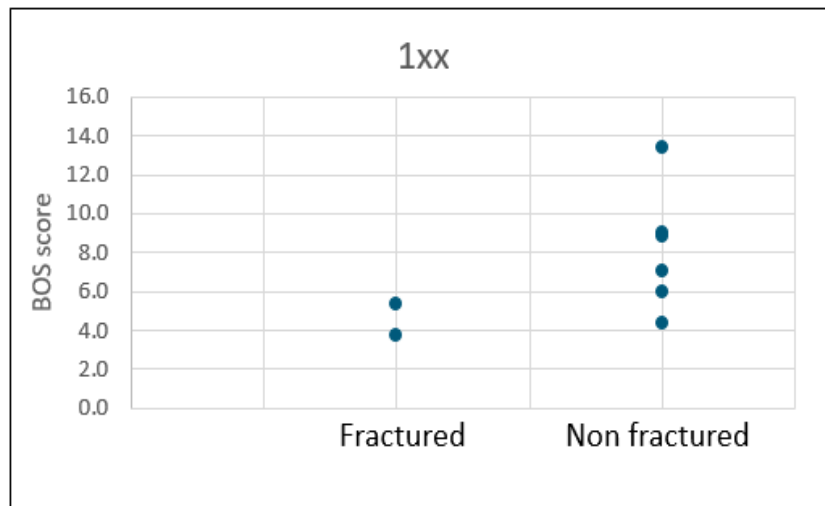
Figure 4.24: The graph shows the coefficient obtained between the ration and body weight obtained with the manual segmentation simulations model.

In this case, the highest fracture risk obtained in the fractured set was 5.4. Moreover, the results showed just one false positive. Excluded the patient wrongly classified, the gap between the low-risk patients and the high-risk patients was equal to 0.6. In this situation there was a lower number of patients that received a wrong prediction and but there was not much gap between the non-fracture and the fracture patients, excluded the false positive.

This technique seemed to improve slightly the prediction of the fracture risk in the model implemented with manual segmentations. However, also in the manual segmentation there was a patient that has been classified in the wrong way. However, the reasons for that could be many, since there were many factors that we were not considering. In fact, the medical condition of these patients was unknown. Usually, the fractures of the femur happened often during daily activity, but in some case the patient was not able to perform the daily activity necessary to fracture the femur. In the worst cases the patient could be

forced to stay in bed. One other reason was the patient could be dead before the fracture happens.

4.3.4 Relation between bone mineral density and difference in reaction force

Next, a relation between the bone difference density means and the difference in reaction force was analyzed. In this way it was possible to check if the difference in reaction force depended only on the weakening of the material properties of the bone. However, even if the threshold was growing, there was not a clear trend and many samples were placed far away from the trendline.
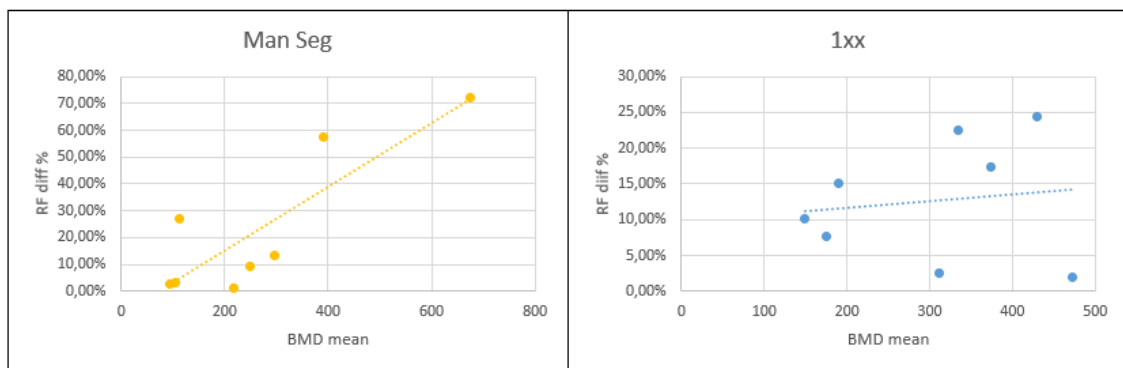
Figure 4.25: Relation between the difference in reaction force and the bone mineral density mean. On the right the model implemented with the automatic segmentation 1xx and on the left the model implemented with the manual segmentation.

4.3.5 Relation between the metastatic volume and the difference in reaction force

In the end, a relation between volume percentage and the difference in reaction force was analyzed. Also, in this case no relation was founded.
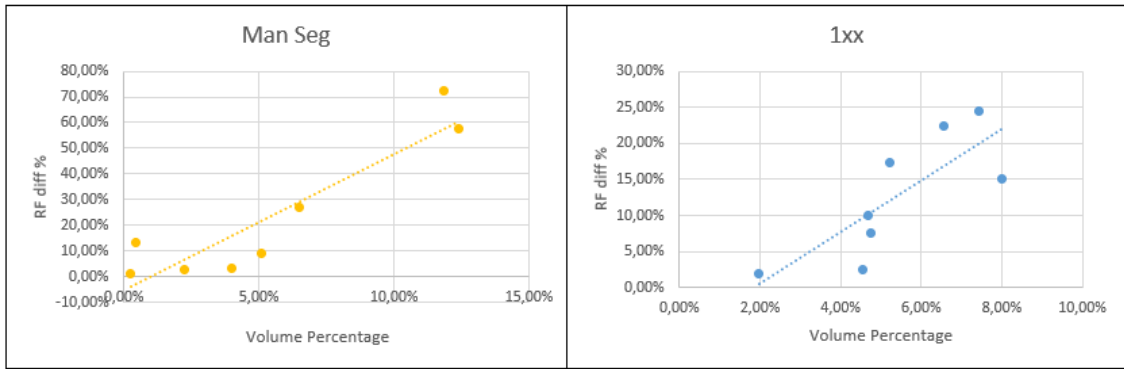
Figure 4.26: Relation between the difference reaction force and the metastatic volume. On the right the model implemented with the automatic segmentation 1xx and on the left the model implemented with the manual segmentation.

Chapter 5:
Automatic Segmentation 2xx

Analysis of the results with the segmentation trained with lytic metastatic bone (easy-medium and hard) and intact bone

5.1 Force displacement-curve and Dice coefficient analysis

The analysis was repeated with this new segmentation. The differences found in Dice coefficient and difference in reaction force between the segmentation were analyzed. The script in the Matlab code and the procedure were maintained as previously. What was going to change was the niifti file as input. After the analysis the difference between the automatic segmentations 2xx with respect to the standard finite element model and the model implemented with the manual segmentation were analyzed in terms of ranking. The relation between Dice coefficient and the difference in reaction force were studied and discussed. The reaction force was also mediated by the body weight so to obtain the BOS score and to classify the patients. In the end, the study of the relation between the bone mineral density means and the difference in reaction force and the volume percentage and the difference in reaction force was carried on.

The eight patients have been analyzed with threshold 0.3.

5.1.1 Patient 1181L
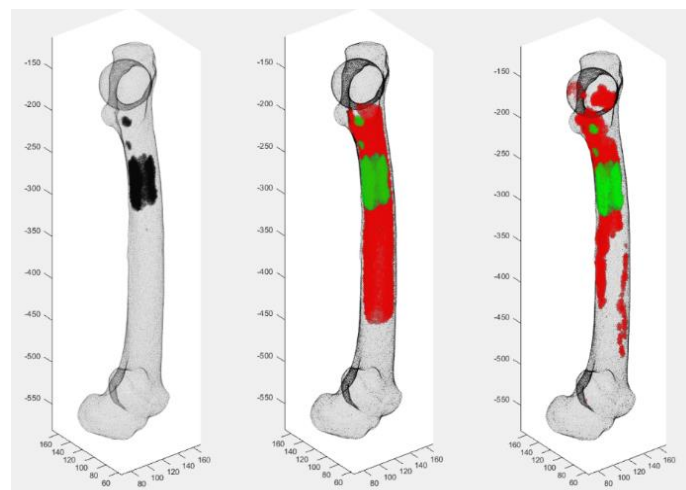
Figure 5.1: ■ Automatic segmentation   ■ Manual segmentation   ■ Overlap between manual and automatic segmentation

The value of the Dice coefficients were the following:

- Manual segmentation and automatic segmentation 2xx: 23.15% (2D) and 23.20% (3D)
- Automatic segmentation 1xx and automatic segmentation 2xx: 29.74% (2D) and 37.11% (3D)

The bone mineral density means of the element set to zero was $485 \frac{g}{cm^3}$. The volume percentage was equal to 1.80%.
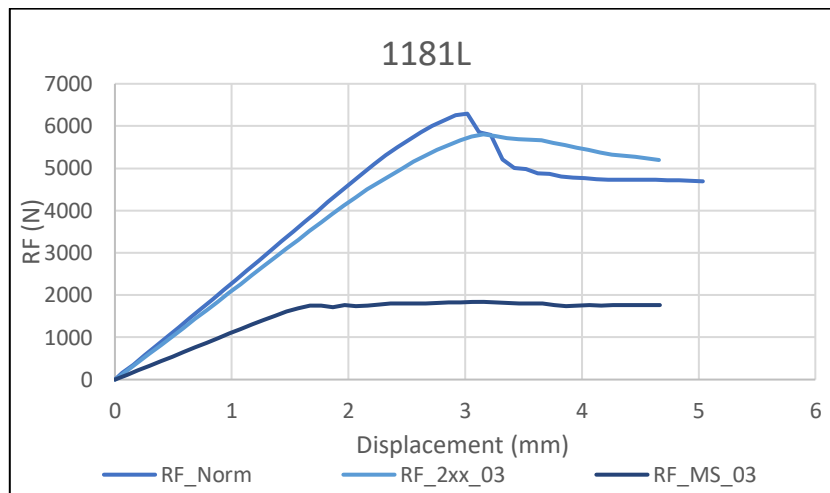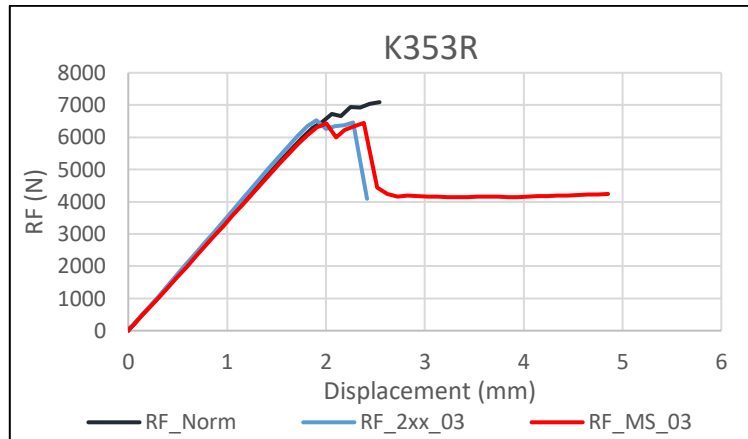

Figure 5.2: Confrontations between the normal model, the model with automatic segmentation 2xx with threshold 0.3 and the model with manual segmentation with threshold 0.3.

The reaction force differences were 8.80% for segmentation 2xx was and 71.29%. for the manual segmentation, respectively.

In this patient there was a very high difference between the results of the reaction forces between the automatic and manual segmentation. In fact, in the manual segmentation 10% more elements were involved in the metastases than in the automatic segmentation. The difference in mean bone mineral density of the metastatic elements was much higher in the manual segmentations compared to the automatic segmentation.

The Dice coefficient showed that the manual segmentation and the automatic segmentation overlapped for about 25%. This means that the deep learning algorithm was not able to detect all the metastasis in this patient. This probably caused the differences between the manual and automatic segmentations and could also cause a difference on

the prediction of the fracture risk. The Dice coefficient between the two automatic segmentations showed that the results were different, but in this case the distance between automatic and manual segmentation, in terms of reaction for difference percentage, was higher than the first segmentation. This mean that for this patient there was not an improvement of the machine learning on detecting the metastasis.
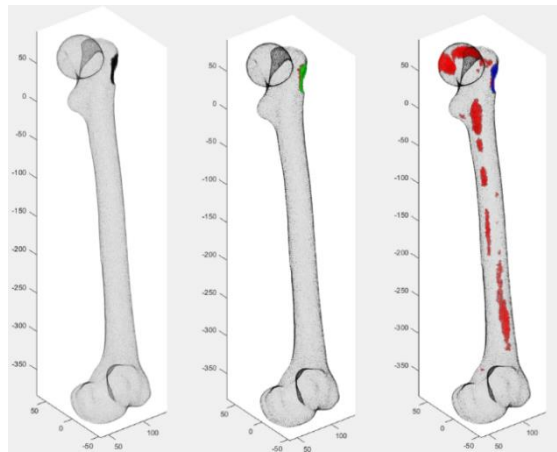
5.1.2 Patient K110R
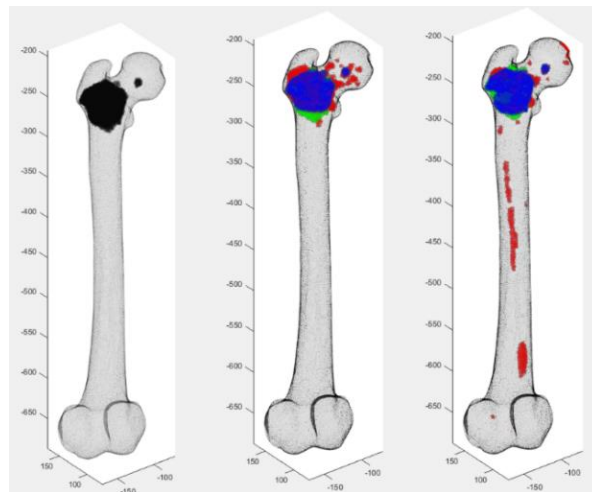
Figure 5.3: ■ Automatic segmentation ■ Manual segmentation ■ Overlap between MS and AS

The value of the Dice coefficients were the following:

- Manual segmentation and automatic segmentation 2xx: 79.17% (2D) and 78.19% (3D)
- Automatic segmentation 1xx and automatic segmentation 2xx: 59.09% (2D) and 76.05% (3D)

The bone mineral density mean of the element set to zero was $85 \frac{g}{cm^3}$. The percentage of the element set to zero was equal to 5.38%.
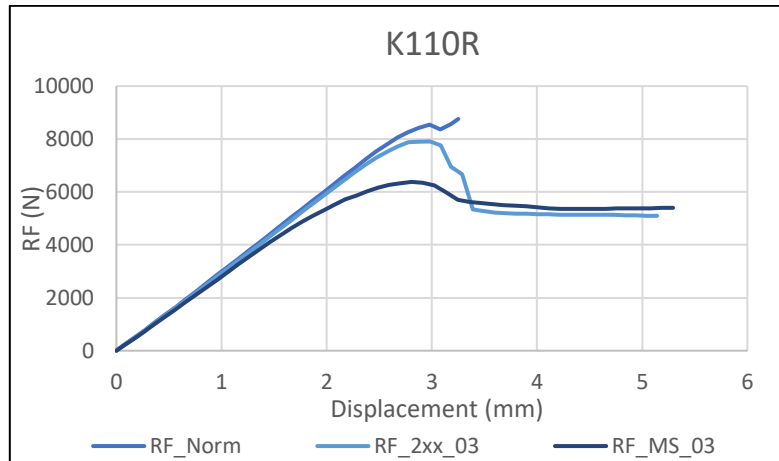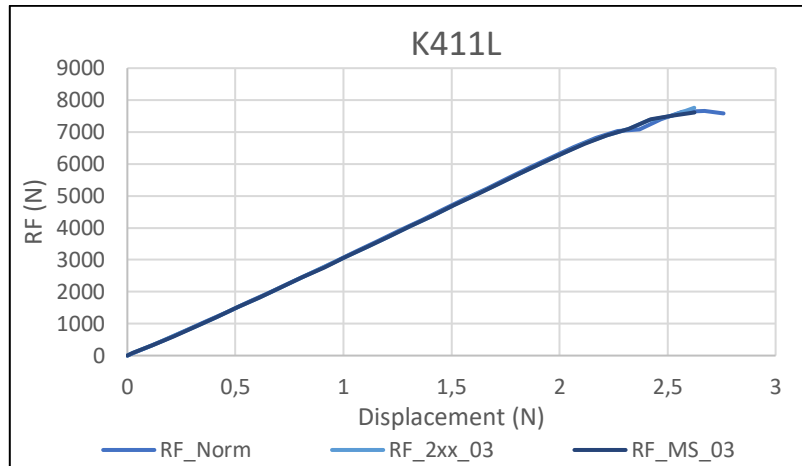
Figure 5.4: Confrontations between the normal model, the model with automatic segmentation 2xx with threshold 0.3 and the model with manual segmentation with threshold 0.3.

The reaction force differences were 8.80% for segmentation 2xx was and 24.16%. for the manual segmentation, respectively.

In this patient there was a small difference between the results of the reaction forces between the automatic and manual segmentation. In the manual segmentation 1.5% more elements were involved in the metastases than in the automatic segmentation. The difference in mean bone mineral density of the metastatic elements was slightly higher in the manual segmentations compared to the automatic segmentation.

The Dice coefficient showed that the manual segmentation and the automatic segmentation overlapped for about 78%. This means that the deep learning algorithm was able to detect almost all the metastasis in this patient. However, one fifth of the metastasis detected from the manual segmentation were not detected from the automatic segmentation. This was probably the reason of the difference on the results. The Dice coefficient between the two automatic segmentations showed that the results were similar, and the results obtained were similar as well. For this patient, the automatic segmentation 2xx was an improvement with respect to the previous one.

5.1.3 Patient K117R
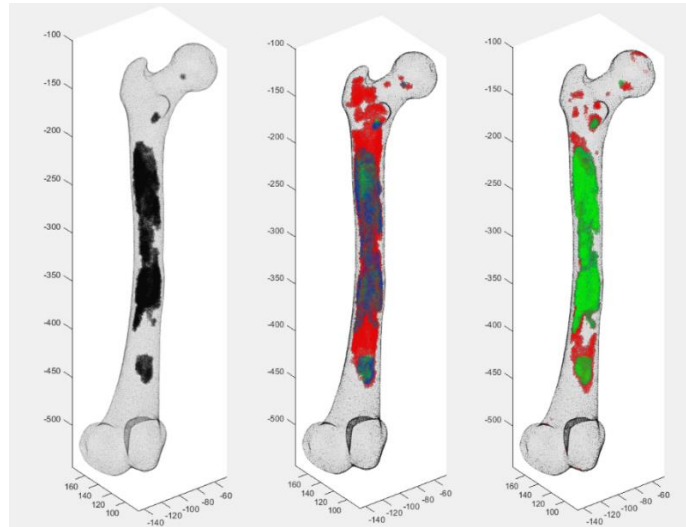
Figure 5.5: ■ Automatic segmentation ■ Manual segmentation ■ Overlap between MS and AS

The value of the Dice coefficients were the following:

- Manual segmentation and automatic segmentation 2xx: 54.88 (2D) and 55.70% (3D)

- Automatic segmentation 1xx and automatic segmentation 2xx: 50.58% (2D) and 78.01% (3D)

The bone mineral density mean of the element set to zero was $307 \frac{g}{cm^3}$. The percentage of the element set to zero was equal to 8.70%.
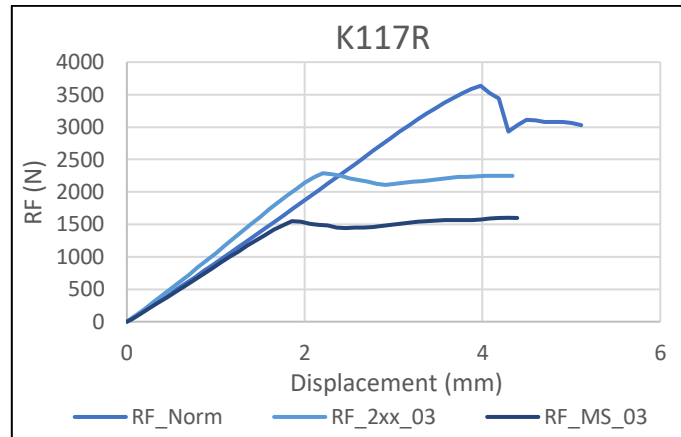
Figure 5.6: Confrontations between the normal model, the model with automatic segmentation 2xx with threshold 0.3 and the model with manual segmentation with threshold 0.3.

The reaction force differences were 37.05% for segmentation 2xx was and 57.49%. for the manual segmentation, respectively.

In this patient there was a high difference between the results of the reaction forces between the automatic and manual segmentation. In the manual segmentation 5% more elements were involved in the metastases than in the automatic segmentation. The difference in mean bone mineral density of the metastatic elements was slightly higher in the manual segmentations compared to the automatic segmentation.

The Dice coefficient showed that the manual segmentation and the automatic segmentation overlapped for about 60%. This means that the deep learning algorithm was not able to detect almost all the metastasis in this patient. This was probably the reason of the difference on the results. The Dice coefficient between the two automatic segmentations showed that the results were similar even if the results were not similar. For this patient, the automatic segmentation 2xx was an improvement with respect to the previous one.

5.1.4 Patient K120L
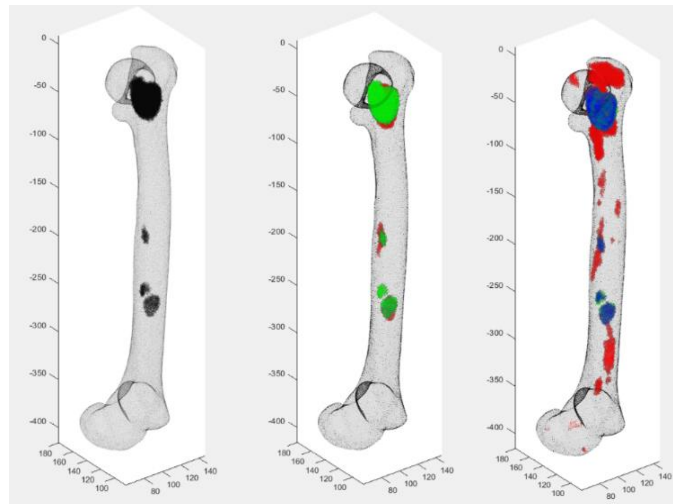
Figure 5.7: ■ Automatic segmentation ■ Manual segmentation ■ Overlap between MS and AS

The value of the Dice coefficients were the following:

- Manual segmentation and automatic segmentation 2xx: 85.43% (2D) and 85.21% (3D)

- Automatic segmentation 1xx and automatic segmentation 2xx: 41.34% (2D) and 61.65% (3D)

The bone mineral density mean of the element set to zero was $102 \frac{g}{cm^3}$. The percentage of the element set to zero was equal to 4.01%.
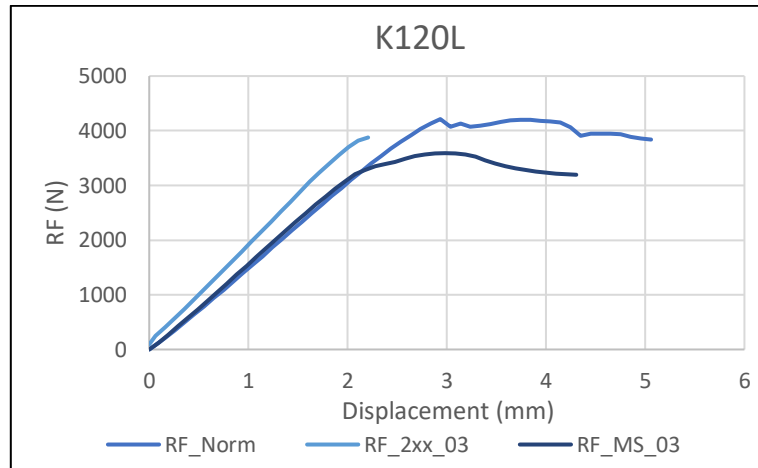
Figure 5.8: Confrontations between the normal model, the model with automatic segmentation 2xx with threshold 0.3 and the model with manual segmentation with threshold 0.3.

The reaction force differences were 7.16% for segmentation 2xx was and 14.78%. for the manual segmentation, respectively.

In this patient there was a low difference between the results of the reaction forces between the automatic and manual segmentation. The elements were involved in the metastases were almost the same. The difference in mean bone mineral density of the metastatic elements was also almost the same.

The Dice coefficient showed that the manual segmentation and the automatic segmentation overlapped for about 85%. This means that the deep learning algorithm was not able to detect almost all the metastasis in this patient but a great part of it. Since the number of elements involved was very similar, it was probable that a small part of healthy bone tissue was considered wrongly metastasis. This was probably the reason of the difference on the results. The Dice coefficient between the two automatic segmentations showed that the segmentations were not similar. For this patient, the automatic segmentation 2xx was an improvement with respect to the previous one.

5.1.5 Patient K304R
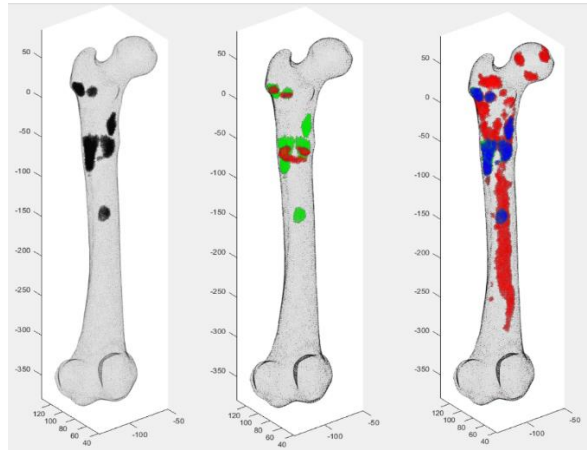
Figure 5.9: ■ Automatic segmentation ■ Manual segmentation ■ Overlap between MS and AS

The value of the Dice coefficients were the following:

- Manual segmentation and automatic segmentation 2xx: 27.29% (2D) and 33.35% (3D)

- Automatic segmentation 1xx and automatic segmentation 2xx: 36.64% (2D) and 45.09% (3D)

The bone mineral density mean of the element set to zero was $271\frac{g}{cm^3}$. The percentage of the element set to zero was equal to 1.82%.
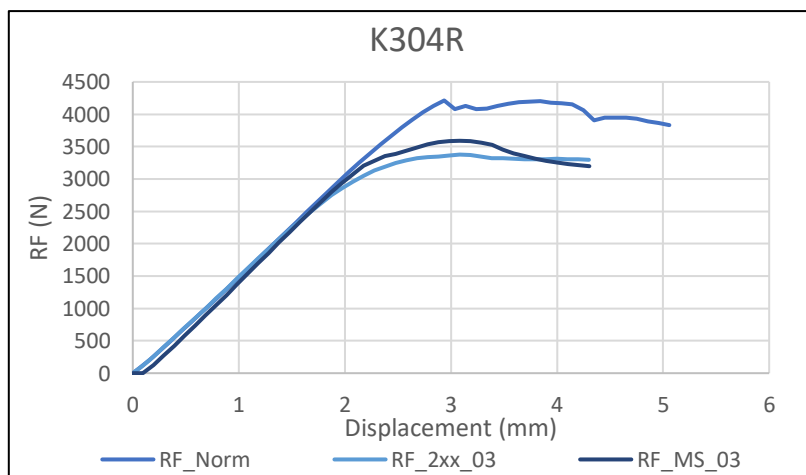
Figure 5.10: Confrontations between the normal model, the model with automatic segmentation 2xx with threshold 0.3 and the model with manual segmentation with threshold 0.3.

The reaction force differences were 14.50% for segmentation 2xx was and 19.58%. for the manual segmentation, respectively.

In this patient there was a low difference between the results of the reaction forces between the automatic and manual segmentation. In the automatic segmentation 5% more elements were involved in the metastases than in the manual segmentation. The difference in mean bone mineral density of the metastatic elements was almost the same.

The Dice coefficient showed that the manual segmentation and the automatic segmentation overlapped for about 33%. In this case, the algorithm considered wrongly some healthy bone tissue as metastatic tissue. This was probably the reason of the difference on the results. The Dice coefficient between the two automatic segmentations showed that the segmentations were not similar. For this patient, the automatic segmentation 2xx was an improvement with respect to the previous one.

5.1.6 Patient K342L
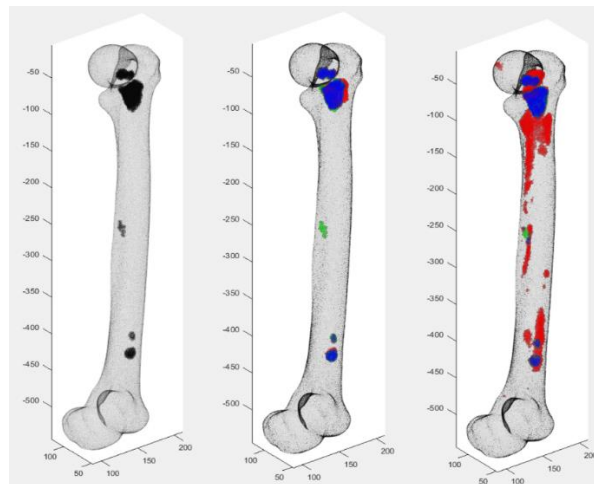
Figure 5.11: ■ Automatic segmentation ■ Manual segmentation ■ Overlap between MS and AS

The value of the Dice coefficients were the following:

- Manual segmentation and automatic segmentation 2xx: 69.47% (2D) and 69.57% (3D)

- Automatic segmentation 1xx and automatic segmentation 2xx: 19.01% (2D) and 41.72% (3D)

The bone mineral density mean of the element set to zero was $271\frac{g}{cm^3}$. The percentage of the element set to zero was equal to 1.82%.
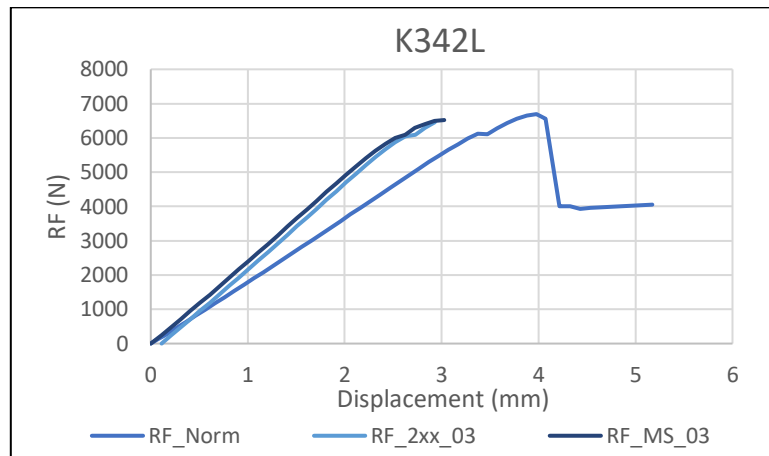
Figure 5.12: Confrontations between the normal model, the model with automatic segmentation 2xx with threshold 0.3 and the model with manual segmentation with threshold 0.3.

The reaction force differences were 0.37% for segmentation 2xx was and 2.59%. for the manual segmentation, respectively.

In this patient there was a very low difference between the results of the reaction forces between the automatic and manual segmentation. In the manual segmentation 1% more elements were involved in the metastases than in the automatic segmentation. The difference in mean bone mineral density of the metastatic elements was almost the same. The Dice coefficient showed that the manual segmentation and the automatic segmentation overlapped for about 70%. In this case there, almost the 30% of the metastasis were not detected from the algorithm. This was probably the reason of the difference on the results. The Dice coefficient between the two automatic segmentations showed that the segmentations were not similar. For this patient, the automatic segmentation 2xx was an improvement with respect to the previous one.

5.1.7 Patient K353R
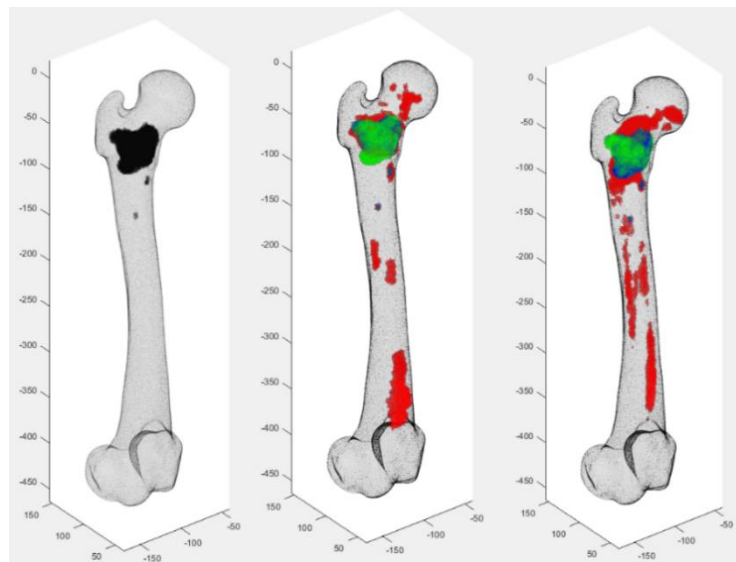
Figure 5.13: ■ Automatic segmentation ■ Manual segmentation ■ Overlap between MS and AS

The value of the Dice coefficients were the following:

- Manual segmentation and automatic segmentation 2xx: 66.45% (2D) and 63.64% (3D)
- Automatic segmentation 1xx and automatic segmentation 2xx: 44.55% (2D) and 58.41% (3D)

The bone mineral density mean of the element set to zero was $76 \frac{g}{cm^3}$. The percentage of the element set to zero was equal to 3.56%.

Figure 5.14: Confrontations between the normal model, the model with automatic segmentation 2xx with threshold 0.3 and the model with manual segmentation with threshold 0.3.

The reaction force differences were 7.92% for segmentation 2xx was and 9.07%. for the manual segmentation, respectively.

In this patient there was a very low difference between the results of the reaction forces between the automatic and manual segmentation. In the manual segmentation 2% more elements were involved in the metastases than in the automatic segmentation. In the manual segmentation the bone mineral density mean was much higher than in the automatic segmentation.

The Dice coefficient showed that the manual segmentation and the automatic segmentation overlapped for about 60%. In this case the algorithm considered wrongly some healthy bone tissue as metastasis. This was probably the reason of the difference on the results. The Dice coefficient between the two automatic segmentations showed that the segmentations were not similar. For this patient, the automatic segmentation 2xx was not an improvement with respect to the previous one.

5.1.8 Patient K411L

Figure 5.15: ■ Automatic segmentation ■ Manual segmentation ■ Overlap between MS and AS

The value of the Dice coefficients were the following:

- Manual segmentation and automatic segmentation 2xx: 77.39% (2D) and 75.67% (3D)
- Automatic segmentation 1xx and automatic segmentation 2xx: 20.39% (2D) and 14.57% (3D)

The bone mineral density mean of the element set to zero was $179 \frac{g}{cm^3}$. The percentage of the element set to zero was equal to 0.24%.

Figure 5.16: Confrontations between the normal model, the model with automatic segmentation 2xx with threshold 0.3 and the model with manual segmentation with threshold 0.3.

The reaction force differences were 1.47% for segmentation 2xx was and 1.38%. for the manual segmentation, respectively.

In this patient there was a very low difference between the results of the reaction forces between the automatic and manual segmentation. The elements involved were almost the same. The difference in mean bone mineral density of the metastatic elements was almost the same.

The Dice coefficient showed that the manual segmentation and the automatic segmentation overlapped for about 78%. In this case the algorithm considered wrongly some healthy bone tissue as metastasis but however the results were very similar. The Dice coefficient between the two automatic segmentations showed that the segmentations were not similar. For this patient, the automatic segmentation 2xx was an improvement with respect to the previous one.

5.1.9 Summary

RF diff %	Manual segmentation	Automatic segmentation 2xx
1181L	71.29%	8.80%
K110R	24.16%	9.71%
K117R	57.49%	37.05%
K120L	17.78%	7.16%
K304R	14.50%	19.58%
K342L	2.59%	0.37%
K353R	9.07%	7.92%
K411L	1.38%	1.47%

Table 5.1: Difference in reaction force between the standard finite element model and the model implemented with the automatic segmentation 2xx and the manual segmentation.

Dice coefficient	Dice 2D	Dice 3D
1181L	23.15%	23.20%
K110R	79.17%	78.19%
K117R	54.88%	55.50%
K120L	85.43%	85.21%
K304R	27.99%	28.88%
K342L	65.47%	69.57%
K353R	66.45%	63.64%
K411L	77.39%	75.67%

Table 5.2: The Dice coefficient obtained from the voxels (2D) and from the element (3D) of the all eight patients.

BMD mean	Manual segmentation	Automatic segmentation 2xx
1181L	674	502
K110R	122	85
K117R	420	307
K120L	105	102
K304R	297	271
K342L	93	103
K353R	249	76
K411L	186	179

Table 5.3: Bone mineral density mean between the standard finite element model and the model implemented with the automatic segmentation 2xx and the manual segmentation.

Volume %	Manual segmentation	Automatic segmentation 2xx
1181L	11.82%	1.80%
K110R	6.57%	5.38%
K117R	12.41%	8.70%
K120L	3.98%	4.01%
K304R	0.45%	1.82%
K342L	2.23%	1.38%
K353R	5.11%	3.56%
K411L	0.24%	0.24%

Table 34: Volume difference percentage between the standard finite element model and the model implemented with the automatic segmentation 2xx and the manual segmentation.

5.2 Analysis of the results

5.2.1 Ranking analysis

The ranking analysis showed a result very similar to the standard finite element model. There were just two sample that have a different rank and they switched the position. It was instead very different from the ranking obtained by the model implemented to the manual segmentation.
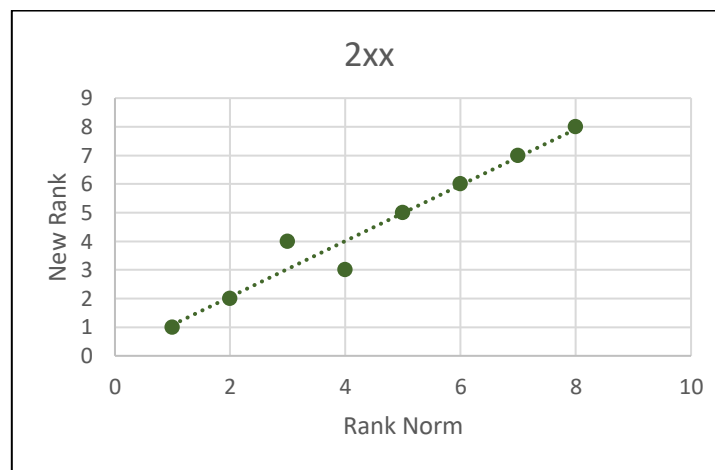
Figure 5.17: Confrontation between the ranking of the standard model with the model implemented with the 2xx segmentation with threshold 0.3.

5.2.2 Dice coefficient and difference in reaction force

Then it has been analyzed how the difference in reaction force and the Dice coefficient were related and if there was a relation.
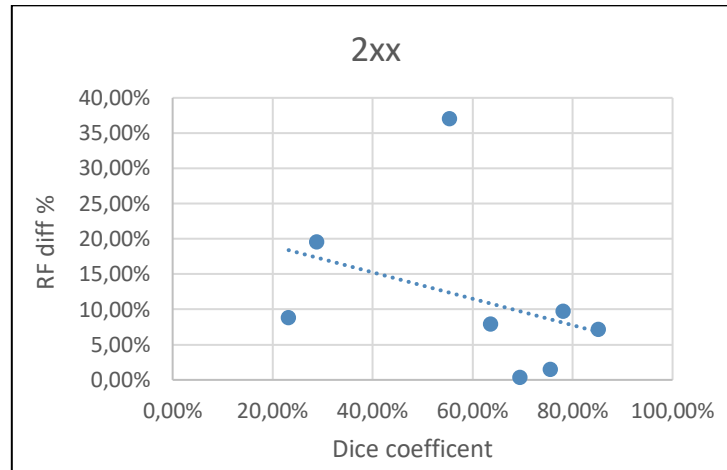
Figure 5.18: This graph show how the difference in reaction force varies with respect to the Dice coefficient.

In the difference in reaction force graphs, however, the samples did not seem to have a linear behavior, meanwhile in the reaction difference percentage this behave seemed closer to a line except for one sample that was very distant from the trend line.

5.2.3 BOS scores

Then, the fracture risk was obtained mediating the reaction force with the body weight and dividing the 8-patient analyzed in patient that had a fracture (represented in the graph by the number 1) and in the patient that did not have a fracture (represented in the graph by the number 2).
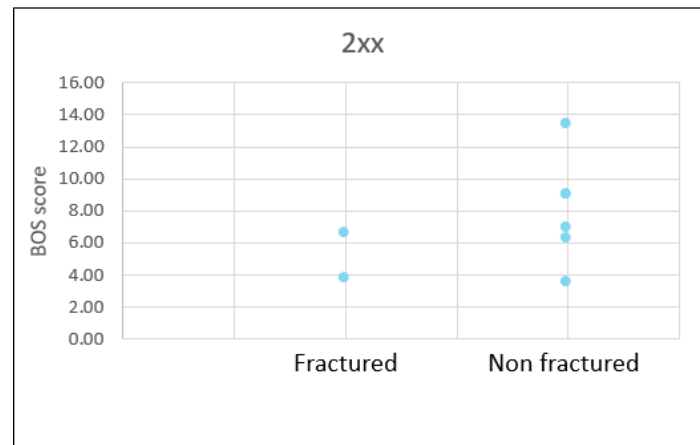
Figure 5.19: The graphs show how the ratio between reaction forces obtained with the model implemented with the 2xx segmentations and body weight was related to a future fracture of the patient.

In this case, the highest BOS score of the fracture set was 6.57. Two patients were below this value in the non-fracture set and another patient got similar results (7.00). So, excluded the patient wrongly predicted, the gap between the patients classified as high fractured risk and the patients classified as a low fractured risk was 0.43. These segmentations seemed not to improve the results obtained by the previous one basing on the BOS score.

5.2.4 Relation between the bone mineral density mean and the difference in reaction force

Then the relation between the bone mineral density mean and the difference in reaction force was compared.
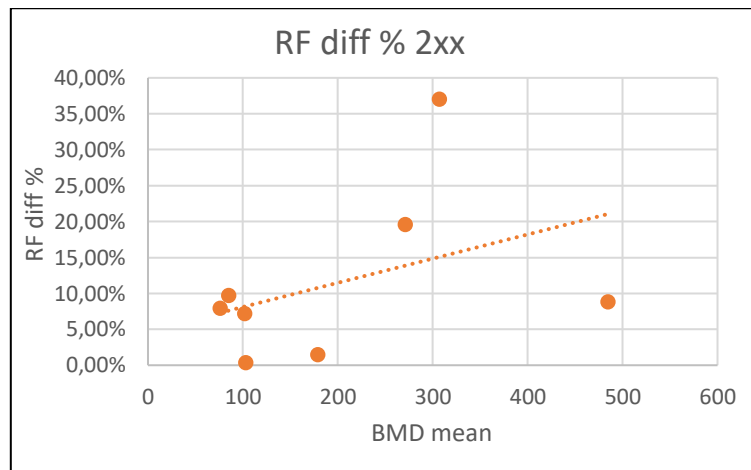
Figure 5.20: The relation between the bone mineral density mean of the element we set to zero with threshold 0.3.

The trend was growing as expected. However, there were many samples that were far away from the trend line, so there was not a strong relationship. That means that the reaction force difference was not simply higher just if elements with a higher bone mineral density were set to zero.

5.2.5 Relation between the metastatic volume and the difference in reaction force

In the end, the relationship between the volume percentage and the difference in reaction force was analyzed.
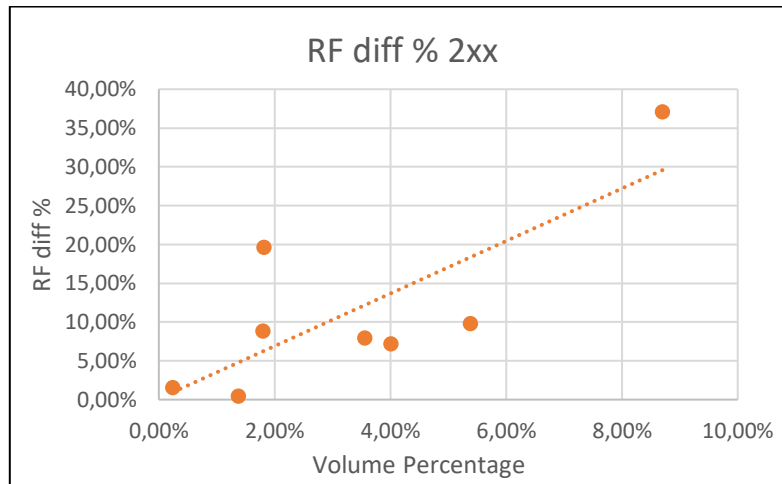
Figure 5.21: The relation between the volume percentage of the element we set to zero with threshold 0.3.

In this case, there were some samples closer to the trendline. However, there were also some samples that were placed quite distance. In conclusion, seemed that the number of elements involved influenced the difference in reaction force, but this does not happen in a linear way.

Chapter 6:

The segmentations 1xx-2xx and all dataset

Analysis of the segmentation obtained by the combination of 1xx and 2xx and the one trained by all dataset (easy-medium-hard lytic metastasis and easy-medium-hard blastic metastasis)

6.1 Force-Displacement curve and Dice coefficient analysis

The aim of the work was verified if the automatic segmentation was more similar to the manual segmentations. In the previous two segmentations promising results were founded. To verify if there was an improvement, two new segmentations were tested. The first segmentation was obtained by training the algorithm with the combination of the two segmentations 1xx and 2xx. This segmentation was named 1xx-2xx. The second segmentation was trained by the slices of lytic metastasis (hard, medium and easy) and by the slice of the blastic metastasis (hard, medium and easy). For this reason, this segmentation was named all dataset.
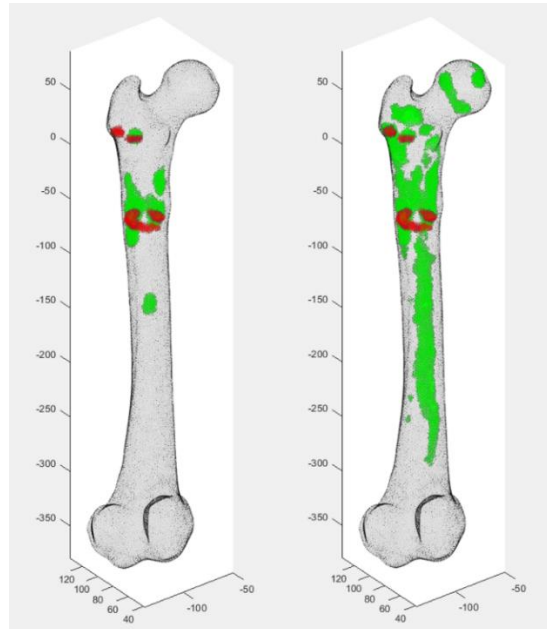
6.1.1 Patient 1181L
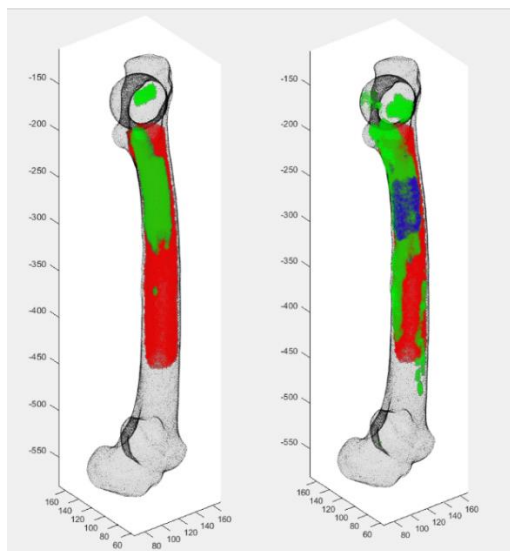
Figure 6.1: ■ Automatic segmentation ■ Manual segmentation ■ Overlap between MS and AS

For the all dataset (AD) segmentation, the Dice coefficient obtained were equal to 32.63% (2D) and 32.91% (3D with threshold 0.3).

For the segmentation obtained by the combination of the segmentation 1xx and 2xx, the Dice coefficient obtained were equal to 14.06% (2D) and 16.71% (3D with threshold 0.3).
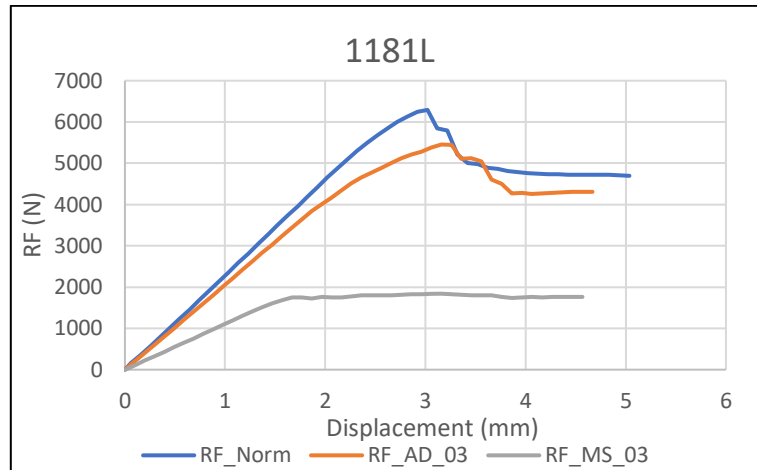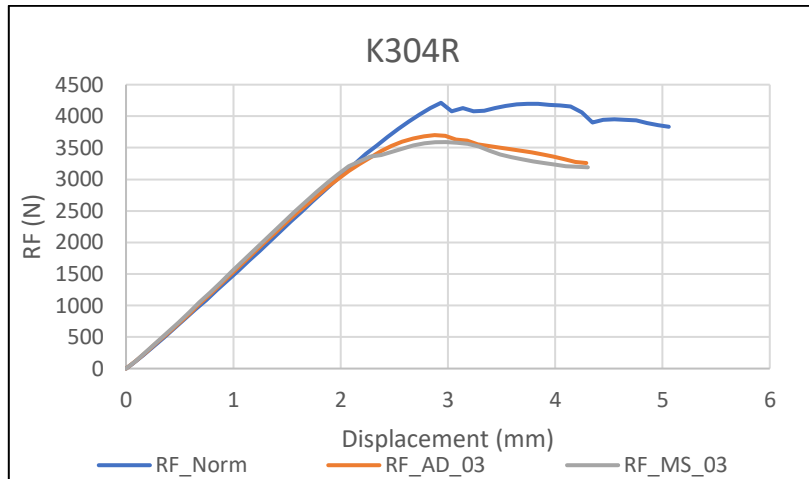
Figure 13: Force-displacement curve of the patient implemented with the automatic segmentation trained with all dataset.

The reaction force differences were 13.33% for the automatic segmentation AD and was 71.29% for the manual segmentation.

In this patient there was a very high difference between the results of the reaction forces between the automatic and manual segmentation. In fact, in the manual segmentation 7% more elements were involved in the metastases than in the automatic segmentation. The difference in mean bone mineral density of the metastatic elements was much higher in the manual segmentations compared to the automatic segmentation.

The Dice coefficient showed that the manual segmentation and the automatic segmentation overlapped for about 37%. This means that the deep learning algorithm was not able to detect all the metastasis in this patient. This probably caused the differences between the manual and automatic segmentations and could also cause a difference on the prediction of the fracture risk.
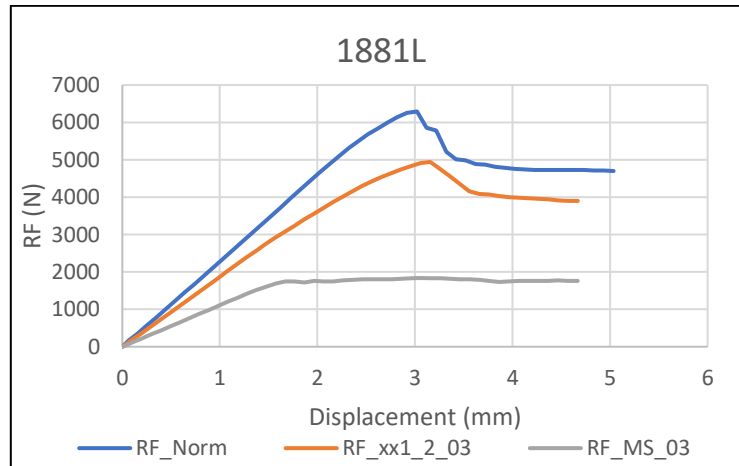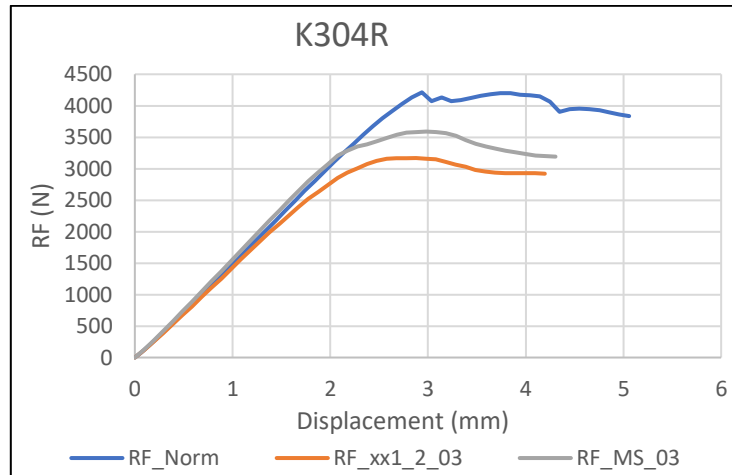
Figure 6.3: Force-displacement curve of the patient implemented with the automatic segmentation obtained by the combination of the automatic segmentation 1xx and 2xx.

The reaction force differences were 21.48% for the automatic segmentation 1xx-2xx and was 71.29% for the manual segmentation.

In this patient there was a very high difference between the results of the reaction forces between the automatic and manual segmentation. In fact, in the manual segmentation 4% more elements were involved in the metastases than in the automatic segmentation. The difference in mean bone mineral density of the metastatic elements was much higher in the manual segmentations compared to the automatic segmentation.

The Dice coefficient showed that the manual segmentation and the automatic segmentation overlapped for about 17%. This means that the deep learning algorithm was not able to detect all the metastasis in this patient. This probably caused the differences between the manual and automatic segmentations and could also cause a difference on the prediction of the fracture risk.
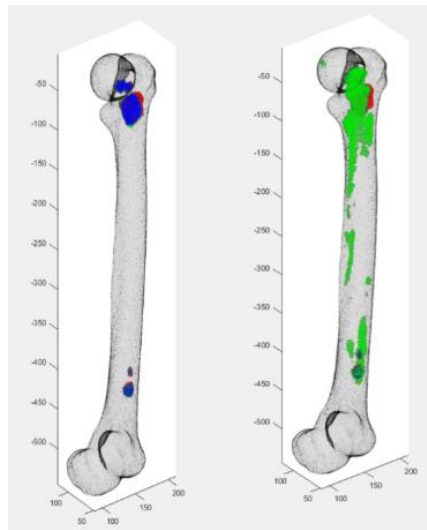
6.1.2 Patient K110R
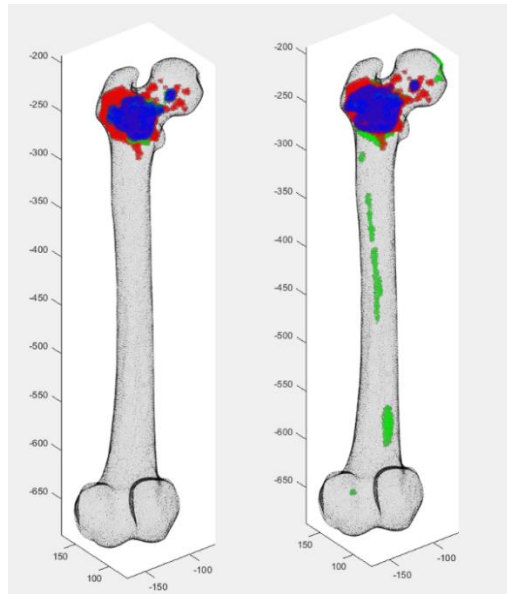
Figure 6.4: ■ Automatic segmentation ■ Manual segmentation ■ Overlap between MS and AS

For the all dataset (AD) segmentation the Dice coefficient obtained were equal to 65.30% (2D) and 64.25% (3D with threshold 0.3).

For the segmentation obtained by the combination of the segmentation 1xx and 2xx the Dice coefficient obtained were equal to 41.82% (2D) and 53.44% (3D with threshold 0.3).
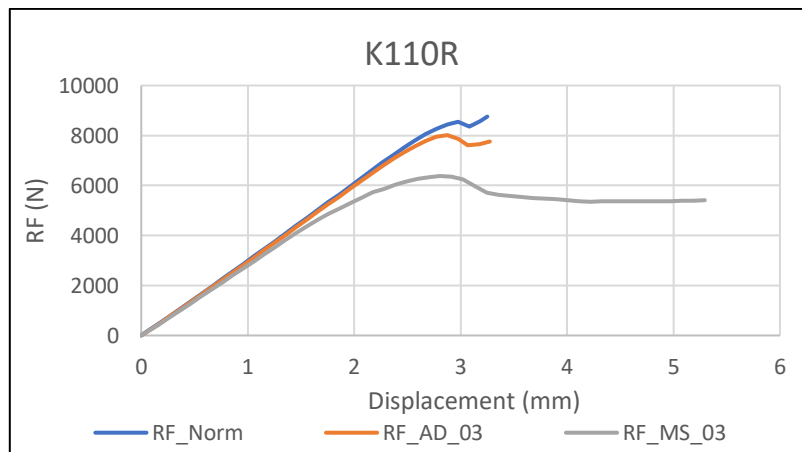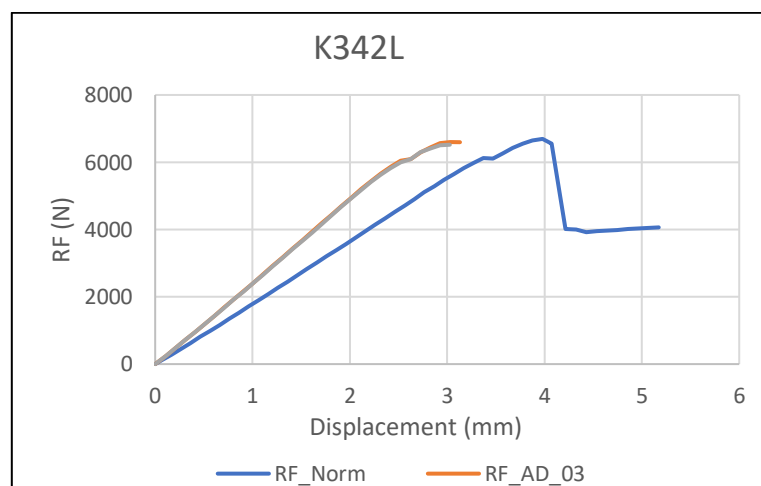

Figure 6.5: Force-displacement curve of the patient implemented with the automatic segmentation trained with all dataset.

The reaction force differences were 8.49% for the automatic segmentation AD and was 24.16% for the manual segmentation.

In this patient there was a low difference between the results of the reaction forces between the automatic and manual segmentation. In fact, in the manual segmentation 5% more elements were involved in the metastases than in the automatic segmentation. The difference in mean bone mineral density of the metastatic elements was slightly higher in the manual segmentations compared to the automatic segmentation.

The Dice coefficient showed that the manual segmentation and the automatic segmentation overlapped for about 65%. This means that the deep learning algorithm was not able to detect all the metastasis in this patient. This probably caused the differences between the manual and automatic segmentations and could also cause a difference on the prediction of the fracture risk.
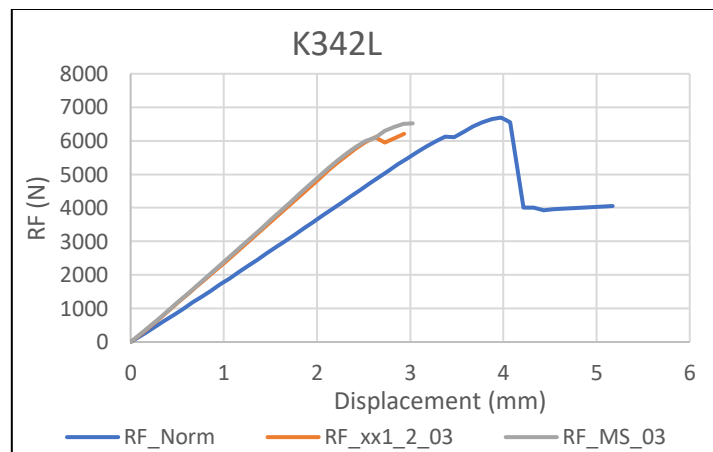

Figure 14: Force-displacement curve of the patient implemented with the automatic segmentation obtained by the combination fo the automatic segmentation 1xx and 2xx.

The reaction force differences were 13.33% for the automatic segmentation 1xx-2xx and was 24.16% for the manual segmentation.

In this patient there was a very low difference between the results of the reaction forces between the automatic and manual segmentation. The elements involved were very similar between the two segmentations. Also, the bone mineral density was very similar between the two segmentations.

The Dice coefficient showed that the manual segmentation and the automatic segmentation overlapped for about 55%. This means that the deep learning algorithm was not able to detect all the metastasis in this patient. This probably caused the differences between the manual and automatic segmentations and could also cause a difference on the prediction of the fracture risk.
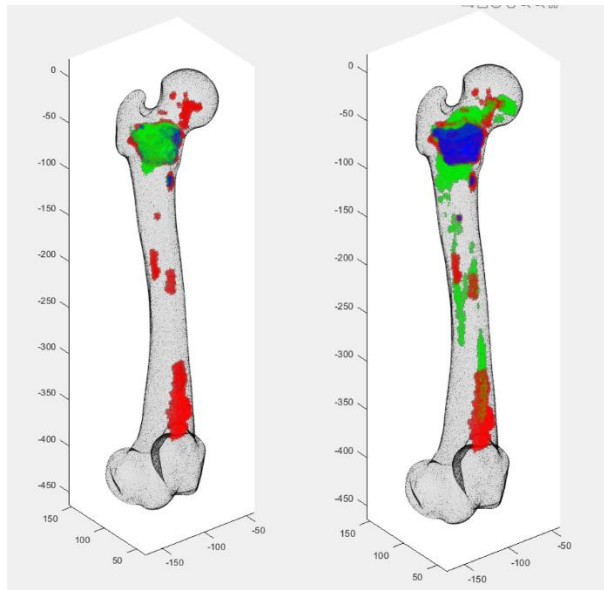
6.1.3 Patient K117R
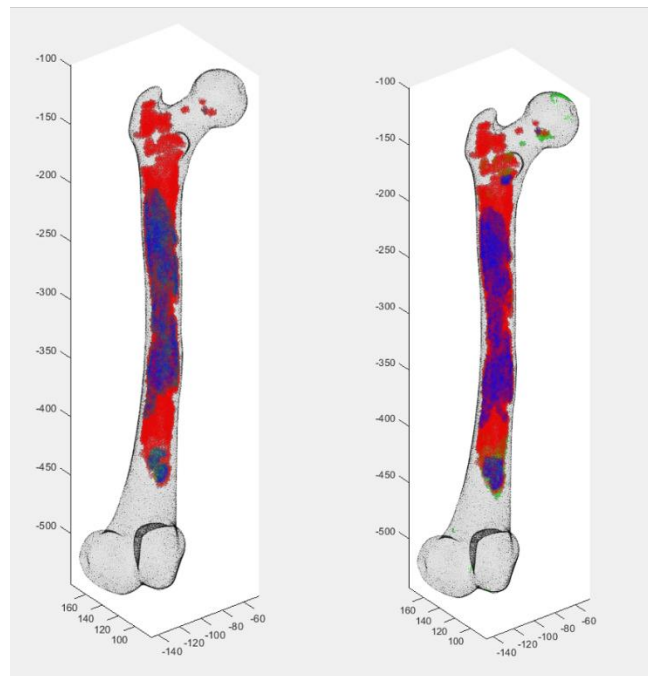
Figure 6.7: ■ Automatic segmentation ■ Manual segmentation ■ Overlap between MS and AS

For the all dataset (AD) segmentation the Dice coefficient obtained were equal to 51.51% (2D) and 52.00% (3D with threshold 0.3).
For the segmentation obtained by the combination of the segmentation 1xx and 2xx the Dice coefficient obtained were equal to 32.43% (2D) and 45.63% (3D with threshold 0.3).
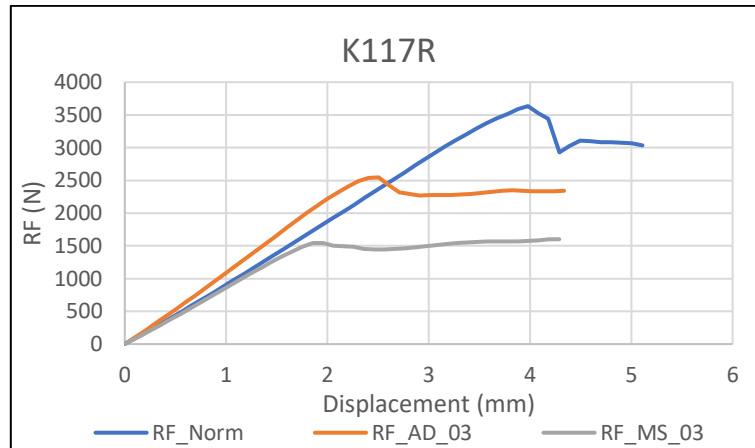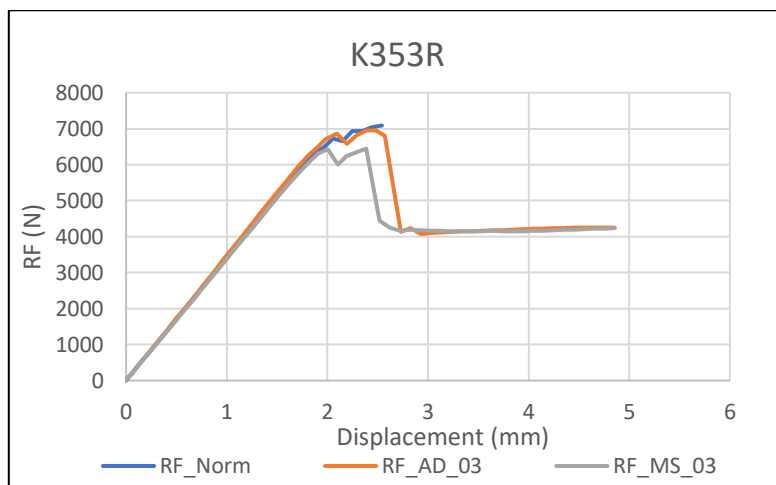
Figure 6.8: Force-displacement curve of the patient implemented with the automatic segmentation trained with all dataset.

The reaction force differences were 29.94% for the automatic segmentation AD and was 57.49% the manual segmentation.

In this patient there was a very high difference between the results of the reaction forces between the automatic and manual segmentation. In fact, in the manual segmentation 8% more elements were involved in the metastases than in the automatic segmentation. The difference in mean bone mineral density of the metastatic elements was much higher in the manual segmentations compared to the automatic segmentation.

The Dice coefficient showed that the manual segmentation and the automatic segmentation overlapped for about 52%. This means that the deep learning algorithm was not able to detect all the metastasis in this patient. This probably caused the differences between the manual and automatic segmentations and could also cause a difference on the prediction of the fracture risk.
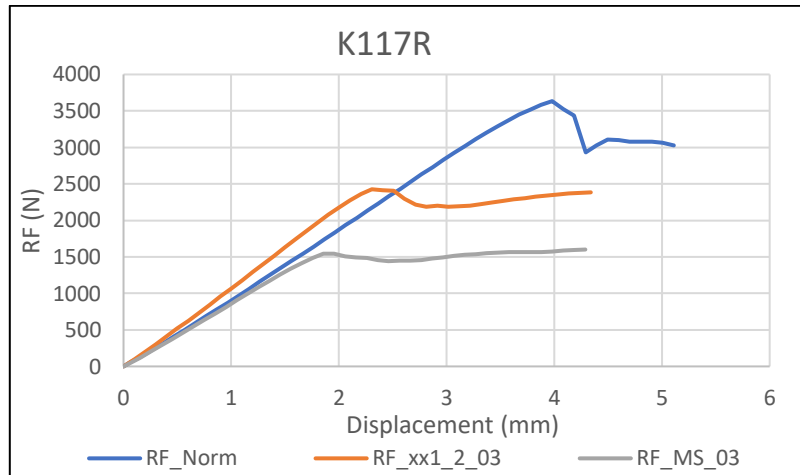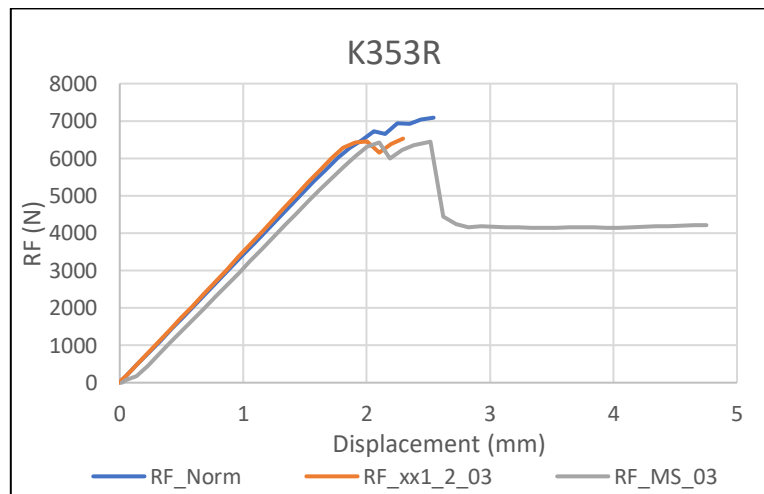
Figure 15: Force-displacement curve of the patient implemented with the automatic segmentation obtained by the combination fo the automatic segmentation 1xx and 2xx.

The reaction force differences were 33.86% for the automatic segmentation 1xx-2xx and was 57.49% for the manual segmentation.

In this patient there was a very high difference between the results of the reaction forces between the automatic and manual segmentation. In fact, in the manual segmentation 5% more elements were involved in the metastases than in the automatic segmentation. The difference in mean bone mineral density of the metastatic elements was much higher in the manual segmentations compared to the automatic segmentation.

The Dice coefficient showed that the manual segmentation and the automatic segmentation overlapped for about 45%. This means that the deep learning algorithm was not able to detect all the metastasis in this patient. This probably caused the differences between the manual and automatic segmentations and could also cause a difference on the prediction of the fracture risk.
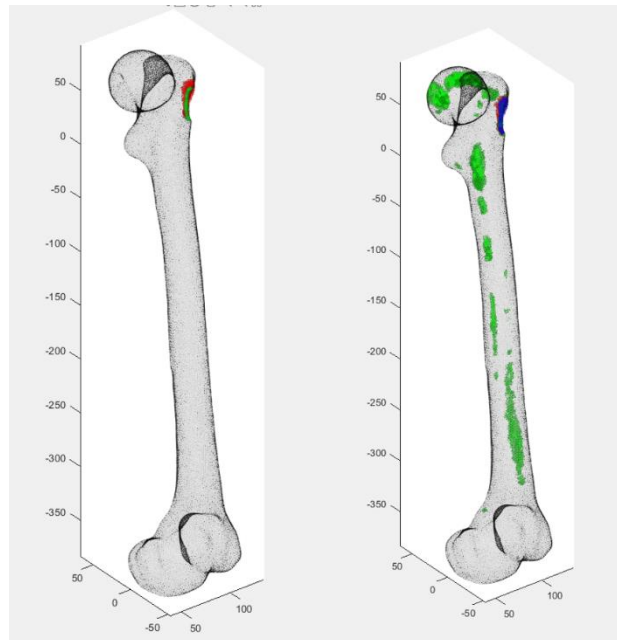
6.1.4 Patient K120L
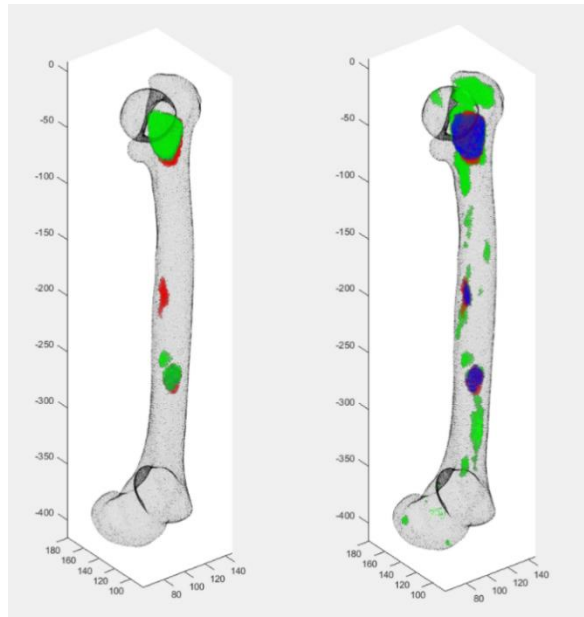
Figure 6.10: ■ Automatic segmentation ■ Manual segmentation ■ Overlap between MS and AS

For the all dataset (AD) segmentation the Dice coefficient obtained were equal to 79.36% (2D) and 79.49% (3D with threshold 0.3).

For the segmentation obtained by the combination of the segmentation 1xx and 2xx the Dice coefficient obtained were equal to 34.87% (2D) and 59.79% (3D with threshold 0.3).
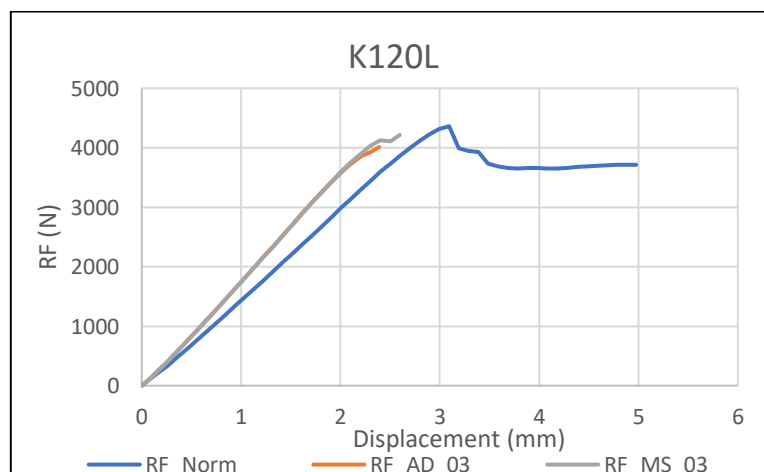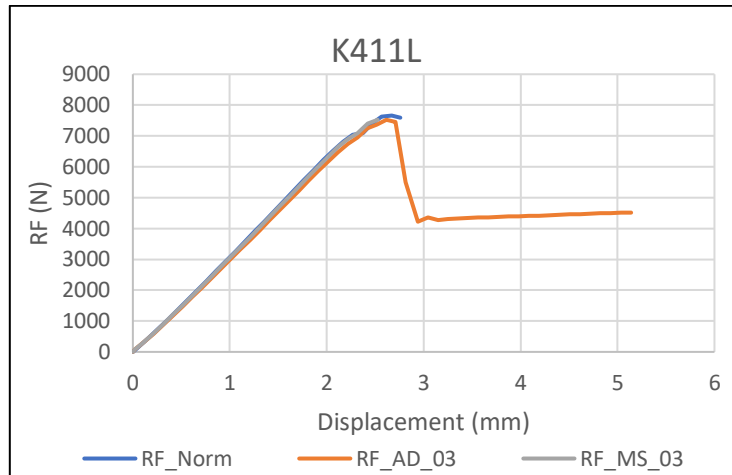

Figure 16: Force-displacement curve of the patient implemented with the automatic segmentation trained with all dataset.

The reaction force differences were 8.01% for the automatic segmentation AD and was 3.38% for the manual segmentation.

In this patient there was a small difference between the results of the reaction forces between the automatic and manual segmentation. The number of elements involved was very similar between the two segmentations. Also, the values of bone mineral density mean was very similar between the two segmentations

The Dice coefficient showed that the manual segmentation and the automatic segmentation overlapped for about 80%. The two segmentations were very similar also in the results, however in this case the algorithm considered a healthy bone tissue as a metastasis.
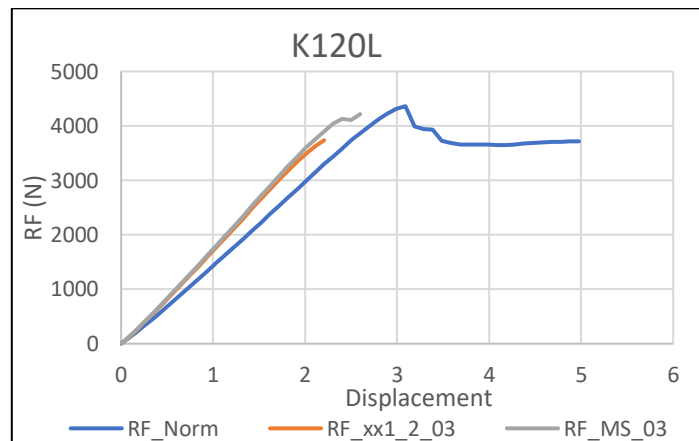
Figure 6.12: Force-displacement curve of the patient implemented with the automatic segmentation obtained by the combination fo the automatic segmentation 1xx and 2xx.

The reaction force differences were 14.36% for the automatic segmentation 1xx-2xx and was 3.38% for the manual segmentation.

In this patient there was a high difference between the results of the reaction forces between the automatic and manual segmentation. In fact, in the automatic segmentation 4% more elements were involved in the metastases than in the manual segmentation. The difference in mean bone mineral density of the metastatic elements was higher in the automatic segmentations compared to the manual segmentation.

The Dice coefficient showed that the manual segmentation and the automatic segmentation overlapped for about 60%. This means that the deep learning algorithm was not able to detect all the metastasis in this patient. This probably caused the differences

between the manual and automatic segmentations and could also cause a difference on the prediction of the fracture risk.

6.1.5 Patient K304R

Figure 6.13: ■ Automatic segmentation ■ Manual segmentation ■ Overlap between MS and AS

For the all dataset (AD) segmentation the Dice coefficient obtained were equal to 22.21% (2D) and 23.60% (3D with threshold 0.3).

For the segmentation obtained by the combination of the segmentation 1xx and 2xx the Dice coefficient obtained were equal to 6.29% (2D) and 10.68% (3D with threshold 0.3).

Figure 6.14: Force-displacement curve of the patient implemented with the automatic segmentation trained with all dataset.

The reaction force differences were 12.16% for the automatic segmentation AD and was 14.50% for the manual segmentation.

In this patient there was a very low difference between the results of the reaction forces between the automatic and manual segmentation. In fact, in the manual segmentation 1% more elements were involved in the metastases than in the automatic segmentation. The values of bone mineral density mean were very similar between the segmentations.

The Dice coefficient showed that the manual segmentation and the automatic segmentation overlapped for about 25%. This means that the deep learning algorithm considered wrongly some healthy bone as a bone metastasis. This probably caused the differences between the manual and automatic segmentations and could also cause a difference on the prediction of the fracture risk.

Figure 6.15: Force-displacement curve of the patient implemented with the automatic segmentation obtained by the combination fo the automatic segmentation 1xx and 2xx.

The reaction force differences were 32.92% for the automatic segmentation 1xx-2xx and was 14.50% for the manual segmentation.

In this patient there was a high difference between the results of the reaction forces between the automatic and manual segmentation. In fact, in the automatic segmentation 5% more elements were involved in the metastases than in the manual segmentation. The difference in mean bone mineral density of the metastatic elements was slightly higher in the automatic segmentations compared to the manual segmentation.

The Dice coefficient showed that the manual segmentation and the automatic segmentation overlapped for about 10%. This means that the deep learning algorithm considered wrongly some healthy bone tissue with metastasis. This probably caused the differences between the manual and automatic segmentations and could also cause a difference on the prediction of the fracture risk.

6.1.6 Patient 342L

Figure 6.16: ■ Automatic segmentation ■ Manual segmentation ■ Overlap between MS and AS

For the all dataset (AD) segmentation the Dice coefficient obtained were equal to 76.57% (2D) and 76.46% (3D with threshold 0.3).

For the segmentation obtained by the combination of the segmentation 1xx and 2xx the Dice coefficient obtained were equal to 15.73% (2D) and 37.81% (3D with threshold 0.3).

Figure 17: Force-displacement curve of the patient implemented with the automatic segmentation trained with all dataset.

The reaction force differences were 1.47% for the automatic segmentation AD and was 2.59% for the manual segmentation.

In this patient there was a very low difference between the results of the reaction forces between the automatic and manual segmentation. The two segmentations had a very similar volume percentage. Also, the difference in bone mineral density mean was very low.

The Dice coefficient showed that the manual segmentation and the automatic segmentation overlapped for about 80%. The two segmentations were very similar but that the deep learning algorithm still was not able to detect completely the metastasis in this patient.

Figure 6.18: Force-displacement curve of the patient implemented with the automatic segmentation obtained by the combination fo the automatic segmentation 1xx and 2xx.

The reaction force differences were 7.80% for the automatic segmentation 1xx-2xx and was 2.59% for the manual segmentation.

In this patient there was a low difference between the results of the reaction forces between the automatic and manual segmentation. In fact, in the manual segmentation 5% more elements were involved in the metastases than in the automatic segmentation. The difference in mean bone mineral density of the metastatic elements was much higher in the manual segmentations compared to the automatic segmentation.

The Dice coefficient showed that the manual segmentation and the automatic segmentation overlapped for about 37%. In this case the algorithm considered some healthy bone as metastasis.

6.1.7 Patient K353R

Figure 6.19: ■ Automatic segmentation   ■ Manual segmentation   ■ Overlap between manual and automatic segmentation

For the all dataset (AD) segmentation the Dice coefficient obtained were equal to 65.40% (2D) and 62.61% (3D with threshold 0.3).

For the segmentation obtained by the combination of the segmentation 1xx and 2xx the Dice coefficient obtained were equal to 29.4% (2D) and 41.95% (3D with threshold 0.3).

Figure 6.20: Force-displacement curve of the patient implemented with the automatic segmentation trained with all dataset

The reaction force differences were 1.93% for the automatic segmentation AD and was 7.90% for the manual segmentation.

In this patient there was a low difference between the results of the reaction forces between the automatic and manual segmentation. In fact, in the manual segmentation 2% more elements were involved in the metastases than in the automatic segmentation. The difference in mean bone mineral density of the metastatic elements was much higher in the manual segmentations compared to the automatic segmentation.

The Dice coefficient showed that the manual segmentation and the automatic segmentation overlapped for about 62%. This means that the deep learning algorithm was not able to detect all the metastasis in this patient. This probably caused the differences between the manual and automatic segmentations and could also cause a difference on the prediction of the fracture risk.

Figure 6.21: Force-displacement curve of the patient implemented with the automatic segmentation obtained by the combination fo the automatic segmentation 1xx and 2xx.

The reaction force differences were 33.86% for the automatic segmentation 1xx-2xx and was 57.49% for the manual segmentation.

In this patient there was a very high difference between the results of the reaction forces between the automatic and manual segmentation. In fact, in the automatic segmentation 2% more elements were involved in the metastases than in the manual segmentation. The difference in mean bone mineral density of the metastatic elements was much higher in the manual segmentations compared to the automatic segmentation.

The Dice coefficient showed that the manual segmentation and the automatic segmentation overlapped for about 40%. This means that the deep learning algorithm was not able to detect all the metastasis in this patient. This probably caused the differences between the manual and automatic segmentations and could also cause a difference on the prediction of the fracture risk.

6.1.8 Patient K411L

Figure 6.22: ■ Automatic segmentation ■ Manual segmentation ■ Overlap between MS and AS

For the all dataset (AD) segmentation the Dice coefficient obtained were equal to 52.63% (2D) and 31.43% (3D with threshold 0.3).
For the segmentation obtained by the combination of the segmentation 1xx and 2xx the Dice coefficient obtained were equal to 15.63% (2D) and 18.85% (3D with threshold 0.3).

Figure 6.23: Force-displacement curve of the patient implemented with the automatic segmentation trained with all dataset.

The reaction force differences were 3.35% for the automatic segmentation and was 1.38%. for the manual segmentation, respectively.

In this patient there was a very high difference between the results of the reaction forces between the automatic and manual segmentation. The difference in volume percentage was very low between the segmentations. Also, the difference in mean bone mineral density of the metastatic elements was very similar.

The Dice coefficient showed that the manual segmentation and the automatic segmentation overlapped for about 30%. This means that the deep learning algorithm was not able to detect all the metastasis in this patient.
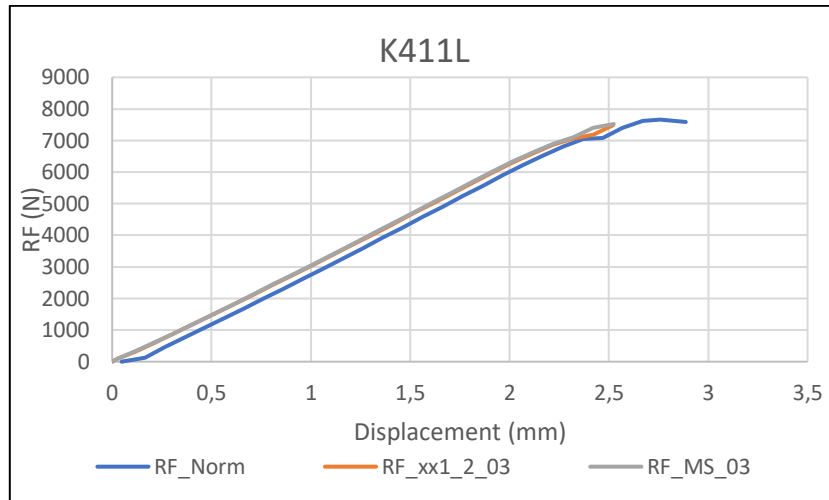
Figure 6.24: Force-displacement curve of the patient implemented with the automatic segmentation obtained by the combination fo the automatic segmentation 1xx and 2xx.

The reaction force differences were 2.32% for the automatic segmentation 1xx-2xx and was 1.38% for the manual segmentation.

In this patient there was a very high difference between the results of the reaction forces between the automatic and manual segmentation. In fact, in the automatic segmentation 1% more elements were involved in the metastases than in the manual segmentation. The difference in mean bone mineral density of the metastatic elements was much higher in the automatic segmentations compared to the manual segmentation.

The Dice coefficient showed that the manual segmentation and the automatic segmentation overlapped for about 18. In this case the algorithm considered wrongly some portions of healthy bone tissue as metastasis.

6.1.9 Summary

RF diff percentage	Manual segmentation	Automatic segmentation AD
1181L	71.29%	13.31%
K110R	24.16%	8.49%
K117R	57.49%	29.94%
K120L	3.38%	8.01%
K304R	14.50%	12.16%
K342L	2.59%	1.47%
K353R	9.07%	1.93%
K411L	1.38%	3.35%

Table 6.1: Difference in reaction force between the standard finite element model and the model implemented with the automatic segmentation AD and the manual segmentation.

RF diff percentage	Manual segmentation	Automatic segmentation 1xx-2xx
1181L	71.29%	21.48%
K110R	24.16%	11.31%
K117R	57.49%	33.86%
K120L	3.38%	14.36%
K304R	14.50%	32.92%
K342L	2.59%	47.80%
K353R	9.07%	7.90%
K411L	1.38%	2.32%

Table 6.2: Difference in reaction force between the standard finite element model and the model implemented with the automatic segmentation 1xx-2xx and the manual segmentation.

Dice coefficient AD	Dice 2D	Dice 3D
1181L	32.63%	32.91%
K110R	65.30%	64.25%
K117R	51.51%	52.00%
K120L	79.36%	79.49%
K304R	22.21%	23.60%
K342L	76.37%	74.46%
K353R	65.40%	65.61%
K411L	52.63%	31.43%

Table 6.3: The Dice coefficient obtained from the voxels (2D) and from the element (3D) of the all eight patients.

Dice coefficient 1xx-2xx	Dice 2D	Dice 3D
1181L	14.06%	16.71%
K110R	41.82%	53.44%
K117R	32.43%	45.63%
K120L	34.87%	59.79%
K304R	6.29%	10.68%
K342L	15.73%	37.81%
K353R	29.40%	41.95%
K411L	15.63%	18.85%

Table 6.4: The Dice coefficient obtained from the voxels (2D) and from the element (3D) of the all eight patients.

BMD mean	Manual segmentation	Automatic segmentation AD
1181L	674	361
K110R	122	79
K117R	420	293
K120L	105	89
K304R	297	270
K342L	93	97
K353R	249	64
K411L	186	200

Table 4: Bone mineral density mean between the standard finite element model and the model implemented with the automatic segmentation AD and the manual segmentation.

BMD mean	Manual segmentation	Automatic segmentation 1xx-2xx
1181L	674	429
K110R	122	128
K117R	420	330
K120L	105	180
K304R	297	356
K342L	93	285
K353R	249	158
K411L	186	453

Table 5: Bone mineral density mean between the standard finite element model and the model implemented with the automatic segmentation AD and the manual segmentation.

Volume %	Manual segmentation	Automatic segmentation AD
1181L	11.82%	4.68%
K110R	6.57%	3.62%
K117R	12.41%	4.76%
K120L	3.98%	3.40%
K304R	0.45%	1.63%
K342L	2.23%	1.56%
K353R	5.11%	3.60%
K411L	0.24%	0.07%

Table 6: Volume % between the standard finite element model and the model implemented with the automatic segmentation AD and the manual segmentation.

Volume %	Manual segmentation	Automatic segmentation 1xx-2xx
1181L	11.82%	7.13%
K110R	6.57%	6.20%
K117R	12.41%	7.19%
K120L	3.98%	7.72%
K304R	0.45%	5.34%
K342L	2.23%	4.40%
K353R	5.11%	6.77%
K411L	0.24%	1.86%

Table 7: Volume % between the standard finite element model and the model implemented with the automatic segmentation AD and the manual segmentation.

6.2 Analysis of the results

6.2.1 Ranking analysis
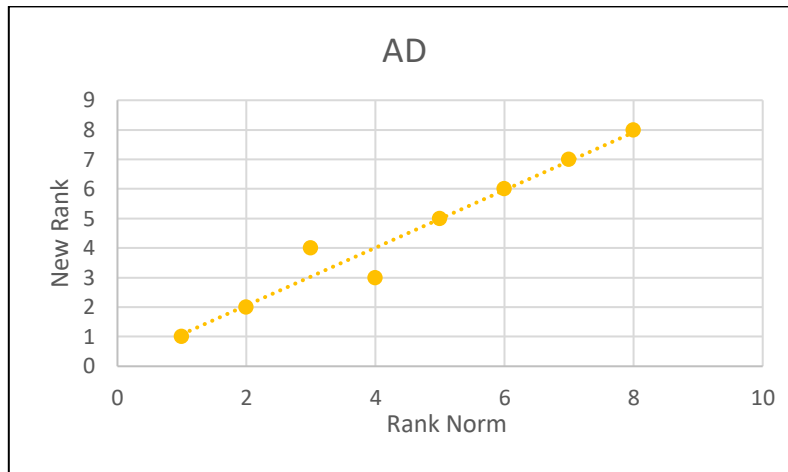
Figure 6.25: Difference between the ranking of the reaction forces obtained in the standard model and the model implemented with the segmentation trained with all dataset.

In the case of the all dataset segmentation, the ranking was very similar to the standard model. There were just two positions that switched. A similar situation was found in the 1xx-2xx segmentation.
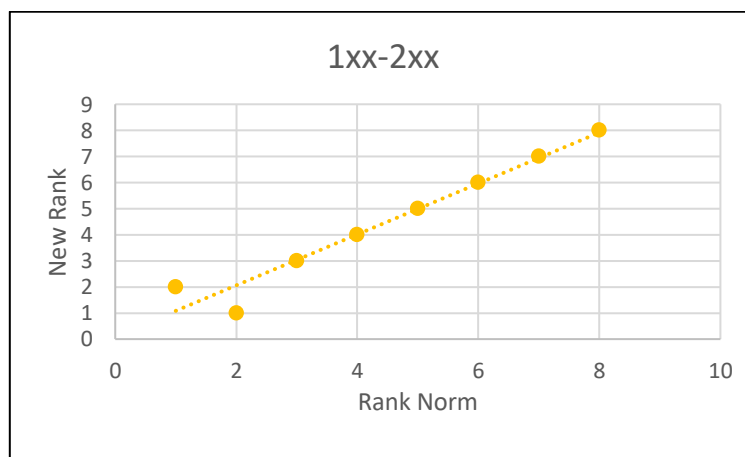
Figure 6.26: Difference between the ranking of the reaction forces obtained in the standard model and the model implemented with the segmentation trained with the combination of the segmentation 1xx-2xx.

Also, in this case there were two samples that switched their position. The results obtained in these two segmentations were different from the results obtained in the manual segmentation. In fact, in the manual segmentation the new ranking changed in a huge way. There were not only sample that just switch the position, but the changes were more important.

6.2.2 Dice coefficient and difference in reaction force

The relation between Dice coefficient and the difference in reaction force did not show any relation between the features in both the segmentations.
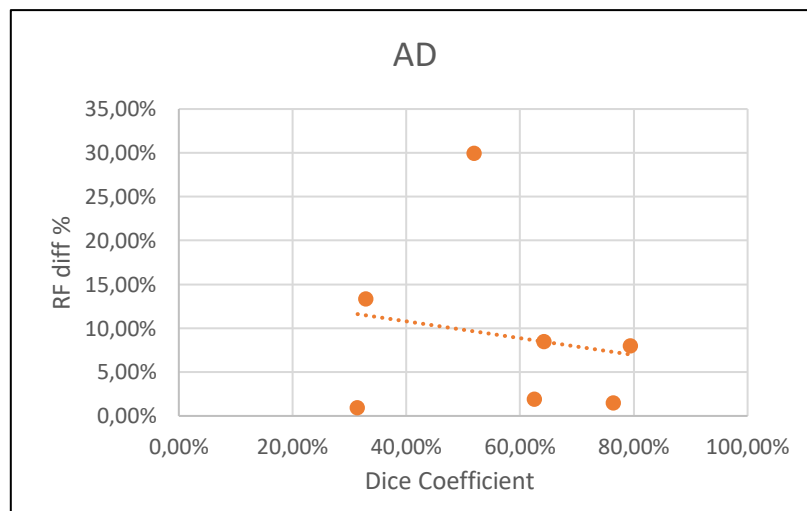
Figure 6.27: The variation of the difference in reaction force with respect to the Dice coefficient.
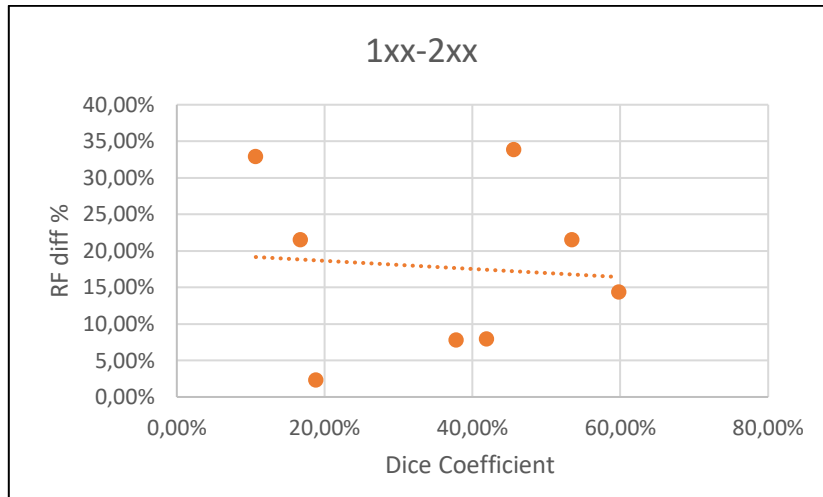
Figure 18: The variation of the difference in reaction force with respect to the Dice coefficient.

6.2.3 BOS score

In each segmentation, two sets were created the fractured set and the non-fractured set. In the manual segmentations, there was one patient in the non-fractured that has the ratio below the highest value of the fractured set. Excluded this patient, the difference between the ratio of the highest value of the fractured set and the ratio immediately higher in the non-fractured set was 2.8.

In the segmentations implemented with all the dataset, there was one patient in the non-fractured set that was wrongly classified as a high risk patient. Excluded this patient, the difference between the BOS score of the highest value of the fractured set and the lowest one in the non-fractured set was 0.31.
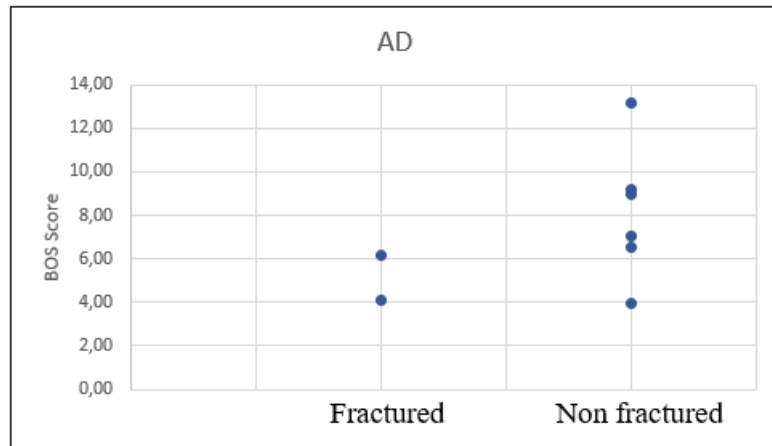
Figure 6.29: The graphs show how the ratio between reaction force and body weight was related to a future fracture of the patient. Two sets have been considered, the fractured set and the non-fractured set. These results were obtained by the model trained with the segmentation trained by all the dataset.

In the 1xx-2xx segmentations, there was one patient in the non-fractured set that was wrongly classified as a high risk patient. Excluded this patient, the difference between the BOS score of the highest value of the fractured set and the lowest one in the non-fractured set was 0.45.
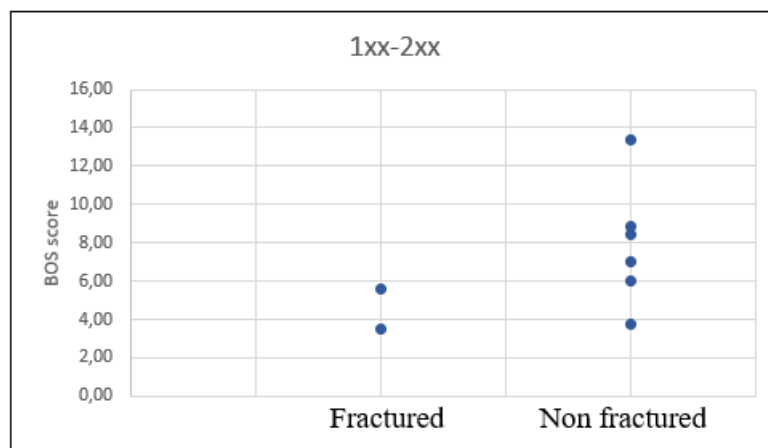
Figure 19: The graphs show how the ratio between reaction force and body weight was related to a future fracture of the patient. Two sets have been considered, the fractured set and the non-fractured set. These results were obtained by the model trained with the segmentation obtained by the combination of the 1xx segmentation and the 2xx segmentation.

6.2.4 Relation between the bone mineral density and difference in reaction force

No relation between the bone mineral density mean and the difference in reaction force was found in both the segmentations. In one case it was possible to see a growing trend but there were a lot of samples that were placed not close to the trendline.
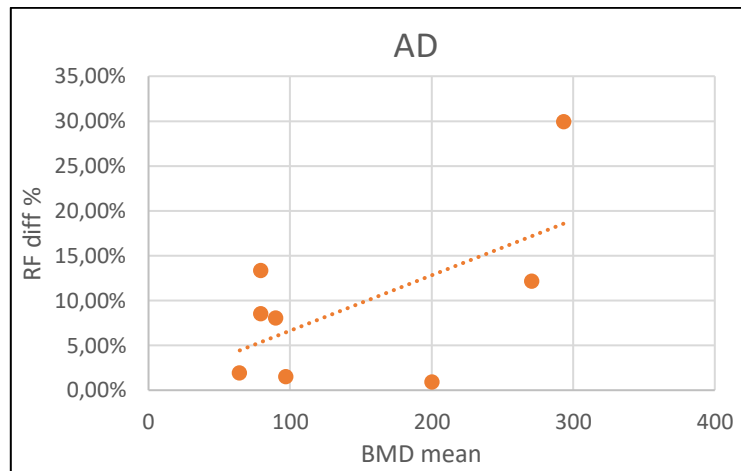
Figure 6.31: Relation between the bone mineral density mean of the element set to zero and the difference in reaction force. The model was obtained with segmentation trained with all the dataset.
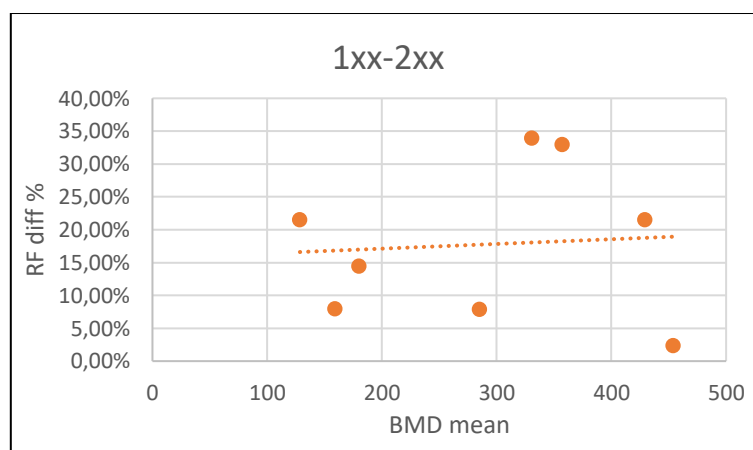
Figure 20: Relation between the bone mineral density mean of the element set to zero and the difference in reaction force. The model as obtained with segmentation trained with the combination of the segmentation 1xx and 2xx.

6.2.5 Relation between the metastatic volume and difference in reaction force

There was a growing trend in the relation between the volume percentage. This trend was not strict, there were many values that were placed far from the trendline. So, also in this case no relation was found.
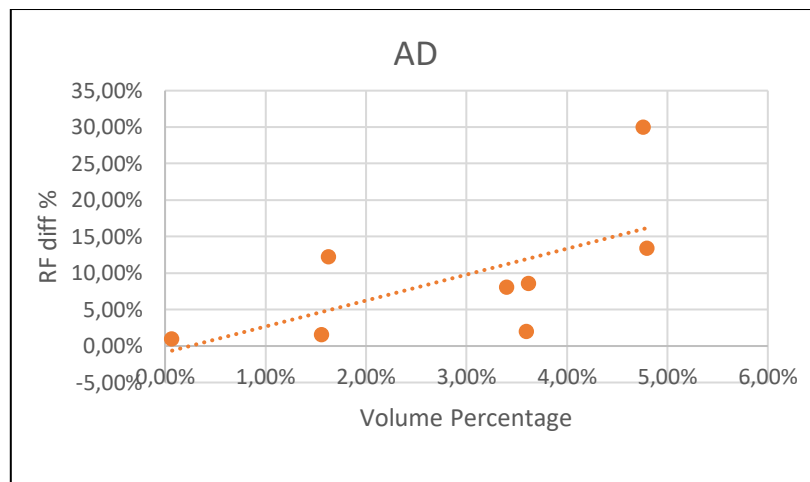
Figure 6.33: Relation between the number element set to zero over the all number of element and the difference in reaction force. The model was obtained with segmentation trained with all the dataset.
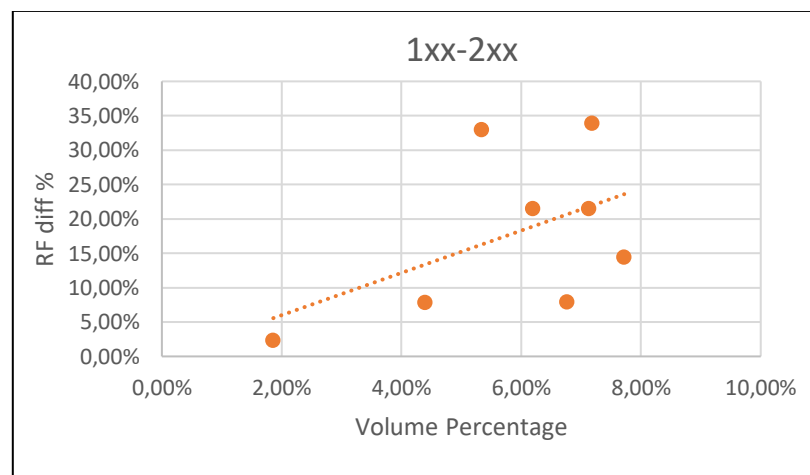
Figure 6.34: Relation between the number element set to zero over the all number of element and the difference in reaction force. The model was obtained with segmentation trained with the combination of the segmentation 1xx and 2xx.

Chapter 7:
The blastic metastasis

Analysis on the best way to implement the material properties of the blastic metastasis in a finite element model.

7.1 The Young's modulus in the blastic metastasis

The aim of this section was to find the best way to adapt the material properties of the blastic metastasis to correct for the overestimation of the bone strength by the FE model. The results of the nanoindentations tests proved that the blastic metastasis have a Young's modulus reduced of 5.8% with respect to the healthy bone [22]. To change the Young's modulus in a similar way, we changed the bone mineral density in our finite element model, because from that the ash density was calculated and from that the elastic modulus was computed. A Matlab's script that modified the calcium file to reduce the bone mineral density in the exact amount to reduce the Young's modulus of 5.8% was written. Next, the simulations were run.

7.1.1 Patient 1031L
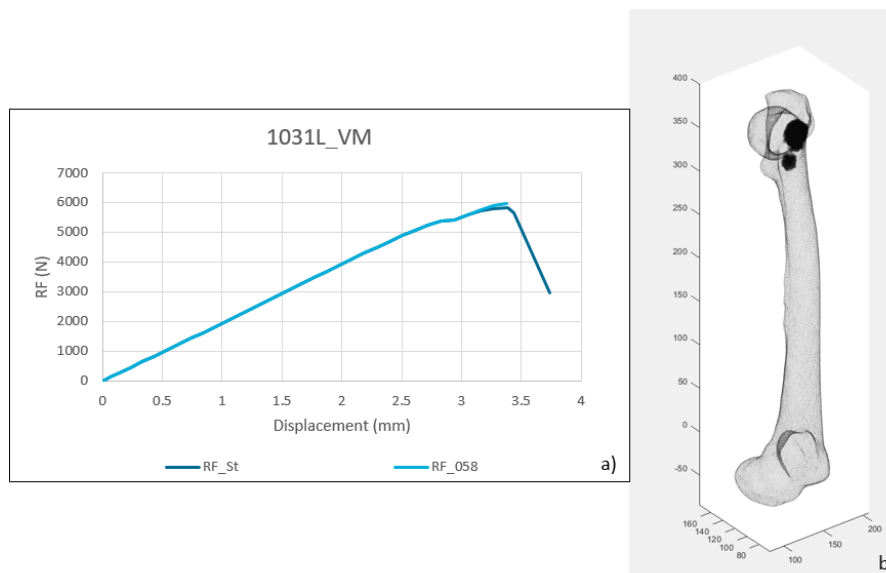
Figure 7.1: a) Force-displacement curve of the standard model and the model with the Young's modulus decreased of 5.8%. b) Disposition of the metastasis in the femur.

In this patient, the metastasis occupied the 0.98% of the volume of the femur. The bone mineral density had an original value of 411.49 $\frac{mg}{cm^3}$ and after the Young's modulus reduction of the bone mineral density was 396.16 $\frac{mg}{cm^3}$. The original Young's modulus

was 3.078 10^3 Mpa and was reduced to 2.899 10^3 Mpa. The difference in reaction force between the two models was -2.95%.

7.1.2 Patient 1061R
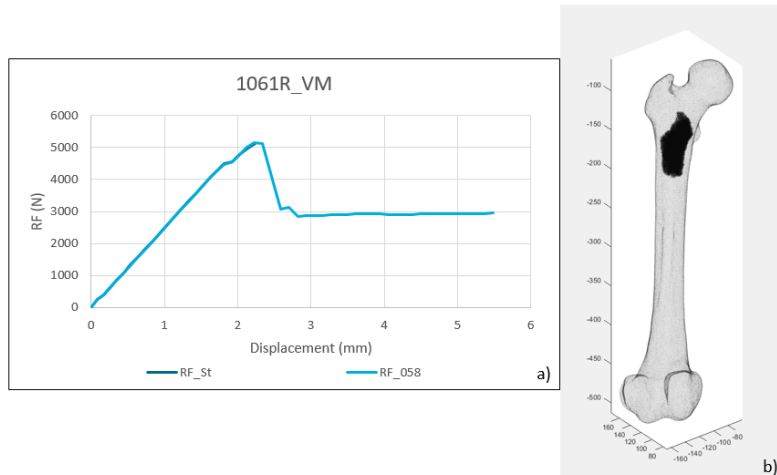
Figure 7.2: a) Force-displacement curve of the standard model and the model with the Young's modulus decreased of 5.8%. b) Disposition of the metastasis in the femur.

In this patient, the metastasis occupied the 2.21% of the volume of the femur. The bone mineral density had an original value of 725.53 $\frac{mg}{cm^3}$ and after the Young's modulus reduction of the bone mineral density was 700.29 $\frac{mg}{cm^3}$. The original Young's modulus was 7.181 10^3 Mpa and was reduced to 7.361 10^3 Mpa. The difference in reaction force between the two models was -0.02%.

7.1.3 Patient 1151R
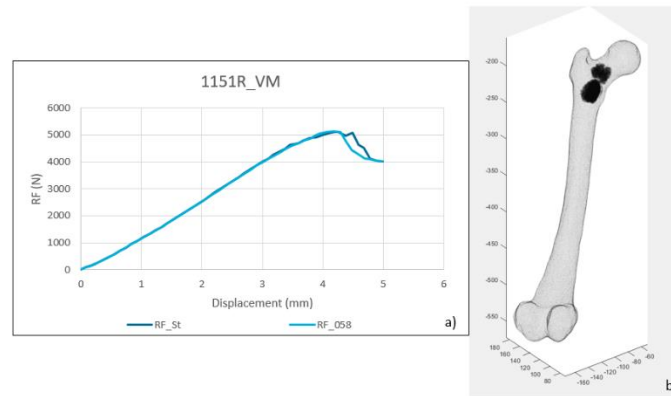
Figure 7.3: a) Force-displacement curve of the standard model and the model with the Young's modulus decreased of 5.8%. b) Disposition of the metastasis in the femur.

In this patient, the metastasis occupied the 0.62% of the volume of the femur. The bone mineral density had an original value of 455.51 $\frac{mg}{cm^3}$ and after the Young's modulus reduction of the bone mineral density was 388.52 $\frac{mg}{cm^3}$. The original Young's modulus was 3.62 10^3 Mpa and was reduced to 3.41 10^3 Mpa. The difference in reaction force between the two models was -2.95%.

7.1.4 Patient K123R
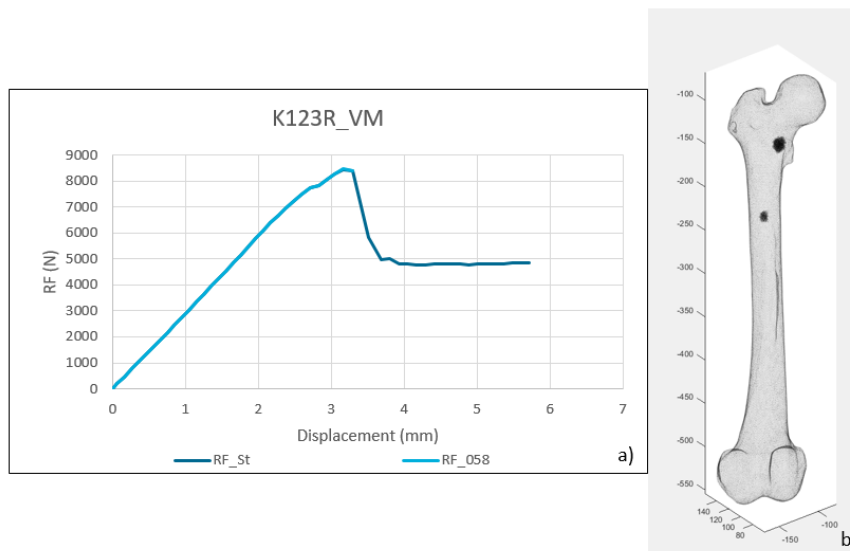
Figure 7.4: a) Force-displacement curve of the standard model and the model with the Young's modulus decreased of 5.8%. b) Disposition of the metastasis in the femur.

In this patient, the metastasis occupied the 0.08% of the volume of the femur. The bone mineral density had an original value of 682.09 $\frac{mg}{cm^3}$ and after the Young's modulus reduction of the bone mineral density was 659.92 $\frac{mg}{cm^3}$. The original Young's modulus was 7.03 10^3 Mpa and was reduced to 6.68 10^3 Mpa. The difference in reaction force between the two models was -0.03%.

7.1.5 Patient K326R
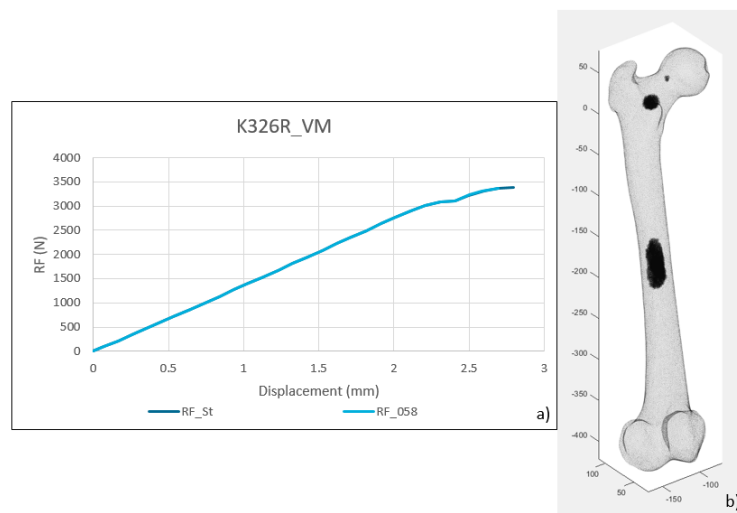
Figure 21: a) Force-displacement curve of the standard model and the model with the Young's modulus decreased of 5.8%. b) Disposition of the metastasis in the femur.

In this patient, the metastasis occupied the 0.94% of the volume of the femur. The bone mineral density had an original value of 472.81 $\frac{mg}{cm^3}$ and after the Young's modulus reduction of the bone mineral density was 455.55 $\frac{mg}{cm^3}$. The original Young's modulus was 3.84 10^3 Mpa and was reduced to 3.62 10^3 Mpa. The difference in reaction force between the two models was 0.55%.

7.1.6 Patient K352L
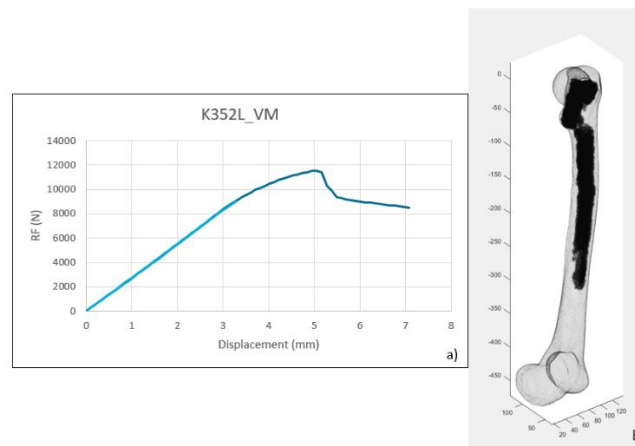
Figure 22: a) Force-displacement curve of the standard model and the model with the Young's modulus decreased of 5.8%. b) Disposition of the metastasis in the femur.

In this patient, the metastasis occupied the 9.49% of the volume of the femur. The bone mineral density had an original value of 601.94 $\frac{mg}{cm^3}$ and after the Young's modulus reduction of the bone mineral density was 584.65 $\frac{mg}{cm^3}$. The original Young's modulus was 5.71 10^3 Mpa and was reduced to 5.38 10^3 Mpa. The difference in reaction force between the two models was -2.95%.

7.1.7 Analysis of the results

Using this technique, the material properties did not, or only slightly decrease. This means that the reduction in the Young's modulus was not large enough to make a difference.

7.2 Young's modulus reduction

For this reason, another analysis was carried on. The Young's modulus was decreased from 5.8% to 95% in 5% steps for each femur to understand which the right percentage was to decrease the Young's modulus. A constant increase of the difference in reaction force with the decreasing of the Young's modulus was expected.

7.2.1 Patient 1031L
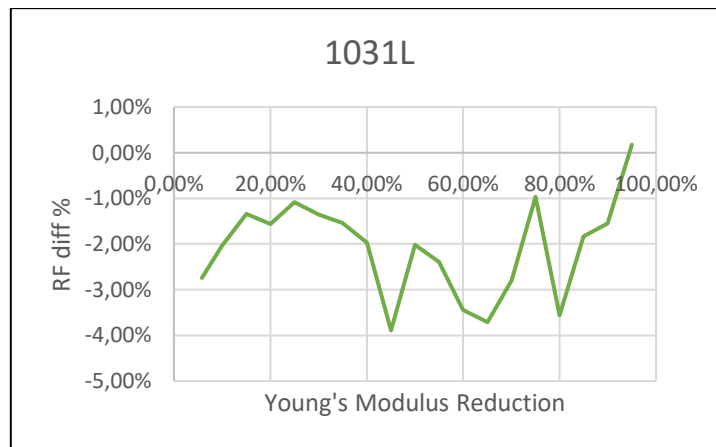
Figure 23: Variation of the difference in reaction force with respect to the Young's modulus.

In this case, the results were not as expected. In many cases, the models had a higher strength than the standard model. Moreover, there was no growing trend between a lower Young's modulus and the difference in reaction force.

7.2.2 Patient 1061R
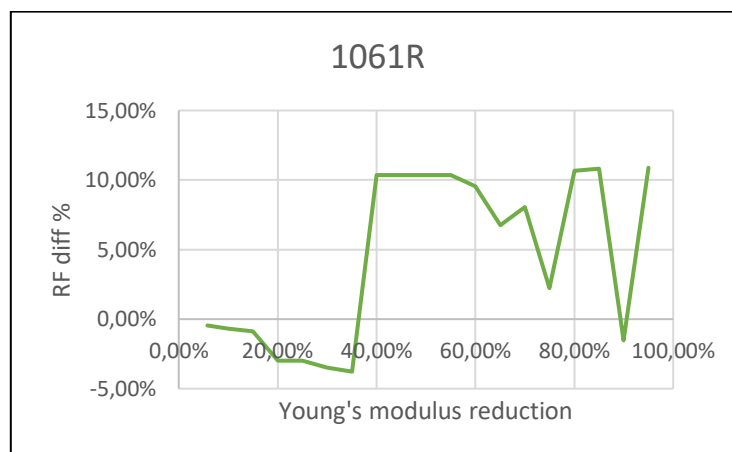
Figure 7.8: Variation of the difference in reaction force with respect to the Young's modulus.

In this case, the results were not as expected. In many cases, the models had a higher strength than the standard model when the modulus were reduced less. Moreover, there

was no growing trend between a lower Young's modulus and the difference in reaction force.

7.2.3 Patient 1151R
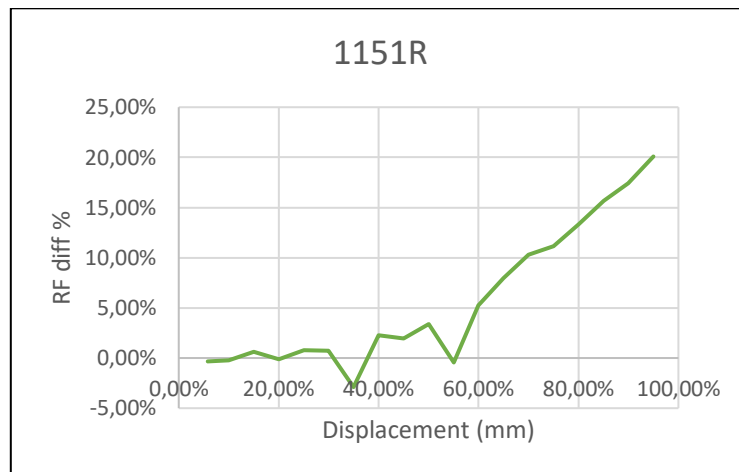
Figure 7.9: Variation of the difference in reaction force with respect to the Young's modulus.

In this case, the results were as expected. In two cases, the models had a lower resistance than the standard model. Moreover, there was a growing trend. The two results that departed from the trend but that can be due to numerical errors of the model.

7.2.4 Patient K123R
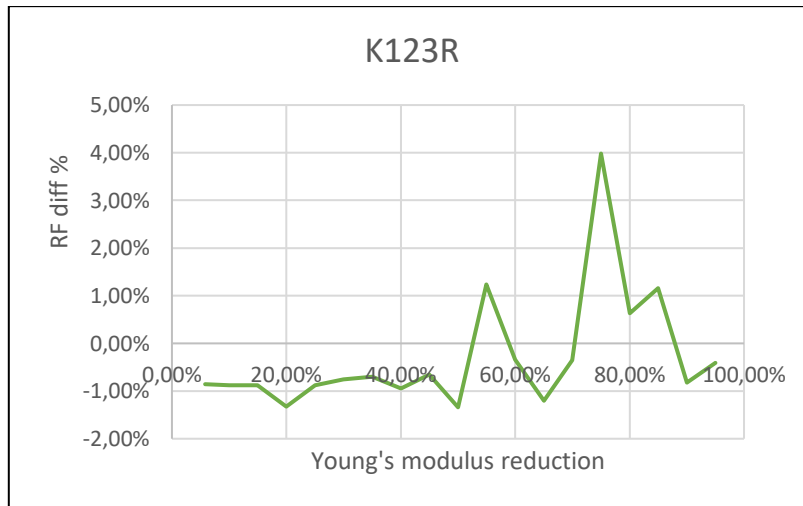
Figure 7.10: Variation of the difference in reaction force with respect to the Young's modulus.

In this case, the results were not as expected. In many cases, the models had a higher strength than the standard model. Moreover, there was no growing trend between a lower Young's modulus and the difference in reaction force.

7.2.5 Patient K326R
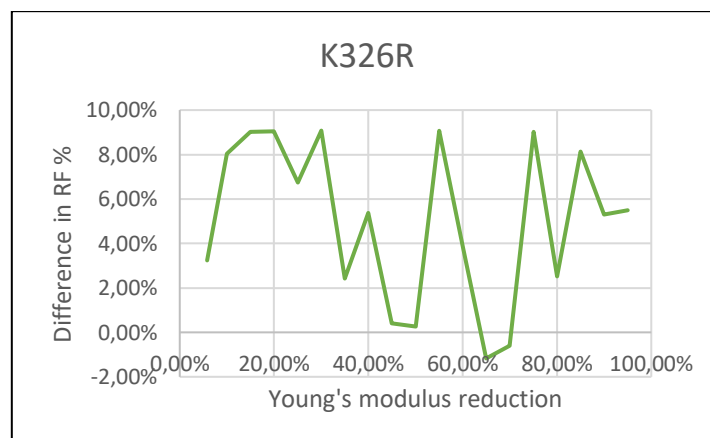
Figure 7.11: Variation of the difference in reaction force with respect to the Young's modulus.

In this case, the results were not as expected. In many cases, the models had a higher strength than the standard model. Moreover, there was no growing trend between a lower Young's modulus and the difference in reaction force.

7.2.6 Patient K352L
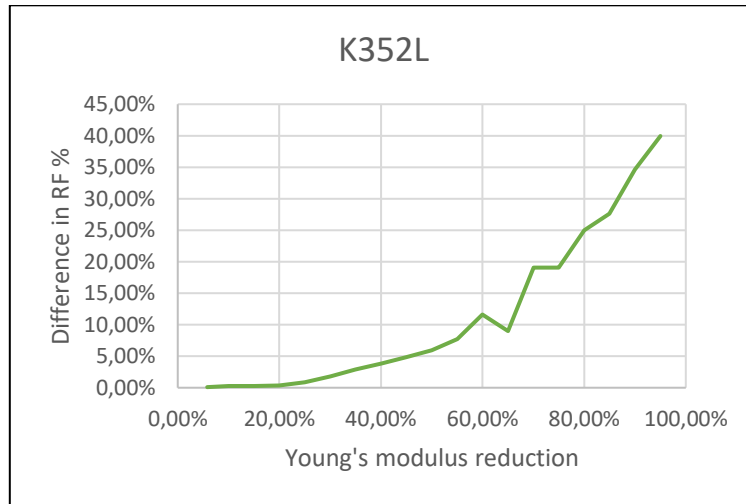
Figure 7.1224: Variation of the difference in reaction force with respect to the Young's modulus.

In this case, the results were as expected. In two cases, the models had a lower resistance than the standard model. Moreover, there was a growing trend. The two results that departed from the trend but that can be due to numerical errors of the model.

7.3 Conclusion

We expected that a reduction in the Young's modulus would result in a reduction of the rection force difference percentage. Patient K352 mostly showed this behavior. This patient had large metastatic lesions spread throughout the femur. Patient 1151R showed a similar behavior when the reduction of the Young's modulus was lower than 60%. In both cases the difference in reaction force showed a large increase when the Young's modulus was lower than 60%. The other femurs had an output that was not expected. They all had the metastasis lesions that were not large. This leads to have slight changes in the material properties, but the slightly different outcome expected did not come out.

This was due to the fact the simulation was incremental, this could lead to the fracture occurring in a slightly different increment, resulting in a slightly different reaction force. However, this does not necessarily mean that the femur was indeed slightly weaker or stronger but could also be due to a small numerical error during the simulation. So, decreasing the material properties of the blastic metastasis in the finite element model only influenced the reaction force if the patient had larger metastatic lesions.

So, small blastic lesions have a small effect on the reaction force, whereas larger blastic lesions apparently do influence the reaction force. How to adapt the blastic lesions to enable to calculate reliable reaction force needs to be researched in the future.

Chapter 8:
Conclusion and future developments

Final remarks and future work proposals.

Bone metastasis often develop in the femur in patients with cancer, in particular if the cancer is in an advanced state. These lesions can cause pain and can lead to a pathological fracture. The surgical treatment of these fracture is complex and it involves often postoperative complications. Doctors usually decide the treatment of metastatic femurs based on the fracture risk. For this reason, a reliable fracture risk prediction is very important. However, the values of sensitivity and specificity of assessing the fracture risk based on the method that were used according to the current guideline are low.

The present work was born to improve the reliability of the assessment of the fracture risk in patients that developed metastasis in the femur. In previous studies, it was seen that the use of a finite element tool improved the reliability of the fracture risk assessment. The finite element tool had however two main drawbacks: the reliability on the prediction was higher but it could be still improved, and the finite element model was not yet usable for patients with blastic metastases, because the mechanical properties of blastic lesions were overestimated in the finite element model. For this reason, we tried to combine the finite element model with a deep learning algorithm that segmented the metastatic lesions by using the segmentations to adapt the material properties of the metastatic lesions. We hypnotized that this would lead to a better prediction compared to the fracture risk based on a finite element model with adapted material propertied based on manual segmentations. However, the automatic segmentations showed an improvement, but not as clear as the manual segmentations. For the blastic metastases, promising results were obtained, in the patients that have metastasis in a very advanced state in the femur.

From the ranking analysis of the lytic metastases, we saw that the impact of the segmentations on the material properties was greater in the manual segmentation models than the automatic segmentations models. From the relation between the Dice coefficient and the difference in reaction force an inconsistency was noted. The segmentations with the highest Dice coefficient were also the ones with reaction forces differed most from the manual segmentations. This worked also in the opposite way. This can be explained by the fact that the difference in reaction forces was due to a weakening of the material properties, since the bone mineral density of the metastatic elements was set to zero. So, if the automatic segmentation considered healthy tissue as metastatic tissue, we would have a low Dice coefficient and a high decrease of the material properties. The manual segmentation is the one that impact most on the material properties of the material. So, if

an automatic segmentation decreases more the material properties, it would obtain similar results to the manual segmentation. The analysis of the BOS scores analysis of the 8 models modified by manual or automatic segmentations seemed to improve in comparison to the BOS scores obtained by the standard model. In particular, the manual segmentations showed the greatest improvement and the results analyzed by a larger number of patients were very promising. 34 Patients were analyzed with the manual segmentations and the results showed an improvement of specificity and positive predictive value and equal results for the sensitivity and negative predictive value with respect to the Eggermont et Al.

When decreasing the Young's modulus of the blastic lesions, four patients showed a trend that was not expected: the reaction force did not decrease as the Young's modulus decreased. The cause could be the metastatic lesions that were small. This led slight changes in the material properties, but apparently not enough to get the outcome as we expected. This could be due to the fact the simulation was incremental, which could lead to the fracture occurring in a slightly different increment, resulting in a slightly different reaction force. However, this does not necessarily mean that the femur was indeed slightly weaker or stronger but could also be due to a small numerical error during the simulation. So, decreasing the material properties of the blastic metastases in the finite element model only influenced the reaction force if the patient had larger metastatic lesions.

On the basis of the aforementioned findings, the following limits and future developments are outlined. For the lytic metastasis, a greater number of samples must be tested to verify if the promising results obtained would maintain in the same way. Then, the algorithm must be improved, to obtain higher Dice coefficients indicating similar results to the manual segmentation because if this process is automatized, it will be easier to use, also by the clinicians. Furthermore, the adaptation of the material properties of the blastic metastases need to be testes for a higher number of patients to get more complete data. The hypothesis is that these results indicate that smaller blastic lesions do not have a significant impact on the reaction force, and therefore only for larger metastases, the material properties require changes.

Bibliography

[1] «IKLN,» Nederlands Kankerregistratie, Integrall Kankercentrum Nederland, June 2018. [Online]. Available: www.cijfersoverkanker.nl.

[2] F. J., «Cancer Incidence and Mortality Worldwide: IARC,» *CancerBase,* n. 11, 2013.

[3] M. F., «Bone metastases: An Overview,» *Oncology reviews,* 2017.

[4] B. K.M., «The bone microeviroment in metastasis, what is special about bone?,» *Springerlink,* 2008.

[5] S. A.B., «Cancer Metastases to Bone: Concepts, Mechanism, and Interactions with Bone Osteoblasts,» *Cancers,* 2018.

[6] C. R.E., «Skeletal complications of malignancy,» *Cancer,* 1997.

[7] M. G.R., «Mechanisms of bone metastasis,» *Cancer,* 1997.

[8] C. E., «Symptom clusters in cancer patients with bone metastases,» *Springerlink,* 2007.

[9] R. R.D., «Bone metastases - the clinical problem,» *European journal of cancer,* 1998.

[10] D. T., «The cost of treatment of skeletal-related events in patients with bone metastases from lung cancer.,» *Oncology,* 2004.

[11] R. M., «Insight opinion to surgically treated metastatic bone disease: Scandinavian Sagrcoma Group Skeletal Metastasis Registry report of 1195 operated skeletal metastasis,» *Surgical oncology,* 2013.

[12] V. d. L. Y.M., «Comparative analysis of risk factors for pathological fracture with femorale metastases,» *The bone & joint journal,* 2004.

[13] V. d. L. Y.M., «Simple radiographic parameter predicts fracturing in metastatic femoral bone lesions: results from a randomised trial,» *Radiotherapy & Oncology,* 2003.

[14] K. S., «Reminalization and pain relief in bone metastases after different radiotherapy fractions (10 times 3 Gy vs. 1 time 8 Gy). A prospective study.,» *Strahlenther Onkol,* 1999.

[15] D. L.C., «Implementation of asymmetirc yielding in case-specific finite element models improves the prediction of femoral fractures.,» *Computer Methods in Biomechanics and Biomedical Engineering,* 2011.

[16] E. F., «Can patient-specific finite element models better predict fractures in metastaatic bone disease than experienced clinicians?,» *Bone joint res.,* 2018.

[17] E. F., «Patient-specific finite element computer model for strehgth assessment of healty and metastatic proximal femur,» *Bone,* 2020.

[18] S. A., «Nonlinear voxel-based finite element model for strength assessment of healthy and metastatic proximal femurs.,» *Bone Reports,* 2020.

[19] K. T.S., «Relationships between material properties and CT scan data of cortical bone with and without metastatic lesions,» *Medical Enginerring & Physics,* 2003.

[20] K. T.S., «Mechanical properties, density and quantitative CT scan data of trabecular bone with and without metastases,» *Medical Engineering & Physics,* 2003.

[21] H. J.A., «Mechanical Properties of Trabecular Bone Within and Adjacent to Osseus Metastases,» *Journal of bone and mineral research,* 1993.

[22] S. M.A., «Conventional finite element models estimate the strenght of metastatic human vertebrae despiute alterations of the bone's tissue and structure,» *Bone,* 2020.

[23] Y. J., «Computer Aided Detection of Lytic Bone Metastases in the Spine using Routine Ct Images,» *IEEE International Symposium on Biomedical Imaging,* 2007.

[24] B. J.E., «Automated Detection of Sclerotic Metastases in the Thoracolumbar Spine at CT,» *Radiology,* 2013.

[25] K. J.H., «Predicting Proximal Femoral Strength Using Structural Engineering Models,» *Clinical orthopaedics and related research,* 2005.

[26] E. F., «Towarrdns clinical implementation of finite element based fracture risk prediction in femoral bone meatastases,» *PhD thesis, Radboud Universiteit.*

[27] C. A., «Criticcal steps in hematogenous metastasis: an overview,» *Surg Oncol Clin,* 2001.

[28] S. G., «Management of bone metastases in cancer: a review,» *Clin Rev Oncol Hematol,* 2005.

[29] C. M., «Molegcular and biological mechanism of bone metastasis,» *EAU update sereies,* 2005.

[30] M. S.C., «Structure and development of the skeleton. In Principles of Bone Biology,» *Academic Press,* 2002.

[31] O. S.M., «Cortical or Trabecular Bone: What's the Difference?,» *American journal of neprology ,* 2018.

[32] P. A.M., «Misconceptions (2): turnover is always higher in cancellous than in cortical bone.,» *Bone ,* 2002.

[33] N. U.S: National Instutes of Health, «Seer Training modules. Cancer registration & Surveilance Modules: Classification of Bones».

[34] C. M., «Osteoblast and osteocyte: Games without frontiers.,» *Arch. Biochem. Biophys.,* 2014.

[35] L. Bonewald, «The amazing osteocyte,» *Bone Miner. Res.,* 2011.

[36] G. C.J., «Ibandronate to treat skeletal-related events and bone pain in metastatic bone disease or multiple myelome: A meta-analysis of randomised clonical trials,» *BMJ open,* 2015.

[37] K. H., «MEtastatic behavior of breat cancer subtypes,» *Clin.Oncol.,* 2010.

[38] A. Liede, «The Incidence of bone metastasis after early-stage breast cancer in canada,» *Breast Cancer Res. Treat.,* 2016.

[39] G. Mundy, «Bone Remodeling and Its Disorders,» *Martin Duniztz Ltd.: London,UK,* 1999.

[40] K. Tu, «Osteoporosis: A review of treatment options,» *Pharm. Ther. 2018.*

[41] T. K.N:, «Osteoporosis: A review of treatment options.,» *Pharm. Ther. ,* 2018.

[42] M. S., «Multiple myeloma and bone: The fatal interaction.,» *Cold Spring Harbor Perspect. Med.,* 2017.

[43] B. R., «Mechanisms of bone destruction in multiple myeloma: The importance of unbalanced process in determining the severity of lytic bone disease,» *Clin. Oncol.,* 1989.

[44] C. S.A., «Histomorphmetric analysis of sclerotic bone metastases from prostatic carcinoma special reference to osteomalacia,» *Cancer ,* 1983.

[45] L. C.E., «Current perspectives on bone metastases in castrate-resistant prostate cancer.,» *Cancer Metastasis Rev.,* 2018.

[46] S. A., «Disruption of collagen7apatite alignment impairs bone mechanical function in osteoblastic metastasis induced by prostate cancer,» *Bone ,* 2017.

[47] C. R., «The clinical course of bone metastases from breast cancer,» *Cancer,* 1987.

[48] R. M., «How is androgen dependent metastatic prostat cancer best treated?,» *Haematol Oncol Clinics North Am,* 1996.

[49] M. R., «Novel therapeutic approaches to cancer patients with bone metastasis,» *Crit Rev Oncol Hematol ,* 2001.

[50] C. R., «Metastatic bone disease: clinical features, pathophysiology and treatment strategies,» *Cancer Treat Reb,* 2001.

[51] H. N., «The management of pathological fractures,» *Trauma,* 1965.

[52] C. D., «Bone cancer pain,» *2003.*

[53] C. R., «Bone health in cancer patients: ESMO clinical practice guidelines,» *Ann Oncol,* 2014.

[54] V. J., «Effect of bone metastases on bone metabolism: implications for diasognis, imaging and assessment of response to cancer treatment,» *Cancer Treat Rev,* 1996.

[55] R. D., «Radiologic diagnosis of bone metastases,» *Cancer,* 1997.

[56] B. J., «Use of bisphosphonates in cancer patients,» *Cancer Treat Rev,* 1996.

[57] G. J.R., «Pharmacologic profile of zoledronic acid: a highly potent inhibitor of bone resorption,» *Drug Dev Res,* 2002.

[58] A. M., «Bone-modifying agnets in the treatment of bone metastases in patients with advanced genitourinary malignancies: a focus on zoledronic acid,» *Ther Adv Urol,* 2012.

[59] Y. A., «Denosumab, a Rank ligand inhibitor, for the management of bone loss in cancer patients,» *Clin Interv Aging,* 2012.

[60] S. G., «Denosunab and bisphosphonates: different mechanism of action and effects,» *Bone,* 2011.

[61] B. R., «Denosumab and bisphosphonates: differen mechanism of action and effects,» *Bone ,* 2011.

[62] A. A., «Efficacy and safety of denosumab in postmenopausal women with osteopenia or osteoporosis: a systematic review and a meta-analysis,» *Horm Metab Res,* 2009.

[63] H. D., «Randomized, double blind study of desonumab versus zoledronica acid in the treatment of bone metastases in patients with advanced cancer (excluding brast and prostaste cancer) or multiple myeloma,» *Clin Oncol ,* 2011.

[64] J. N., «Radiation of bone metastases: conventional techniques and the rof of systemic radiopharmaceuticals,» *Cancer,* 1997.

[65] T. C., «The palliation of symptomatic osseus metastases: final results of the study by the Radiation Therapy Oncology Group,» *Cancer ,* 1982.

[66] P. C., «A report of RTOG 8206: a phase III study of whether the addition of single dose hemi-body irradiation to standard fractionated local field irradiation is more effective than local field irradiation alone in the treatment of symptomatic osseus metastases,» *Radiat Oncol Biol Phys,* 1992.

[67] R. R., «Clinical expierence with strontium89 in prostatic and breast cancer patients,» *Semin Oncol,* 1993.

[68] T. P., «Palliation of painful metastatic disease involving bone with image-guided treatment: comparison of patients immediate response to radiofrequency ablation and cryoablation,» *Roentgenol,* 2011.

[69] C. M:, «percutaneous image-guided cryoablation of painful metastases involving bone: multicenter trial,» *Cancer,* 2013.

[70] C. R., «Management of long bone metastases: recommendations from the Italian Orthopaedic Society bone metastasis study group,» *Expert review of Anticancer Therapy ,* 2014.

[71] S. M.S., «Pathologic and impending fractures: biological and clinical aspects,» *Journal of Biological Regulators and Homeostatic Agents,* 2015.

[72] M. H., «Metastatic disease in long bones. A proposed scoring system for diagnosing impending pathologic fractures,» *Clinical Orthopaedics and Related Research ,* 1989.

[73] B. M., «Prediction of strength and strain of the proximal femur by a CT-based finite element method,» *J Biomech ,* 2007.

[74] S. A., «Pathological fracture risk assessment in patients with femoral metastases using CT-based finite element methods. A retrospective clinical study.,» *Bone ,* 2018.

[75] S. A., «When and where do patients with bone metastases actually break their femurs?,» *Bone Joint J,* 2005.

[76] F. C., «Mechanical behavior of metastatic femurs through patient-specific computational models accounting for bone-metastasis interaction,» *Journal of the Mechanical Behavior of Biomedical Materials,* 2019.

[77] U. D., «Finite element analysis of trabecular bone structure: a comparison of image-based meshing techniques,» *Journal of Biomechanics,* 1998.

[78] C. S., «Bone poroelasticity,» *J. Biomech 1999.*

[79] B. M., «General theory of three-dimensional consolidation,» *J. Appl.,* 1941.

[80] B. E., «Automated Detection of Sclerotic Metastases in the Thoracolumbar Spine at CT.,» *Radiology,* 2013.

[81] V. L., «Wathersheds in Dicital Spaces: An Efficient Algorithm Based on Immersion Simulations,» *IEEE Trans. Patterns Anal. Machine Intell. ,* 1991.

[82] H. J.H:, «Complications of bone metastases: surgical managemente,» *Cancer,* 2000.

[83] K. Y., « The risk assessment of pathological fracture in the proximal femur using a CT-based finite element method,» *Journal of Orthopaedic Science ,* 2017.

List of Figures

List of Tables